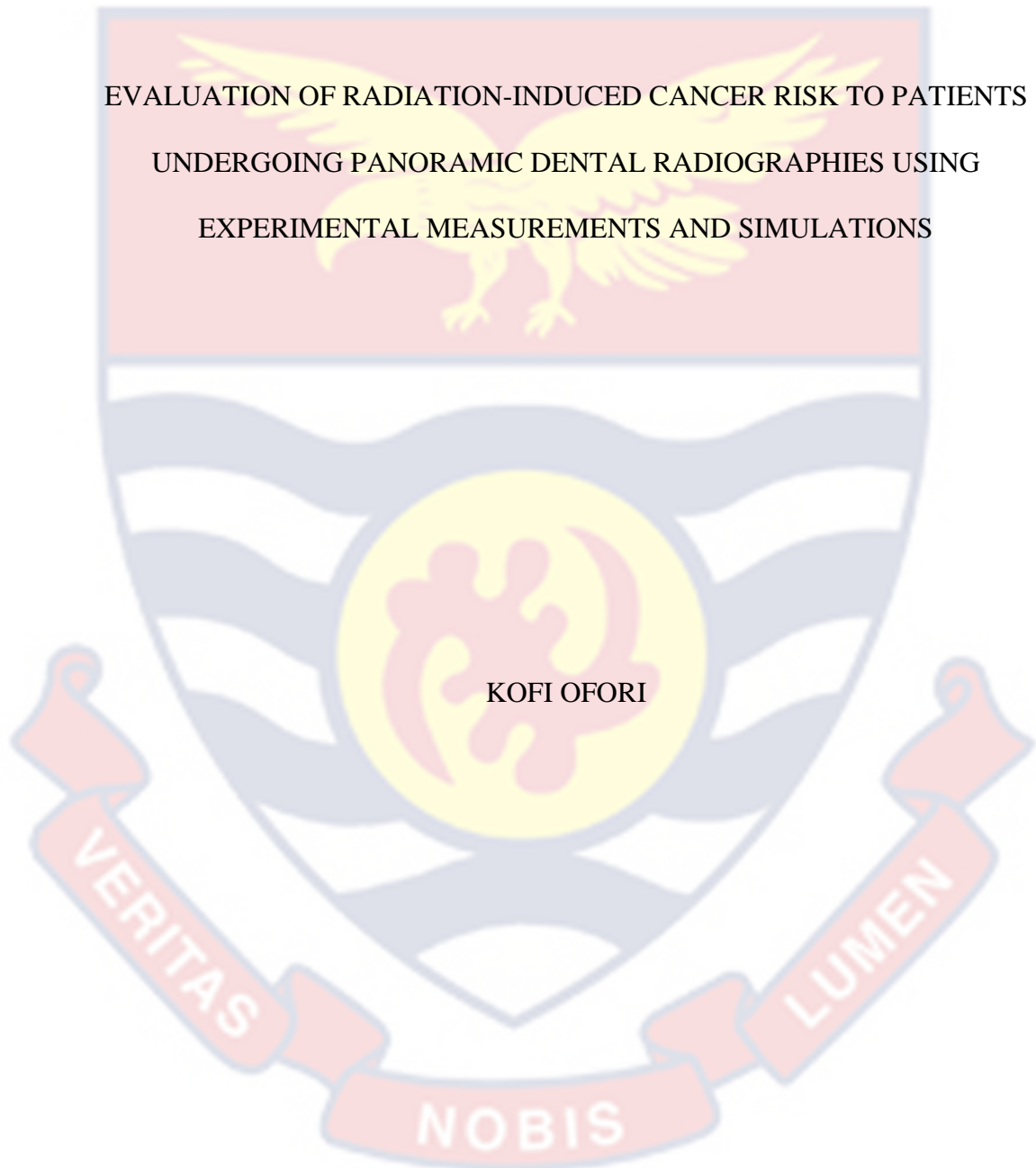


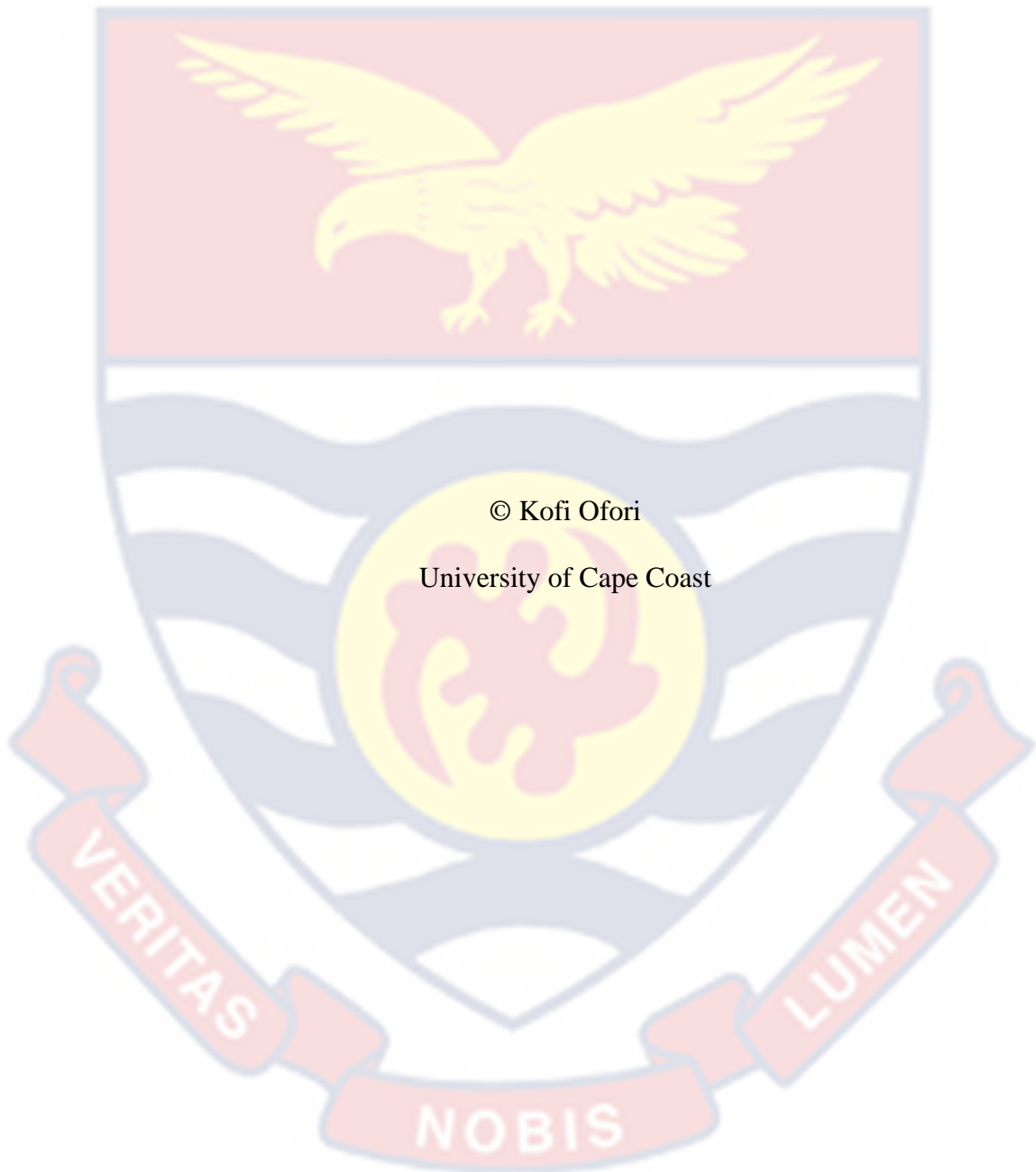
UNIVERSITY OF CAPE COAST



EVALUATION OF RADIATION-INDUCED CANCER RISK TO PATIENTS
UNDERGOING PANORAMIC DENTAL RADIOGRAPHS USING
EXPERIMENTAL MEASUREMENTS AND SIMULATIONS

KOFI OFORI

2023



© Kofi Ofori

University of Cape Coast

UNIVERSITY OF CAPE COAST

EVALUATION OF RADIATION-INDUCED CANCER RISK TO PATIENTS
UNDERGOING PANORAMIC DENTAL RADIOGRAPHIES USING
EXPERIMENTAL MEASUREMENTS AND SIMULATIONS

BY

KOFI OFORI

Thesis submitted to the Department of Physics of the School of Physical
Sciences, College of Agriculture and Natural Sciences, University of
Cape Coast, in partial fulfilment of the requirements for the award
of Doctor of Philosophy degree in Physics

NOVEMBER 2023

DECLARATION

Candidate's Declaration

I hereby declare that this thesis is the result of my own original research and that no part of it has been presented for another degree in this University or elsewhere.

Candidate's Signature: Date:

Name: Kofi Ofori

Supervisors' Declaration

We hereby declare that the preparation and presentation of the thesis were supervised in accordance with the guidelines on supervision of thesis laid down by the University of Cape Coast.

Principal Supervisor's Signature: Date:

Name: Prof. Mary Boadu

Co-Supervisor's Signature: Date:

Name: Dr. Baah Sefa-Ntiri

ABSTRACT

Patient doses related with panoramic dental radiographies are comparatively low, but the frequency at which these examinations are taken is high. Hence, it is necessary to justify these examinations to ensure that doses to patients, especially children are kept as low as reasonably allowable. The risk of exposure-induced cancer deaths to the four standard age groups, comprising 5-, 10-, 15-year-olds and adults were evaluated in this research. The mean REIDs were estimated based on the patients' age, mass, height, gender, as well as the input doses, exposure factors, beam geometries and simulation parameters. The respective ranges of REID estimates (per ten million) were 6.45-2.04 for males, 8.32-2.62 for females; 7.45-2.51 for males, 9.02-3.62 for females; 8.50-2.03 for males, 11.02-4.12 for females; 7.99-2.65 for males, 10.52-3.90 for females; 8.45-1.95 for males, 10.68-3.09 for females; 9.85-3.21 for males, 11.05-4.09 for females. Individual radiogenic cancers were observed for leukaemia, lung cancers, liver cancers, stomach cancers and other cancers for all ages and gender. Breast cancer was observed in female patients, with negligible risk in males. In an instance, the respective REIDs for the cancer types for the age groups were 2846.00×10^{-9} - 786.00×10^{-9} in males, 2415.00×10^{-9} - 613.00×10^{-9} in females; 630.00×10^{-9} - 147.00×10^{-9} in males, 1114.00×10^{-9} - 240.00×10^{-9} in females; 19.99×10^{-9} - 3.89×10^{-9} in males, 9.56×10^{-9} - 1.89×10^{-9} in females; 26.65×10^{-9} - 5.40×10^{-9} in males, 28.45×10^{-9} - 6.60×10^{-9} in females; 15230.00×10^{-8} - 2560.00×10^{-8} in males, 18790.00×10^{-9} - 4499.00×10^{-9} in females; and 2250.00×10^{-10} - 78.00×10^{-10} in females only. According to the findings of this study, radiation exposure generally increased the risk of cancer in youngsters more than adults, and more in female patients compared to male patients.

KEY WORDS

Dental Panoramic Radiography

Dose Area Product

Effective Dose

Organ Absorbed Dose

Risk of Exposure-Induced Cancer Death

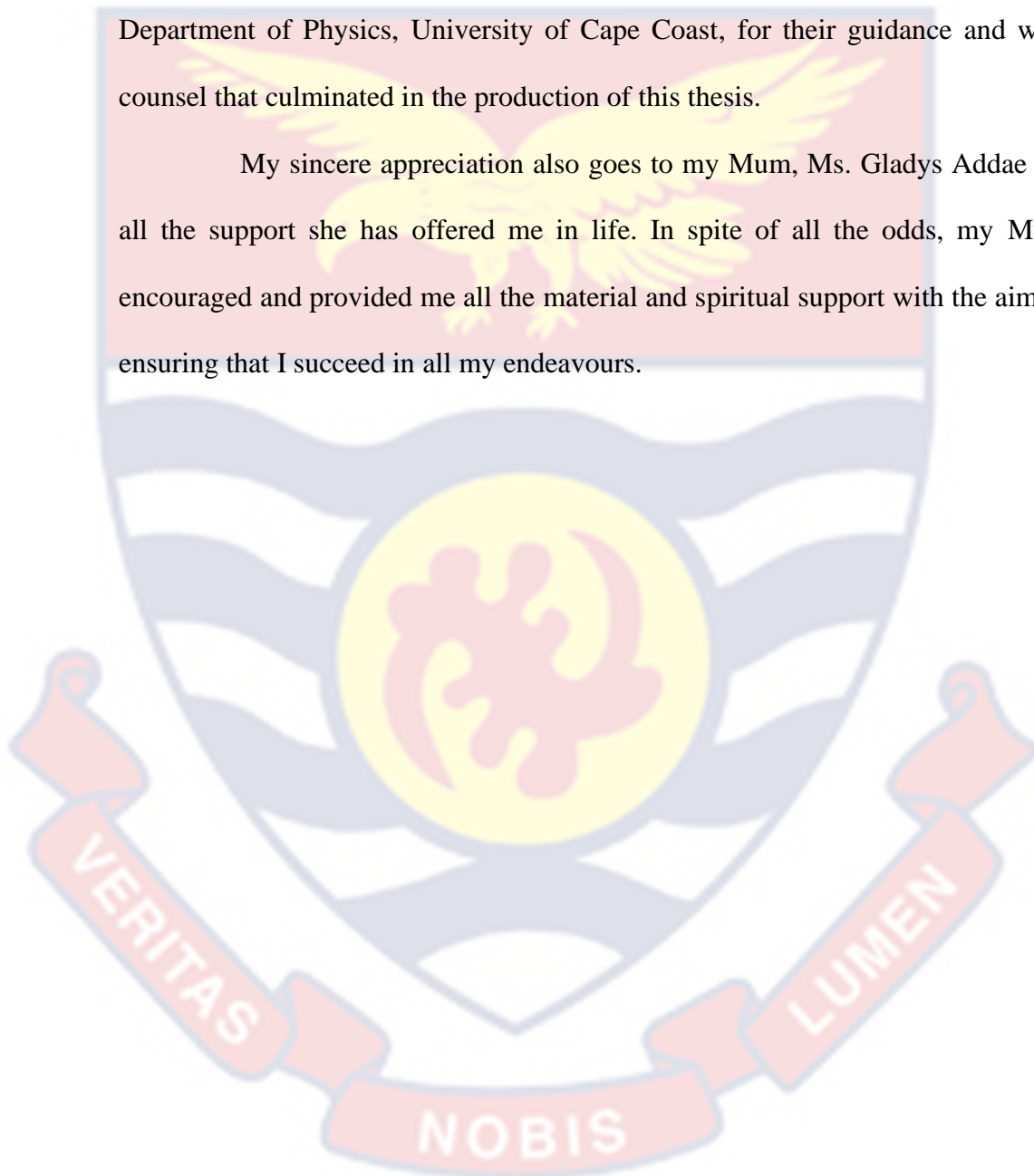
Simulation



ACKNOWLEDGEMENTS

I would like to convey my sincere gratitude to my supervisors, Prof. Mary Boadu, Director of the Radiological and Medical Research Institute of the Ghana Atomic Energy Commission and Dr. Baah Sefa-Ntiri, Senior Lecturer at the Department of Physics, University of Cape Coast, for their guidance and wise counsel that culminated in the production of this thesis.

My sincere appreciation also goes to my Mum, Ms. Gladys Addae for all the support she has offered me in life. In spite of all the odds, my Mum encouraged and provided me all the material and spiritual support with the aim of ensuring that I succeed in all my endeavours.



DEDICATION

To my lovely mum, Ms. Gladys Addae.



TABLE OF CONTENTS

DECLARATION	ii
ABSTRACT	iii
KEY WORDS	iv
ACKNOWLEDGEMENTS	v
DEDICATION	vi
LIST OF TABLES	xi
LIST OF FIGURES	xiii
LIST OF ABBREVIATIONS	xvi
CHAPTER ONE: INTRODUCTION	1
Background to the Study	1
Statement of the Problem	7
Purpose of the Study	7
Objectives of the Study	8
Significance of the Study	8
Delimitations	9
Limitations	9
Organisation of the Study	10
CHAPTER TWO: LITERATURE REVIEW	12
Introduction	12
Radiation Dosimetry	12
X-Ray Interactions	12
Photoelectric Effect	13
Compton Scattering	13

Coherent Scattering	14
Radiation Dosimetry and Measurement	15
Incident Radiation	15
Kerma Area Product (KAP)	16
Absorbed Radiation	16
Absorbed Dose	16
Equivalent Dose	17
Effective Dose	17
Radiation Dose and Risk in Dental Radiology	18
Radiation Damage	18
The Risks	19
Dental Radiography Equipment Variables Affecting Radiation Doses to Patients	23
Generation of X-Rays and Kilovoltage	23
Filtration	25
Collimation	25
Collimation in Panoramic Radiography	26
Choice of Image Receptor in Dental Radiography	27
Intra-Oral Radiography	27
Extra-Oral Radiography	27
Digital Receptors in Panoramic Radiography	28
Background of Monte Carlo Applications in Dental Radiology	29
Radiation Dose Quantities in PCXMC	32
Calculation of Incident Air Kerma	33

Mathematical Phantoms	34
The Monte Carlo Technique	37
Risk Assessment	39
Chapter Summary	44
CHAPTER THREE: METHODOLOGY	46
Introduction	46
Panoramic Dental X-Ray Equipment	46
Magic Max Universal Multimeter for Performance Testing	47
Performance Testing	48
Condition of Measurement for each Performance Parameters	49
kVp accuracy	49
Timer Accuracy	50
kVp Reproducibility	50
Timer Reproducibility	50
Exposure Reproducibility	51
mA Linearity	51
Half-Value Layer (HVL)	51
Patient Data Collection	51
Examination Factors and Dose Area Product Measurement	52
PCXMC Simulations for the various Dental Radiographies	53
Computation of Organ and Effective Doses	56
Computation of the Cancer Risk	57
Chapter Summary	59

CHAPTER FOUR: RESULTS AND DISCUSSION	61
Introduction	61
Performance Tests	61
Dose Area Product	62
Organ Absorbed and Effective Doses	67
Risk of Exposure-Induced Cancer Death (REID)	76
Individual/Organ Specific Radiogenic Cancers	85
Chapter Summary	107
CHAPTER FIVE: SUMMARY, CONCLUSIONS AND RECOMMENDATIONS	109
Overview	109
Summary	109
Conclusions	110
Recommendations	110
REFERENCES	113
APPENDICES	132
APPENDIX A: THE PCXMC 2.0 MODIFIED PRINCIPAL DIMENSIONS OF THE MATHEMATICAL PHANTOMS.	132
APPENDIX B: PCXMC 2.0 PERCENTAGE BY WEIGHT OF THE ELEMENTS IN THE PHANTOM TISSUES	133

LIST OF TABLES

	Page
1 ICRP 103 Tissue weighting factors	18
2 Stochastic impacts (nominal lifetime probability)	20
3 The age-risk relationship	20
4 Effective doses and risks from stochastic effect	21
5 Estimate of the total number of images from dental examinations performed annually in European countries	23
6 Organs and tissues with their weighting factors	31
7 Panoramic equipment information and technical specifications	46
8 Parameters for performance test and acceptable criteria	49
9 Patient data for the various age groups	52
10 Major parameters measured and their acceptance criteria	61
11 kVp, mAs, and DAP (mGy.cm ²) for the 5-year-old group	63
12 kVp, mAs, and DAP (mGy.cm ²) for the 10-year-olds	64
13 kVp, mAs, and DAP (mGy.cm ²) for the 15-year-olds	65
14 kVp, mAs, and DAP (mGy.cm ²) for the Adults	66
15 Organ absorbed and effective dose (\pm SD) from Kh-0.5-105 panoramic equipment	70
16 Organ absorbed and effective dose (\pm SD) from CS8100SC panoramic equipment	71
17 Organ absorbed and effective dose (\pm SD) from OPX105 panoramic equipment	72
18 Organ absorbed and effective dose (\pm SD) from PHT-6500 panoramic equipment	72

- 19 Organ absorbed and effective dose (\pm SD) from GX100-20DC panoramic equipment 74
- 20 Organ absorbed and effective dose (\pm SD) from 1117340V1010 panoramic equipment 75



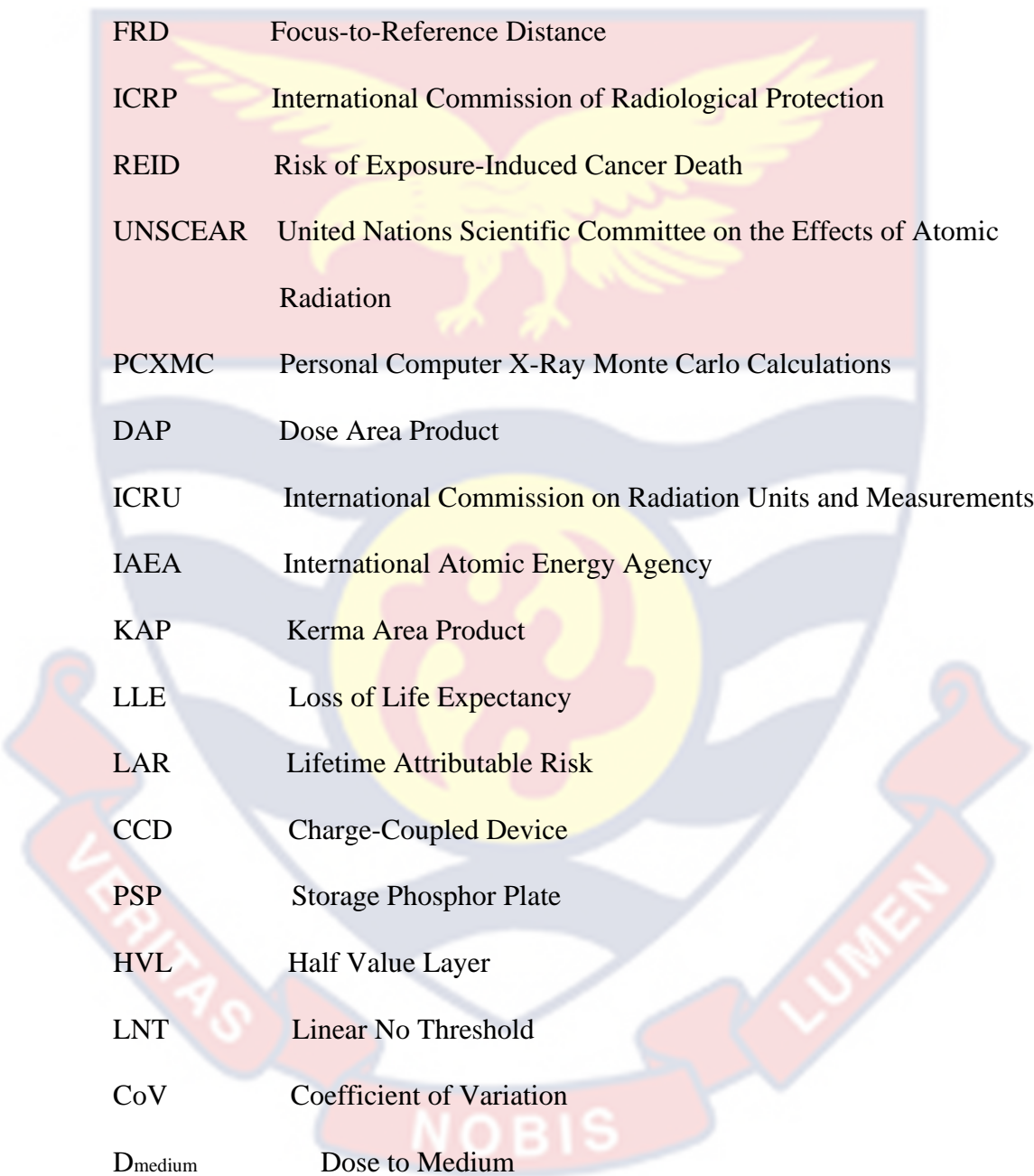
LIST OF FIGURES

	Page
1 Patient undergoing Panoramic Dental Radiography	3
2 X-ray Source and Detector Movement during the Radiography	4
3 Photon Interactions with the Body	4
4 Panoramic Radiograph	5
5 Coherent Scatter, Photoelectric effect, Compton scatter	14
6 Air Kerma of an X-ray Tube	16
7 Magic Max Universal Tool	48
8 The DAP Meter	53
9 Set-Up for DAP Measurement	53
10 An Illustration of Geometry	55
11 The PCXMC 20Rotation's Interface	56
12 REID Values from Device Model Kh-0.5-105	79
13 REID Values from Device Model CS8100SC	80
14 REID Values from Device Model OPX105	81
15 REID Values from Device Model PHT-6500	82
16 REID Values from Device Model GX100-20DC	83
17 REID Values from Device Model 1117340V1010	84
18a The REID Values for Leukemia from the Kh-0.5-105 Panoramic Equipment Model	85
18b The REID Values for Lung Cancer from the Kh-0.5-105 Panoramic Equipment Model	86
18c The REID Values for Liver Cancer from the Kh-0.5-105 Panoramic Equipment Model	87
18d The REID Values for Stomach Cancer from the Kh-0.5-105 Panoramic Equipment Model	87
18e The REID Values for Other Cancers from the Kh-0.5-105 Panoramic Equipment Model	87
19a The REID Values for Leukemia from the CS8100SC Panoramic Equipment Model	88

19b	The REID Values for Lung Cancer from the CS8100SC Panoramic Equipment Model.	88
19c	The REID Values for Liver Cancer from the CS8100SC Panoramic Equipment Model	89
19d	The REID Values for Stomach Cancer from the CS8100SC Panoramic Equipment Model	89
19e	The REID Values for Other Cancers from the CS8100SC Panoramic Equipment Model	90
20a	The REID Values for Leukemia from the OPX105 Panoramic Equipment Model	90
20b	The REID Values for Lung Cancer from the OPX105 Panoramic Equipment Model	91
20c	The REID Values for Liver Cancer from the OPX105 Panoramic Equipment Model	91
20d	The REID Values for Stomach Cancer from the OPX105 Panoramic Equipment Model	92
20e	The REID Values for Other Cancers from the OPX105 Panoramic Equipment Model	92
21a	The REID Values for Leukemia from the PHT-6500 Panoramic Equipment Model	93
21b	The REID Values for Lung Cancer from the PHT-6500 Panoramic Equipment Model	93
21c	The REID Values for Liver Cancer from the PHT-6500 Panoramic Equipment Model	94
21d	The REID Values for Stomach Cancer from the PHT-6500 Panoramic Equipment Model	94
21e	The REID Values for Other Cancers from the PHT-6500 Panoramic Equipment Model	95
22a	The REID Values for Leukemia from the GX100-20DC Panoramic Equipment Model	95
22b	The REID Values for Lung Cancer from the GX100-20DC Panoramic Equipment Model	96

22c	The REID Values for Liver Cancer from the GX100-20DC Panoramic Equipment Model	96
22d	The REID Values for Stomach Cancer from the GX100-20DC Panoramic Equipment Model	97
22e	The REID Values for Other Cancers from the GX100-20DC Panoramic Equipment Model	97
23a	The REID Values for Leukemia from the 1117340V1010 Panoramic Equipment Model	98
23b	The REID Values for Lung Cancer from the 1117340V1010 Panoramic Equipment Model	98
23c	The REID Values for Liver Cancer from the 1117340V1010 Panoramic Equipment Model	99
23d	The REID Values for Stomach Cancer from the 1117340V1010 Panoramic Equipment Model	99
23e	The REID Values for Other Cancers from the 1117340V1010 Panoramic Equipment Model	100
18f	REID for Breast Cancer from the Kh-0.5-105 Panoramic Equipment Model.	101
19f	REID for Breast Cancer from the CS8100SC Panoramic Equipment Model	101
20f	REID for Breast Cancer from the OPX105 Panoramic Equipment Model	102
21f	REID for Breast Cancer from the PHT-6500 Panoramic Equipment Model	102
22f	REID for Breast Cancer from the GX100-20DC Panoramic Equipment Model	103
23f	REID for Breast Cancer from the 1117340V1010 Panoramic Equipment Model.	103

LIST OF ABBREVIATIONS

The background of the page features a large, semi-transparent watermark of the University of Cape Coast crest. The crest is a shield-shaped emblem with a yellow eagle with outstretched wings in the center. Below the eagle is a yellow sun. The shield is flanked by two red banners with white text. The left banner reads 'VERITAS' and the right banner reads 'LUMEN'. At the bottom of the shield, the word 'NOBIS' is written in white. The entire crest is set against a light blue background.

BEIR	Biological Effects of Ionizing Radiation
CBCT	Cone-Beam Computed Tomography
FOV	Field of View
FRD	Focus-to-Reference Distance
ICRP	International Commission of Radiological Protection
REID	Risk of Exposure-Induced Cancer Death
UNSCEAR	United Nations Scientific Committee on the Effects of Atomic Radiation
PCXMC	Personal Computer X-Ray Monte Carlo Calculations
DAP	Dose Area Product
ICRU	International Commission on Radiation Units and Measurements
IAEA	International Atomic Energy Agency
KAP	Kerma Area Product
LLE	Loss of Life Expectancy
LAR	Lifetime Attributable Risk
CCD	Charge-Coupled Device
PSP	Storage Phosphor Plate
HVL	Half Value Layer
LNT	Linear No Threshold
CoV	Coefficient of Variation
D_{medium}	Dose to Medium
$\mu(E)/\rho$	Mass Energy Absorption Coefficient
μSv	micro-Sievert

mR milli-Roentgen

mA milli-Ampere

kVp kilovoltage peak

Gy Gray

J/kg Joule Per kilogram

mGy milli-Gray

R Roentgen

mAs milli-Ampere second

keV kilo-electron Volt

Sv Sievert

HVL Half Value Layer

D Absorbed Dose

Wr Radiation Weighting Factor

H Equivalent Dose

E Effective Dose

Wi Tissue Weighting Factor

Ka, e Entrance Surface Air Kerma

Ka Air Kerma

nGy nano-Gray



CHAPTER ONE

INTRODUCTION

Background to the Study

The United Nations Scientific Committee on the Effect of Atomic Radiation (UNSCEAR) 2008 reports that dental radiography is among the often types of radiological examinations undertaken. Data from UNSCEAR shows that 300 examinations are conducted on 1000 people annually (UNSCEAR, 2010).

Radiographs in dentistry are essential for a patient's diagnosis, therapy planning, monitoring, and follow-up. Depending on the purpose of the radiographs, they could be obtained from the different types of dental X-ray modalities such as the cone-beam computed tomography, panoramic, cephalometric or intra-oral. The most used technique is Intra-oral radiography. Additionally, it is inexpensive compared to other radiography procedures, both in terms of radiation dose and monetary cost. The ideal placement of the detector with optimal projection geometry mainly determines the level of radiographic clarity. The effectiveness of the image's contrast and greyscale also affects quality.

Despite the fact that radiographic screening for oral illnesses should not be done, panoramic dental X-ray examinations has been utilized as a technique for screening (Granlund et al., 2016; Molander et al., 1995) and is frequently suggested as a crucial component of orthodontic planning and therapy (Granlund et al., 2016). Compared to the more modern imaging methods that are three-dimensional in nature used in oral radiography, like cone-beam dental computed

tomography, panoramic radiography is regarded as a low-dose technique (Granlund et al., 2016).

Even though the exposures associated with panoramic radiography are relatively low, justification and optimization must be taken in account to keep radiation risks as minimal as is practicable (Teunen, 1998). In order to always keep patient exposure within the recommended levels, and also to identify possible equipment malfunction or inadequate technique, it is recommended that dose assessment and risks associated with the dental procedures be performed on regular basis (Horner et al., 2015).

Currently, the majority of dental X-ray machines in Ghana are intra-oral in nature. There are forty-two of them in operation in the country as against only six panoramic units, with no cone-beam computed tomography (CBDCT) dental unit available at the moment.

Intra-oral radiographs are limited due to the fact that patients do not have the tolerance during the placement of the detectors in their mouth and also its inability to provide images of the whole positions or locations of interest (i.e., the oral cavity) (Granlund et al., 2016). Utilizing extra-oral technology, such as panoramic radiography, which is now commonly used, is an alternative. (Granlund et al., 2016; Molander et al., 1995).

Panoramic radiography, a two-dimensional examination shows the entirety of the mouth, including all of the teeth in both the upper and lower mandible, adjacent structures and tissues on a single radiograph. This X-ray examination detects the dentistry and medical issues like advanced periodontal disease, cysts in the jaw bones, jaw tumors and oral cancers, impacted teeth, including wisdom teeth, jaw disorders (also known as temporomandibular joint

or TMJ disorders), sinusitis, and the location of completely emerged as well as emerging teeth (Horner et al., 2015).

Figures 1 to 4 show the processes leading to the acquisition of image during panoramic radiography: starting with positioning of the subject between the radiation source and the image acquisition device, the process continues with the movement of the source of X-ray and detectors, X-ray interaction with the body systems, leading to the acquisition of panoramic radiograph.



Figure 1: Patient undergoing Panoramic Dental Radiography (FARDT, 2019)

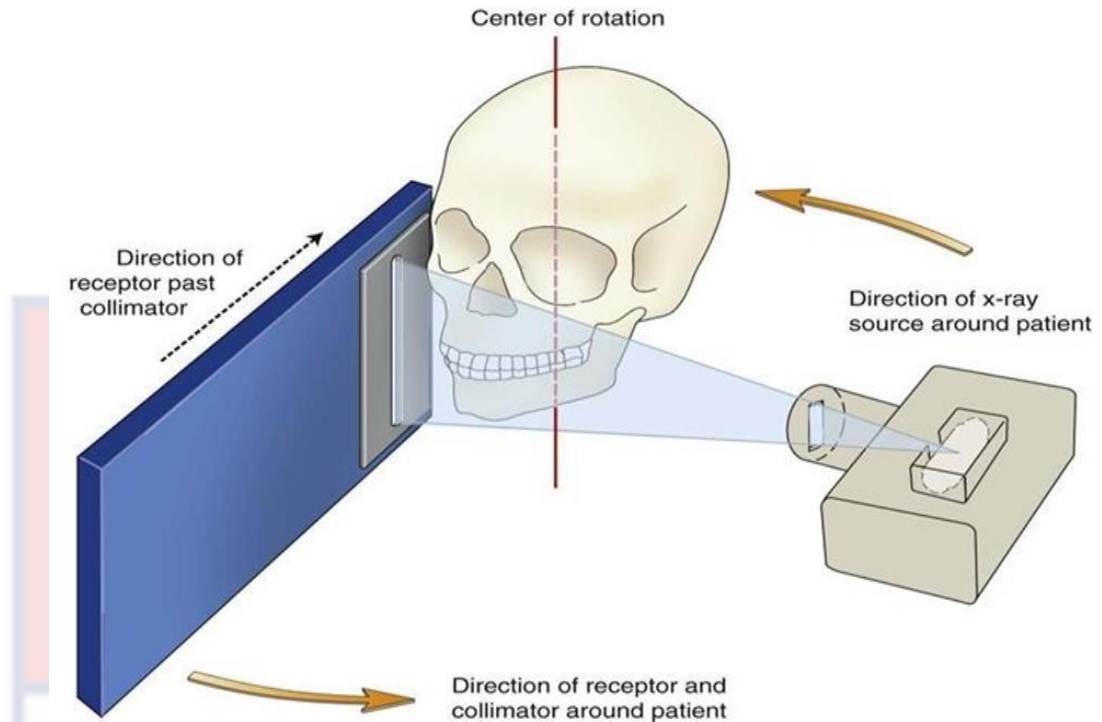


Figure 2: X-ray Source and Detector Movement during the Radiography (Dentistry, 2015)

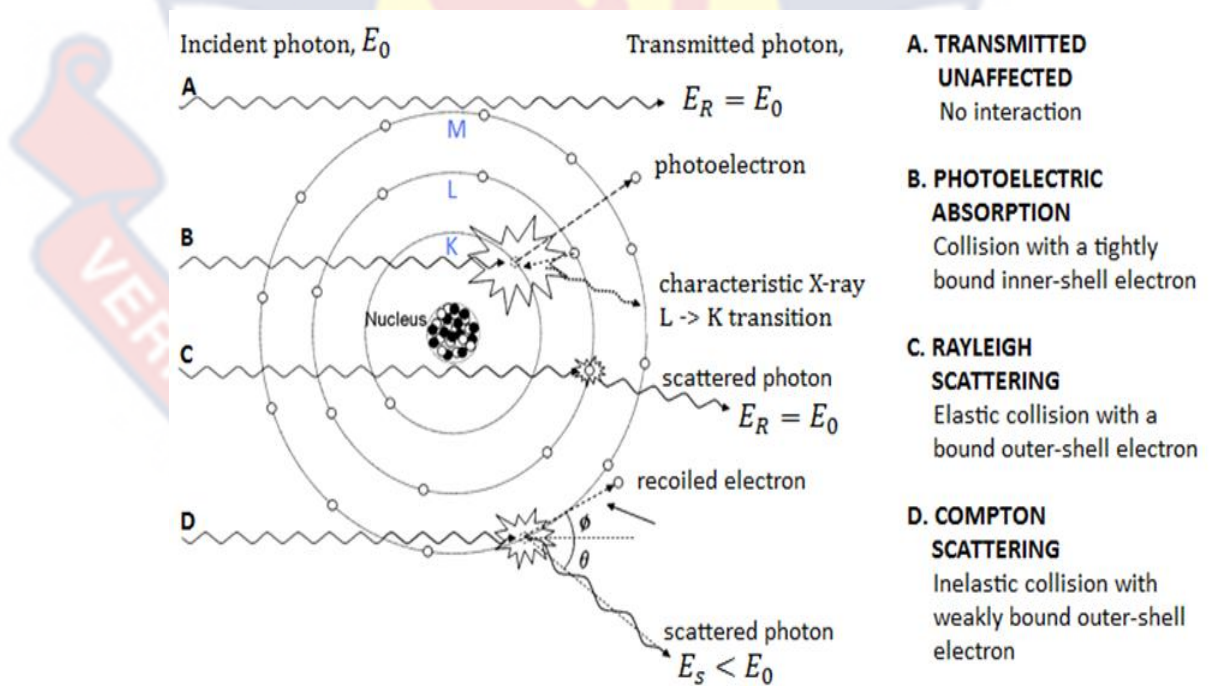


Figure 3: Photon Interactions with the Body: 15-150 keV (Carestream Health, 2007)



Figure 4: Panoramic Radiograph (Izzetti et al., 2021)

It is important to consider the potential carcinogenic effects of the X-rays utilised in these dental examinations despite the benefits of these radiographies to patients (Niroomand-Rad, 2003). Therefore, radiographers, dental practitioners and patients alike must be aware of the risk of carcinogenesis associated with these procedures.

In panoramic radiography, among the parts that are vulnerable are the thyroid and salivary glands. Frequently within the main beam are the salivary glands during panoramic radiography (Granlund et al., 2016). During panoramic scans, the greatest radiation doses are administered to the salivary glands and mouth mucosa of all the tissues (Ludlow et al., 2008).

Observations of the radiation dose from dental radiographies have been reported by several studies but their findings concentrated on only reporting dose at the entrance surface, dose-width-product, different organ and effective doses for a few age categories. Through the use of PCXMC software, Aps

calculated the radiation dosage to the thyroid gland from radiographs obtained in pediatric patients with dento-alveolar injuries. He considered the patient's age, vertical projection angle, exposure duration, exposure voltage, current, as well as beam collimation (Aps, 2013). Walker and van der Putten analysed dose-width-product and entrance surface doses for both panoramic and intra-oral units, and compared their findings to computer simulations of these procedures created using Monte-Carlo methods (Walker & van der Putten, 2012). In order to determine radiation-induced cancer values, they multiplied the effective dose by a constant factor or co-efficient (Horner et al., 2015; Ludlow et al., 2008). Souza et al. used a Monte Carlo code with the Female Adult voxel (FAX) and Male Adult voxel (MAX) phantoms to ascertain the absorbed dosages to the thyroid gland during intra-oral dental exams. The lifetime incidence of cancer related to adult dental exams was also determined (Souza et al., 2008).

It is occasionally criticised that the effective dose is used to explain the stochastic harm that ionizing radiation causes to patients (ICRP, 2007; McCollough et al., 2010; Pradhan et al., 2012). In spite of the fact that the risk of exposure-induced cancer death (REID) is a function of age and gender, the effective dose is not stated as a function of gender or age (ICRP, 1991). Female patients exhibit greater radio sensitivity than male patients, according to Hall et al., and the risk is approximately 15%/Sv for patients in their first decade of life compared to 1%–2%/Sv for adults in their late middle years (Hall, 2002). Therefore, it was advised that the risk calculation be carried out using the risk coefficients from the Biological Effects of Ionizing Radiations VII Committee Report (Council, 2005). These risk coefficients take into consideration the site for cancer, gender, exposure age, and dose specific to each organ dose (Hall &

Brenner, 2008).

Statement of the Problem

During Intra-oral, Panoramic, and other dental radiographies, the organs and tissues at risk are those around the head, neck and chest regions. Studies done elsewhere in the past have shown that exposure to dental X-rays in general is linked to a possible risk of cancer (Brenner et al., 2003; Hall & Brenner, 2008). Studies have linked dental X-ray exposure to an increased risk of developing brain cancer (Neuberger JS et al., 1991; Preston-Martin et al., 1989), tumors of the parotid gland (Preston-Martin et al., 1985), cancer of the breast (Ma et al., 2008) and cancer of the thyroid (Memon et al., 2010; Wingren et al., 1997).

In Ghana, the widely available dental modality is the intra-oral and some very few panoramic. According to Granlund et al. (2016), panoramic dental exposures produce higher doses compared with intra-oral modality. However, work have not been done to determine the radiation-induced cancer risk posed to patients who undergo such examinations.

Again, previous works done elsewhere in time past based on ICRP 60 (ICRP, 1991) underestimated the risk evaluation because the salivary glands and brain tissues were not assigned weighting factors.

Purpose of the Study

This study's goal was to determine the dose-area products (DAPs), organ doses, effective doses, and use these parameters in estimating the radiation-induced cancer risk to patients of various ages, both male and female from panoramic radiographies.

Objectives of the Study

This study's main objective was to assess the radiation-induced cancer risk to patients exposed to panoramic dental radiographies in some selected dental diagnostic facilities within Accra and Kumasi.

The specific objectives were as follows:

- Analyze the dose-area products (DAPs) for the different age categories (5, 10, 15-year-old and adult) and gender from the various dental panoramic X-ray equipment under study using patients' examination factors including the kVp, mA and time.
- Use the DAPs, technique factors and with the aid of the PCXMX simulation tool, evaluate the absorbed and effective doses to patients who underwent the dental procedures based on ICRP 103 (2007).
- Assess the radiation-induced cancer risk to patients based on their ages and gender.
- Determine the individual/specific radiogenic cancers.

Significance of the Study

Firstly, risk evaluation based on the updated ICRP 103 (ICRP, 2007) will provide correct estimation of the effective doses and the radiation-induced cancer risk.

Secondly, the dose and risk values that may be recorded for specific organs and tissues will serve notice to radiographers and dental practitioners as to the specific areas to be protected, and the level of protection needed during the panoramic radiographies.

Thirdly, based on the REID values, referral dental practitioners will realise the need to justify the request for dental examination by weighing the benefits against the risk since any small amount of dental exposure to radiation has the potential of inducing cancer.

Lastly, the REID values from the dental procedures would provide information to interested parties (the regulator, the operator, the patient, and the staff of the facility), as to the level of risk posed by the procedure under study.

Delimitations

This study focused on estimating the radiation-induced cancer risks to both male and female patients of four age categories; 5-year-olds, 10-year-olds, 15-year-olds and adults from six different dental panoramic equipment situated in six different dental diagnostic facilities in Ghana. The dose area products of the patients were measured with the dose area product meter as part of the procedures to establish the risks of radiation-induced cancer risks. The dose area product measurements, in addition to the patients' examination protocols, i.e., kVp, mA and time, were used to compute the absorbed and effective doses which in effect were employed to calculate the patients' risk of exposure-induced cancer mortality.

Limitations

One of the study's drawbacks was the patients' wide age and body size variation. Four typical age groups were selected to address this issue. The standard age groups representations were the 5-, 10-, and 15-year-old, and adult patients. The age categories that were defined were chosen on the premise of the benefit of matching the phantoms that are commonly used in other researches

(Aps, 2013; Carestream Health, 2007; Chen et al., 2011) as well as Monte Carlo simulation programmes (Eckerman et al., 1996).

This is so because majority of the findings from the other studies only applied to adults. Additionally, some of them did not specifically state the kind of panoramic dental X-ray equipment (whether conventional, computed radiography or direct digital radiography). When they used ambiguous terms like "dental radiography" in a number of instances, it was unclear which types of radiographies were surveyed. This study compared the studies that have defined the sort of dental examination in order to address this issue.

Organisation of the Study

This study is broken up into five major chapters.

The introduction covers the background to the study, statement of the problem, purpose of the study, objectives of the study, significance of the study, delimitations, limitations of the study and organisation of the study.

The second chapter examines relevant literature works in detail. The major areas concentrated on are radiation dosimetry, X-ray interactions in diagnostic X-rays (i.e., photoelectric effect, Compton scattering and coherent scattering). Other areas covered include radiation dose and measurements, radiation dose and risk in dental radiology, equipment factors that influence radiation doses to patients in dental radiology, the choice of image receptors in dental radiology and Monte Carlo applications in dental radiology.

Chapter three describes the methodology employed in conducting the study. The main areas covered are the details and technical parameters of the equipment studied, performance testing measurements on the equipment considered for this study, information and data on patients studied, measurements

of the dose area products, computations of the organ and effective doses using the PCXMC, computation of the cancer risk using the PCXMC, and the statistical tools deployed in analysing the results.

Chapter four is about the results and analysis of the performance testing conducted on all the six equipment as against the criteria used in including them in the study, dose area product measurements, organ absorbed, and effective doses depending on ages of patients and the overall REID and organ specific REID values based on ages and gender of the patients.

Chapter five offers overview of the study, summary, conclusions and recommendations.



CHAPTER TWO

LITERATURE REVIEW

Introduction

This chapter focuses on radiation dosimetry, X-ray interactions with matter, measurement of radiation doses, doses of radiation and its related risk in dental radiology, equipment factors that influence radiation doses in patients during dental radiology, choice of image receptors in dental radiology and the Monte Carlo application in dental radiology.

Radiation Dosimetry

Radiation doses originate from energy that is locally deposited due to interactions between the photons of the X-ray and the atom's medium.

X-Ray Interactions

The energy of X-ray which is defined by its composition of energetic photons and is a type of electromagnetic radiation, is determined using equation (1):

$$E = h\nu \quad (1)$$

where ν is the electromagnetic wave's frequency, and h is Planck's constant with a value of 6.63×10^{-34} J.s.

When X-rays interact with matter, their photons' energy is transferred to electrons in the matter. X-rays are classified as indirectly ionizing radiation because the energetic electrons interact with different electrons in close by atoms, forfeit energy, and create ionizations. At the diagnostic X-ray energy level, there are three major kinds of reactions: photoelectric effect, Compton scattering, and coherent scattering (Beutel et al., 2014; Huda, 2016; Sharma,

2021) as shown in Figure 5.

Photoelectric Effect

In 1905, Albert Einstein discovered the photoelectric effect (Beutel et al., 2014). It happens when an electron in an inner shell of a medium interacts with a photon incident on the medium. (Figure 5B). The electron in the inner shell that is expelled from the atom completely absorbs the incident photon, absorbing all of its energy in the process. If E_0 is the incident X-ray energy and E_B is the binding energy of the electron in the inner shell, the ejected photoelectron's kinetic energy will be expressed in equation (2) as:

$$E_k = E_0 - E_B \quad (2)$$

The excess energy is then released as characteristics X-rays, which the electrons in the outer shell use to occupy the vacancies created. Photoelectric effect happens in diagnostic imaging only when the atomic number (Z) of the medium is high and the incoming photon energy is just above the K edge.

Compton Scattering

Compton scattering occurs between the incident X-ray photons and the outer-shell electrons (Figure 5C). It typically occurs when the incident X-ray photon energy (E_0) exceeds the outer shell electron's binding energy by a considerable amount. The results of the Compton interaction are an outer shell electron loss in a positive atomic ion and a scattered photon with energy (E') less than the initial photon energy. The relationship between the energies and the scattering angle θ is described by the Klein-Nishina equation expressed in equation (3) as:

$$\frac{E'}{E_0} = \frac{1}{1 + \alpha (1 - \cos \theta)} \quad (3)$$

Where

$$\alpha = \frac{E_o}{m_o c^2} = \frac{E_o}{511keV} \quad (4)$$

Equations (3) and (4) show that as the scattering angle increases, the scattered X-ray photon energy reduces. In diagnostic radiology, Compton scattering is the primary source of scattered radiation.

Coherent Scattering

An X-ray with minimal energy is scattered from an atom in a process known as coherent scattering, also known as Rayleigh scattering (Figure 5A), with no energy loss. The X-ray has no effect on the substance. The scattered X-ray course in relation to the incident X-ray has a negative effect on medical imaging. Mostly, coherent scattering occurs when low energy X-rays are incident on high atomic number (Z) materials.

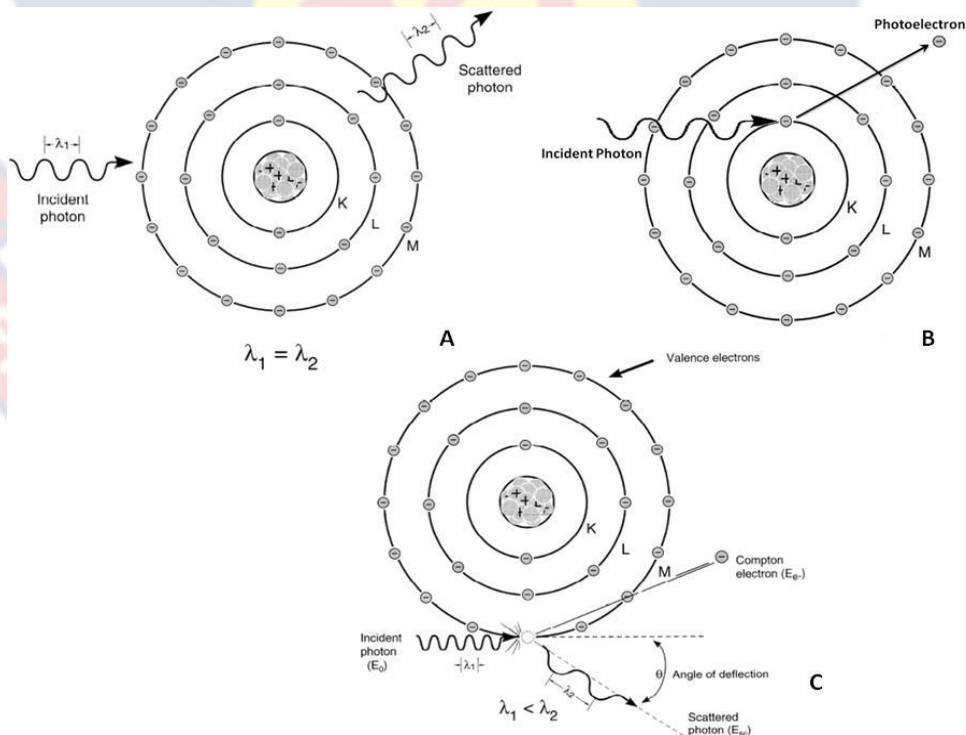


Figure 5: (A) Coherent Scatter; (B) Photoelectric effect; (C) Compton scatter

(Huda, 2016)

Radiation Dosimetry and Measurement

Incident Radiation

Exposure

A measure of an X-ray source's performance is termed exposure (Beutel et al., 2014). It has the SI measure of C/kg and is mathematically defined in equation (5) as:

$$Exposure = \frac{Q}{M} \quad (5)$$

Q is the quantity of charge on the ions and M is the unit mass of air.

Roentgens was the unit of exposure.

Medical radiation dosimetry measures exposure by simply placing an ion chamber in an X-ray beam. Air kerma is increasingly taking the place of exposure because using exposure with the SI system to measure X-ray beam intensities is cumbersome (Huda, 2015).

Air Kerma

It is the quantity of energy transferred from X-ray photons to electrons per unit mass of air. The unit is Gray (Gy). 1 Gy equals 1 J/kg. While the focal point and filtration distance have a negative function with the intensity of the X-ray beam, the mAs and kV have a positive correlation. Figure 6 shows the connection between the intensity of a typical X-ray beam at 100 centimeters from the focal point, the tube voltage and beam filtration.

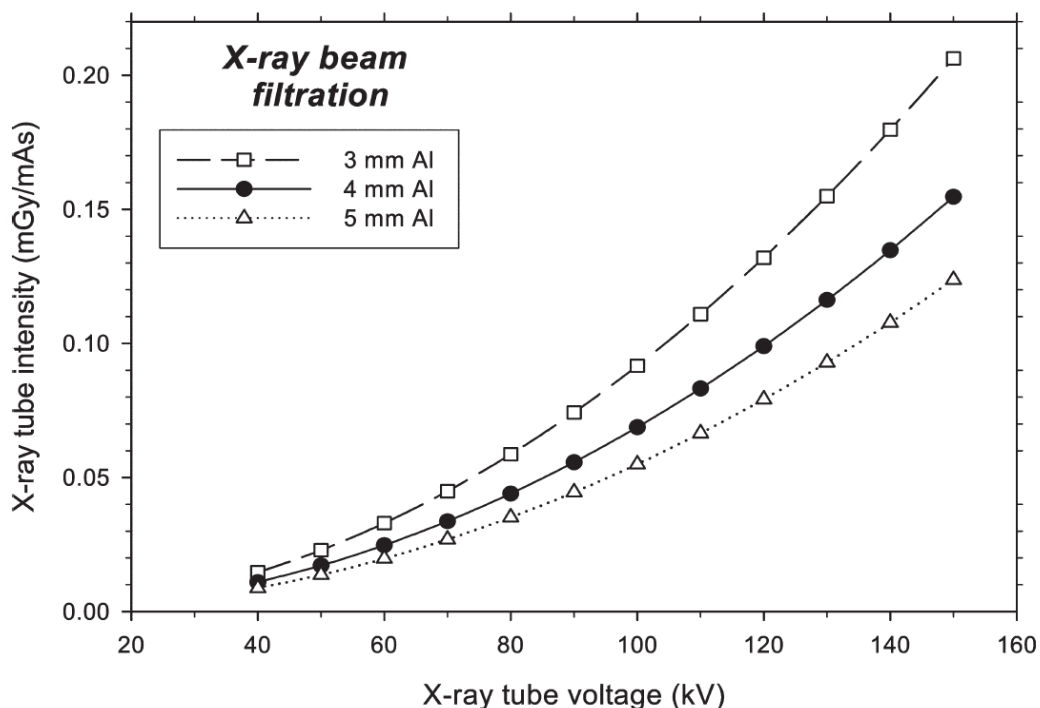


Figure 6: Air Kerma of an X-ray Tube (Huda, 2015)

Kerma Area Product (KAP)

It is used to calculate the amount of radiation incident on a patient. It is calculated by multiplying the intensity of the X-ray beam by the corresponding cross-sectional area value of the beam without taking backscattering radiation into consideration. When a patient is exposed to the same amount of radiation, the patient's physical traits have an impact on the energy absorption pattern.

Absorbed Radiation

Absorbed Dose

Regarding a particular X-ray beam strength, the physical properties of the substance affects the absorbed dose, measured in Gy or J/kg. Materials with higher atomic number (Z) capture more radiation energy than those with lower atomic number. For a medium with mass M , receiving energy E_n , the absorbed dose is given as:

$$D_{medium} = \frac{E_n}{M} \quad (6)$$

Doses to the skin and other organs in medical radiology are the most significant absorbed dose quantities. A diagnostic radiologic exam's skin dosage is about 50% greater than incident air kerma's value (Huda, 2015). Doses to other organs are less than equivalent doses to the skin and are affected by the beam's quality and the area being exposed.

Equivalent Dose

Various radiation types can have varying relative biological effectiveness, which gives an indication of the biological harm. Examples of these radiation types include X-rays, gamma rays, and others (Beutel et al., 2014). The equivalent dose H (unit: Sv) is to account for the relative biological effectiveness (RBE). It is described as

$$H = D \cdot W_r \quad (7)$$

where D represents the tissue's absorbed dose and the radiation weighting component is W_r (For X-rays utilized in diagnostic radiography, $W_r = 1$).

Effective Dose

It is used to normalize the dose by considering the dose provided to the exposed body portion with that of exposure of the whole body (Beutel et al., 2014), and thereby enable risk assessment. It is calculated using equation (8)

expressed as:

$$E = \sum_i W_i H_i \quad (8)$$

Where H_i is the equivalent dose to organ i , and w_i is the tissue weighting factor,

which represents the proportional radiosensitivity of the specific organ. This is presented in Table 1.

Table 1: ICRP 103 Tissue Weighting Factors

Tissue	W_i
Breast, colon, lung, stomach, remainder tissues, red bone-marrow	0.12
Gonads	0.08
Liver, thyroid, stomach, esophagus	0.04
skin, salivary glands, brain, bone surface	0.01

(Source: ICRP, 2007)

The summation in Equation (8) includes all of the tissues and organs that were exposed to radiation for a particular test.

Radiation Dose and Risk in Dental Radiology

Radiation Damage

Patients undergoing X-ray examination have their bodies exposed to millions of photons. Despite the fact that ionization can damage any molecule, chromosomal DNA damage cannot be underestimated. While most DNA damage is rapidly repaired, the structure of a chromosome is rarely irreversibly altered. This could eventually result in the development of tumour. It could take a long time between being exposed and realising that a tumor has been diagnosed clinically. Knowing the doses received by radiological techniques is crucial because with that, it is possible to predict the likelihood that a particular X-ray dose will cause the growth of a tumor. Despite the low doses and risks associated with dental radiology, several epidemiological studies have demonstrated an elevated chance of brain (Hwang et al., 2018; Longstreth et al., 2004), salivary gland (Horn-Ross et al., 1997; Preston-Martin & White,

1990) and thyroid (Hwang et al., 2018; Memon et al., 2019) dental imaging tumors.

As the risk is directly related to the dose, the aforementioned effects can be classified as "chance" (stochastic) effects. They are thought to have no radiation dose level below which they will not happen (Hallquist et al., 1994). The development of cataracts, erythema of the epidermis, and effects on reproduction are some of the other harmful effects of radiation. Undoubtedly, there is a threshold dose below which they do not appear. Although the amount of these threshold doses vary, they are all significantly higher than those used in dental radiography. Therefore, these deterministic impacts are not further considered, save in exceptional cases.

The Risks

The total harm a person exposed to radiation will likely suffer is known as radiation detriment. Hereditary factors, non-fatal cancer, and the lifetime risk of getting cancer are all examples of stochastic effects. The breakdown of the summed number into its component parts is provided in Table 2 (adapted from (ICRP, 1991)). Dental radiography is thought to have negligible hereditary impacts (White, 2014).

Table 2: Stochastic Impacts (nominal lifetime probability)

Detriment (10^{-2} Sv^{-1})	
Fatal cancer	5.0
Non-Fatal Cancer*	1.0
Severe hereditary effect	1.3
Total	7.3

* It is not representative of true incidence, which would be much higher.

(Source: ICRP, 1991)

One's risk is a function of age, being higher in younger people and least in older people as shown in Table 3.

Table 3: The Age-Risk Relationship

Age Groups (years)	Multiplication factor for risk
< 10	x 3
10-20	x 2
20-30	x 1.5
30-50	x 0.5
50-80	x 0.3
80+	Negligible

(Source: ICRP, 1991)

For the two sexes, it adopts the multiplicative risk projection model. In actuality, women always face a greater relative risk than men.

Beyond the age of 80, the risk is minimal because a patient's life expectancy will likely be exceeded by the latent time between exposure and a tumor's symptomatic manifestation. Younger people's tissues, on the other hand, are more radiosensitive, and are more likely to live longer than the latent phase.

Some of the doses and related risks from dental radiographies are shown in Table 4.

There is a particular problem when the salivary glands are included or excluded in the dose calculation. The International Commission on Radiation Protection's (ICRP, 1991) description of effective dose calculations does not explicitly include the salivary glands as an organ, which results in an underestimation of risk. However, several investigators resorted to special weighting factor to include salivary gland doses in dose calculations that would normally be disregarded, but for the clear association between dental radiography and a greater risk of salivary gland tumors. The risks and effective doses of this method are higher.

Table 4: Effective Doses and Risks from Stochastic Effect

X-ray procedure	Effective Dose (μSv)	Risk of fatal cancer (per million)	References
Intra-oral radiograph (bitewing/periapical)	1-8.3	0.02-0.6	(Avendanio et al., 1996; Cederberg et al., 1997; Dula et al., 2001; Gijbels et al., 2002; Hall, 2002; Pasler, 2021; Velders et al., 1991)
Anterior maxillary occlusal	8	0.4	(Velders et al., 1991)
Panoramic	3.85-30	0.21-1.9	(Danforth & Clark, 2000; Dula et al., 2001; Frederiksen et al., 1994; Gori et al., 2000; Hall, 2002; Lecomber A. R. & Faulkner K, 1998; Lecomber et al., 2000; Pasler, 2021)
Lateral cephalometric radiograph	2-3	0.34	(Gijbels et al., 2001; Gori et al., 2000; Maillie & Gilda, 1993; Pasler, 2021; Visser et al., 2001)

Cross-sectional tomography (single slice)	1-189	1-14	(Dula et al., 1997, 2001; Frederiksen et al., 1994; Scaf et al., 1997)
CT (mandible)	364-1202	18.2-88	(Dula et al., 2001; Frederiksen et al., 1995; Scaf et al., 1997)
CT (maxilla)	100-3324	8-242	(Dula et al., 2001; Frederiksen et al., 1995; Scaf et al., 1997)

(Source: Horner et al., 2015)

The White paper (Gori et al., 2000) marked a recalculation of publications that were mostly published before ICRP 60. Only works published after 1990 are explicitly cited, along with White. For intraoral and panoramic radiography, it has been expected that films that fall within the E-speed category and intensifying screens that are within the rare-earth group will be used, respectively.

According to the aforementioned data, dental radiographies have low doses and risks. In spite of the low doses from dental procedures, a lot of radiographs are taken in the European Union each year (Table 5).

Table 5: Estimate of the Total Number of Images from Dental Examinations Performed Annually in European Countries

European Country	Images per annum x 10 ³ (one image means one exposure)	Images per annum per 1000 populations*
Denmark	2,400	449
Germany	22520	274
Spain	5,515	138
Luxembourg	191	433
Netherlands	2,700	169
Portugal	986	96
Finland	1,484	286
Sweden	15,000	1,660
United Kingdom	12,500	209

(Source: UNSCEAR, 2001)

Dental Radiography Equipment Variables Affecting Radiation Doses to Patients

Generation of X-Rays and Kilovoltage

The X-ray beam's mean and maximal X-ray energies are governed by the voltage which is the difference in potential across the X-ray tube when it is in operation. Patients receive greater skin doses due to low voltages resulting in lower X-ray energy (Horner et al., 2015). They also need lengthier exposure times than an X-ray set with a higher voltage would need with the same current. These necessitated lower voltage limits—typically in the 50–60 kV range—being set in legislation from various nations. Lower skin dose is produced by greater voltages, whereas higher deep dose is produced by more X-ray scattering (Hayakawa et al., 1993).

Examining the image quality at different voltages and the film's spectral sensitivity is important for dental (intra-oral) radiography. Increases in voltage that go much beyond 70 kV would produce a spectrum that is not ideal for dental film sensitivity (Horner et al., 2015). Images with "low" voltages have higher contrast than those with higher kilovoltages. This represents the various ways that low and high energy radiation are attenuated.

For intraoral radiography, a voltage of roughly 60–70 kV is regarded as an acceptable compromise in relation to dose limitation options and general efficacy of the diagnosis (Horner et al., 2015).

In contrast to intraoral radiography, the primary exposure management method for panoramic radiography uses voltage. As a result, the majority of panoramic X-ray devices provide the operator with a variety of voltages. The main factors influencing the choice of voltage are the essence to regulate the X-ray intensity and the film/screen combination's energy sensitivity.

For both dental (intraoral) and panoramic/cephalometric devices, X-ray generation from direct current (constant potential) is a contemporary substitute for conventional pulsating kilovoltage. These X-ray generation techniques generate proportionally fewer low energy X-rays (Horner et al., 2015; McDavid et al., 1982; Stenström et al., 1987) and as a result, patients receive lower cutaneous doses. The average X-ray energy from X-ray set with constant potential (DC) is higher than X-ray set with alternating potential (AC) at equal operating voltage (Helmrot et al., 1994).

Filtration

Filtration removes X-ray photons with lower selectively from the X-ray beam. As a result, it is essential if patients' skin doses are to be reduced. Aluminum filtering is a well-known feature of dentistry X-ray equipment. Since this filtration is installed during manufacturing, the dentist has little direct influence over it.

Numerous scholars have looked into added filters using materials other than aluminium as a way to lower the dose in intraoral dental radiography (Horner et al., 2015; Kapa et al., 1990; Macdonald-Jankowski & Lawinski, 1992; MacDonald-Jankowski & Lawinski, 1991; Mauriello et al., 1996; Tetradis et al., 1995; Wakoh et al., 1995; White & Gratt, 1991). They are used primarily because they "shape" the X-ray spectrum to better fit the spectral sensitivity of dental film. The data suggests that all provide dose reductions (Horner et al., 2015; Kapa et al., 1990; Macdonald-Jankowski & Lawinski, 1992; MacDonald-Jankowski & Lawinski, 1991; Mauriello et al., 1996; Tetradis et al., 1995; White & Gratt, 1991) however, this must be weighed against the cost (White & Gratt, 1991), alterations to image quality (Tetradis et al., 1995) and the possible rise in times of exposure connected with their usage. Additionally, dose reduction for panoramic radiography has been proven (Kapa & Tyndall, 1989).

Collimation

A clear method of reducing the dose to patients is to limit the beam to the specific region to be imaged. By reducing the beam area on the skin's surface, less of the patient is exposed to radiation. The field size and the X-ray source's proximity to the skin both have an impact on dose restrictions. Raising this distance decreases the divergence of the beam within the patient, which

diminishes the volume irradiated.

Collimation in Panoramic Radiography

The initial purpose of panoramic radiography was to examine the mandible and teeth. However, the radiographed area is much larger than the area of interest for diagnosis. Dentistry lacked the means to lessen the area to be exposed. To reduce patient dose, however, a number of devices now provide programmed field-size trimming. When specific diagnostic data is needed, field limitation can greatly reduce patient exposure. Beam limitation should be automatically selected on new equipment, though manual selection is permissible (NRPB, 2001). The beam's height at the secondary collimator must be kept to a minimum and should in no instance be greater than that which is required to expose the target region (should ordinarily be 120 or 150 mm). Typically, the width of the beam should not exceed 5 mm.

A "child-imaging setting" on some modern panoramic machines minimizes the region of interest to be exposed by 27 to 45% (Horner et al., 2015). Others provide more advanced programmes that permit radiographing particular areas and joints around the neck and head regions. In a research, Lecomber and Faulkner (Lecomber & Faulkner, 1993) found that the effective dose could be decreased by more than 50% by using an Orthophos X-ray unit's field size program that is limited to the jaws' tooth-bearing areas. Such facilities provide an easy method of dose reduction, so the acquisition of machines equipped with them ought to be promoted.

Choice of Image Receptor in Dental Radiography

Intra-Oral Radiography

Film of group D was the fastest intraoral film commercially accessible up until 1980. E-speed films, which can reduce the quantity of radiation by about 50%, became available in 1981, but somehow had a decreased inherent contrast (Thunthy & Weinberg, 1995). This was likely the primary factor why few dentists used this style of film (Bohay et al., 1994; Button et al., 1999; Hintze, 1993; Platin et al., 1998; Svenson & Petersson, 2009; Syriopoulos K et al., 1998).

Following improvements technology, several film manufacturers have created enhanced E-speed and group F films that comply with ISO speeds (White & Yoon, 2000). Comparing a well-known brand of F-speed film to the same manufacturer's E-speed film has shown to decrease doses by 20–25% (Geist & Brand, 2001; Ludlow et al., 2001; Syriopoulos et al., 2001).

Fast films that are known to be consistent with achieving acceptable diagnostic results for intra-oral radiography should be used. Use of E or F film is advised since they greatly minimise doses when compared to films with group D-speed. Due to its slower speeds and image quality limitations, instant process film should only be used in urgent situations, like endodontics or pre-extraction cases during after-hours treatment (Czajka et al., 1996).

Extra-Oral Radiography

It is recommended to use a combination of fast film-intensifying screen that matches with the diagnostic results for extraoral radiographies. The combination of the film and screen cannot be less than 400. Intensifying screens

made from rare-earth and films have been shown to result in dose reductions of about 50% for cephalometric and panoramic radiography (Horner et al., 2015). Manufacturers generally recommend the pairings of rare-earth screens and orthochromatic film because they have a better ability to convert the radiation to light as compared to the others (Wakoh et al., 2001).

Numerous investigations have been conducted to assess the sensitometry characteristics of these film-screen combinations (Thunthy & Weinberg, 1997; Wakoh et al., 2001). Higher contrast films do not perform well for panoramic radiography as compared to wide latitude films.

Digital Receptors in Panoramic Radiography

The goal of digital radiography is to produce images with excellent quality for diagnosis that are at the very least at par with traditional radiographic film. Furthermore, no equipment or processing chemicals are required because the images are presented instantly on the computer screen.

Through optical lenses or fiber optic connection, the light is delivered to the CCD. The observed light pattern is transformed into an electronic signal to produce an image on a computer.

The second type of digital system employs photostimulable phosphor (PSP) image plates, or photostimulable storage phosphors. The plates are made of a polyester substrate covered in a crystallized halide made of compounds called barium fluorohalides that have been activated by europium. When the plate is subjected to radiation, the absorbed energy of the X-ray is stored as a hidden image within the phosphor crystals. The energy stored is released as visible light, in a scanner, which is transformed to an electrical signal and then

digitalized. The final image is displayed on the computer. Storage phosphor systems are cordless in comparison to CCD systems.

Both digital systems kind have benefits and drawbacks. When 'instant' radiographs are desired, CCD systems may be more helpful because image acquisition is quicker than with PSP systems. PSP devices, in comparison, use a larger image plate and are wireless. The lower radiation dose is one of digital radiography's most significant benefits.

In CCD devices, a long, vertical CCD replaces the conventional film. Cephalometric radiography employs the same sensor, with the patient's head positioned between cephalostat's CCD mount and the tube. Scans of the patient's head are performed using X-ray beam that is flat and fan-shaped. The patient must remain still throughout the approximately 15-second scanning procedure. According to some studies, if density and contrast can be modified using software features, an image of enhanced features could be obtained for easy diagnosis (Dula et al., 1998; Gijbels et al., 2001; Hagemann et al., 2000; Lim & Foong, 1997; Visser et al., 2001). Digital radiography has the advantage of allowing for post-image optimization of an image's density and sharpness.

Background of Monte Carlo Applications in Dental Radiology

The mean absorbed doses (or equivalent doses) are currently used to determine the stochastic harm caused by ionizing radiation to humans (ICRP, 2007). For various reasons, referencing effective dose allows an individual to evaluate and report the harm more clearly. However, using effective dose in explaining patient radiation exposure has occasionally been called into question, and has been proposed that appropriate risk values be used rather (ICRP, 2007).

Consequently, PCXMC 2.0 has been designed to assess the risk of cancer caused by the exposure. The risk evaluation is carried out in accordance with the BEIR VII Committee's model (Council, 2005).

During X-ray examinations, the effective and organ doses cannot be determined directly in patients. Again, acquiring them through experimental observations using physical phantoms is difficult and time-consuming. They can however be computed to an acceptable degree of approximation if enough information on the X-ray examination technique is provided. Nowadays, these calculations are typically performed using the Monte Carlo technique, which uses random numbers to simulate complex medium's radiation movement—in this instance, the human body (Jones & Wall, 1985; Zankl et al., 1994).

STUK (Finland's Radiation and Nuclear Safety Authority) used the Monte Carlo code PCXMC 20Rotation, a supplemental program of PCXMC 2.0 (Tapiovaara & Siiskonen, 2008), to simulate and compute the absorbed and effective doses of each type of examination conducted. The doses of 29 organs and tissues computed are presented in Table 6.

Table 6: Organs and Tissues with their Weighting Factors

Tissue or Organ	Weighting Factor in ICRP Publication 60	Weighting Factor in ICRP Publication 103
Gonads	0.20	0.08
Red bone marrow	0.12	0.12
Colon	0.12	0.12
Lung	0.12	0.12
Stomach	0.12	0.12
Bladder	0.05	0.04
Liver	0.05	0.04
Esophagus	0.05	0.04
Thyroid	0.05	0.04
Breast	0.05	0.12
Bone surface	0.01	0.01
Skin	0.01	0.01
Brain	Remainder organ	0.01
Salivary glands	None	0.01
Remainder organs	0.05	0.12
Adrenal glands	0.005	0.0086
Kidneys	0.005	0.0086
Muscle	0.005	0.0086
Pancreas	0.005	0.0086
Small intestine	0.005	0.0086
Spleen	0.005	0.0086
Thymus	0.005	0.0086
Uterus and cervix	0.005	0.0086
Brain	0.005	See above
Upper large intestine	0.005	None
Extrathoracic region	None	0.0086
Gallbladder	None	0.0086
Heart	None	0.0086
Lymphatic nodes	None	0.0086
Oral mucosa	None	0.0086
Prostate	None	0.0086
Total	1.00	1.00

(Source: ICRP, 2007)

The Personal Computer Programme for X-ray Monte Carlo Code (PCXMC) enables the calculation of patient's organ doses of different ages and sizes under examination conditions used in projection radiography, fluoroscopy and X-ray projections that are freely adjustable. The software has undergone numerous improvements since 1997. Cristy's mathematical phantom model was minimally modified in PCXMC versions 1.0-1.5 (Cristy M, 1980). The latest version of the phantom (PCXMC 2.0) has been revised to the Cristy and

Eckerman models (Cristy & Eckerman, 1987), having minor additional modifications (head modifications, Cristy and Eckerman data corrections in relation to some apparent errors and addition of prostate and salivary glands, extrathoracic airways and oral mucosa which are all new organs). The effective dose can now be evaluated based on the weighting factors in ICRP 103 due to these phantom modifications (ICRP, 2007). Now, the software can evaluate radiation risks based on a person's age and sex.

Radiation Dose Quantities in PCXMC

The PCXMC calculates organ doses as a function of incident air kerma ($K_{a,i}$), at the point where the X-ray beam's central axis penetrates the patient. The user must provide exposure-area product and air kerma-area product, among other parameters. The focal spot-to-skin distance (FSD), total filtration, kV, mAs, and measured radiation output data can all be used in calculating this datum. It can also be discovered by measuring air kerma of the entrance surface or the dose area product of real patient examinations. One can use PCXMC's capacity to reasonably predict $K_{a,i}$ from the current-time product (mAs). Other parameters needed must nonetheless be captured if real radiation measurements are not available.

If the entrance dose of the subject was measured in relation to tissue dose rather than air kerma, the measured datum must be changed to air kerma before being used. The change of dose to the tissue, D_{tissue} , to the air kerma K_a is entirely dependent on the make-up of the tissue and the radiation energy spectrum. It is possible to use the roughly equivalent equation $K_a = 0.94 \cdot D_{soft\ tissue}$ for the energies of diagnostic radiology. Tissue's kerma and tissue's absorbed dose can be thought of as being equivalent in range of energy of photon examined in

PCXMC (photon energies below 150 keV), with the exception of bone-soft tissue interfaces (Tapiovaara & Siiskonen, 2008).

Calculation of Incident Air Kerma

When the only known information is the current-time product of the tube (mAs), the PCXMC calculates the incident kerma using the examination factors listed. The entry data for the test must include the voltage (kV) of the X-ray tube, overall filtration, and FSD. If the user has stated that the FSD is infinite, then this option cannot be used (actually: 100 m).

It is crucial to remember that X-ray tube output varies between units in practice. Variation in X-ray tubes is caused by no less than one of the following factors:

- the discrepancy between the kV, mAs, and filtration values as displayed and as actually measured
- differences between off-focal radiation and how collimation removes it
- true filter components in the path of the beam
- X-ray tube anode surface smoothness
- An X-ray tube's anode angle
- Voltage waveform of an X-ray device (PCXMC takes the form of a maintained (constant) potential or low-ripple generator) (Tapiovaara & Siiskonen, 2008).

It should be noted that the PCXMC's computation of the tube's output is dependent on measurements of diagnostic X-ray tube output. The fundamental information was gathered using X-ray tubes and/or filter options from 46 different devices.

Mathematical Phantoms

There are a variety of phantom models for the human body that can be used in Monte Carlo computations. They consist of computational models with mathematically defined bodily contours and organs. PCXMC version 2.0 employs computer-generated hermaphrodite phantoms of people of various age groups. Cristy and Eckerman (1987) defined these phantoms; however, PCXMC has made a few changes. These phantoms' primary bodily measurements are listed in appendix A and appendix B. Previous versions of PCXMC used phantom models that were slightly different; they were built on Cristy's (Cristy M, 1980) model with minor modifications (Tapiovaara et al., 1997).

Cristy and Eckerman's (1987) phantom models were designed to be employed for the dose measurement of inner sources of photons. Eckerman and Ryman (1993) modified the phantom models' head, neck, and upper spine after they were first published to make them more suitable for computations involving external irradiation. Eckerman and Ryman included the oesophagus (1993). The changes are incorporated, albeit considering minor additional changes:

- The cranium's back was drawn as a cone that was circular instead of a cylinder that was elliptic in shape as in Eckerman, Cristy, and Ryman (1996). The PCXMC head model is similar to the MIRD head model, but not identical (Bouchet et al., 1999).
- In order to accommodate the parotid glands, the facial skeleton's lateral width has been reduced.
- The facial skeleton is situated below where it would be because of a correction made in reaction to an evident inaccuracy in the downward position

- Correction had been made with regard to the thyroid's obvious positional error in Eckerman, Cristy, and Ryman's (1996) data. Eckerman and Ryman's material corresponds to the information utilized in PCXMC for the adult phantom (1993).
- The phantom's salivary glands are modeled (parotid, sublingual and submandibular glands). Based on information from ICRP Publication 89 (ICRP, 2002), the glands' size and position were calculated.
- In the phantoms, the extrathoracic passageways are modelled (pharynx, larynx, part of trachea, paranasal sinuses). Despite being mentioned as one of the tissues of the extrathoracic airways in Publication 89 of ICRP, the mouth was not previously considered a component of the extrathoracic airways (ICRP, 2002). In PCXMC, the mouth mucosa is treated individually.
- The mucosa of the pharynx is modeled in the Phantoms. Between the epidermis and the facial skeleton is a portion of the tissue, and behind the skeleton is another portion.
- The prostate is modeled in the phantom. ICRP Report 89 (ICRP, 2002) served as sources of guidance for the modeling.
- The phantoms' arms can be eliminated to enable for more precise computations for X-ray projections that are lateral in nature.
- The phantoms' height and mass can be adjusted to fit the information about specific patients.
- The phantoms do not include lymph node modelling. Instead, based on the doses in surrogate organs, the dosage in the lymph nodes is calculated using equation (9) expressed as:

$$\begin{aligned}
D_{\text{lumph nodes}} = & 0.25. D_{\text{small intestines}} + 0.15. D_{\text{pancreas}} + \\
& 0.13. D_{\text{extrathoracic airways}} + 0.10. D_{\text{gallbadder}} + \\
& 0.08. D_{\text{salivary glands}} + 0.07. D_{\text{lungs}} + \\
& 0.05. D_{\text{thyroid}} + 0.05. D_{\text{total body}} + \\
& 0.04. D_{\text{oesophagus}} + 0.04. D_{\text{heart}} + \\
& 0.03. D_{\text{stomach}} + 0.01. D_{\text{testes}} +
\end{aligned} \tag{9}$$

The PCXMC allows for the modification of these fundamental phantoms. The user is given the option to alter any of their height or mass to achieve this. The programme uses these primary values of the body size to calculate the scaling factors given in equations (10) and (11) as

$$S_z = \frac{h}{h_0} \tag{10}$$

and

$$S_{xy} = \sqrt{\frac{h_0 \cdot M}{h \cdot M_0}}, \tag{11}$$

where h_0 and M_0 are the unscaled phantom's height and weight, and s_z is the scaling factor in the z-axis orientation (height of phantom), s_{xy} is the scaling factor in the x- and y-axes orientations. The organ masses are then adjusted as necessary by multiplying all phantom measurements by these scaling factors. The coordinates, (x_0, y_0, z_0) , are used to compute the coordinates of the transformed phantom, (x, y, z) by

$$\begin{aligned}
X &= S_{xy} X_0 \\
y &= S_{xy} y_0 \\
Z &= S_z Z_0
\end{aligned} \tag{12}$$

This procedure enables the phantoms' shapes to be altered so that they more closely match the real patient. This method cannot replicate the variability in phantom shapes caused by variations in the amount of fat tissue since every measure in a specific direction (whether horizontal or vertical) must be multiplied by the same scaling factor. The variability in phantom shapes caused by, for example, variations in the amount of fat tissue cannot be simulated by this technique. The origin continues to be in the middle of the base of the trunk, meaning that this change has no impact on the coordinate system used to enter the geometry of the X-ray beam. The location of the organs will vary when replicating the irradiation of the same body (Tapiovaara & Siiskonen, 2008).

The Monte Carlo Technique

The computation of photon transport is premised on simulation (stochastic in nature) of photon-matter interactions.

A point isotropic source emits photons into the solid angle determined by the dimensions of the focal distance and the X-ray field, where they are then tracked when interacting at random with the phantom in accordance with the probability distributions of the various physical processes they could experience, such as photo-electric absorption, coherent (Rayleigh) scattering, or incoherent (Compton) scattering. This series of encounters creates a "photon history" (Tapiovaara & Siiskonen, 2008). Storm and Israel (1970) provided the coherent scattering's cross sections, photo-electric effects, and in-coherent scattering (Storm & Israel, 1970), while Hubbell et al. (1975) provided the functions of the atomic form factors and incoherent scattering (Hubbell et al., 1975). Further interactions are ignored in PCXMC since the maximum potential particle energy is limited to 150 keV. The range of secondary electrons in soft tissue at such

energies is only a small proportion of a millimeter, and is assumed that the energy of the secondary electrons is absorbed at the location where the photon is impacted. The energy deposited to the organ at each interaction point is computed and saved for dose computation. The estimates of the averages of the phantom's energy depositions are employed to determine the dose in the mentioned organs from the many independent random photon histories.

The skeletons of the mathematical phantoms were modeled as a uniform blend of organic and mineral bone, including active bone marrow (Cristy & Eckerman, 1987). Determining the dose to the active bone marrow necessitates taking secondary electrons from the bone matrix into account due to the active bone marrow's location in tiny spaces in bone called trabecular bone, causing the dose to be greater than the kerma (Rosenstein, 1976). The fraction of energy deposited in the active bone marrow of a particular skeletal part, $\Delta E_{ABM, i}$, for an energy deposit ΔE within that portion of skeleton i from an energy E photon, is determined using equation (13)

$$\Delta E_{ABM, i} = \Delta E \cdot \frac{(\mu_{en}(E))_{ABM}}{(\mu_{en} E/\rho)_{bone}} \cdot \frac{m_{ABM, i}}{m_{bone, i}} \cdot f_i(E) \quad (13)$$

where $m_{bone, i}$ and $m_{ABM, i}$ represent the skeletal component's mass i and its active bone marrow's mass, respectively. The mass-energy absorption is $\mu_{en}(E)/\rho$. In PCXMC, all bones and phantom ages are applied with the same factor. The energy deposits in the residual skeleton components is $\Delta E - \Delta E_{ABM, i}$. The active bone marrow dose is calculated by adding up all the energy distributed all over the skeleton and dividing it by the total mass of active bone marrow.

The PCXMC determines the organ doses for monochromatic photons with energies of 10, 20, ..., 150 keV. Linear interpolation could be used with

sufficient precision to calculate the amount of energy per photon absorbed at other photon energies. The mean of these batches is used to compute the overall estimate of absorption at every one calculated energy value, and the standard deviation used to compute the statistical error. The voltage of the X-ray tube, the X-ray tube's angle of tungsten target, and the filter values are all defined in terms of the Birch and Marshall theory (Birch & Marshall, 1979), which is utilized in computing the spectra of the X-ray. The user can specify a couple of filters of any atomic number and thickness concurrently in the current version of the program. The filter datasets are taken from combined X-ray interaction data (McMaster et al., 1970). Using photon fluence measurements based on conversion coefficients, the air kerma is calculated (Büermann et al., 2006).

It is significant to remember that the organ's number of simulated interactions affects how precisely the estimated dose and the statistical error approximation are calculated. When the interactions are low, the estimation has a biased abnormal distribution, which is demonstrated by an elevated number of the statistical error, and the real errors in statistics could be greater than what was anticipated (Tapiovaara et al., 1997).

Risk Assessment

For the purpose of calculating the likelihood of developing cancer as a result of exposure to ionizing radiation, several mathematical models have been created. The BEIR VII (Council, 2005) group developed the incidence of cancer and cancer fatality risk models. In comparison to dose rates that are high and doses that are large, dose rates that are low and doses that are small are currently thought to produce cancer risks that are comparatively low. The risk reduction factor is accounted for by the dose and dose reduction factors (DDREF).

It should be mentioned that age-dependent mortality rates are used to determine the lifetime risk of developing cancer. Leukemia, solid cancers in particular organs, and all cancers that are classified as solid, taken together are all given risk categories.

Limitations in the epidemiologic data for cancer caused by radiation are just one example of the factors that contribute to risk estimation uncertainty.

According to the committee on BEIR VII, the projections of risks must be gauged with a reasonable dose of skepticism, with more emphasis being placed on the risk's magnitude.

The models of the excess relative and absolute risk for solid cancers (ERR and EAR, respectively) at achieved age take the shape expressed in equation (14) (Council, 2005).

$$\text{ERR}(t, e, D) \text{ or } \text{EAR}(t, e, D) = \beta_s D_{\text{exp}} (\gamma e^*) (t/60a)^\eta \quad (14)$$

where e is age at exposure in years, $e^* = (e - 30 \text{ a})/10 \text{ a}$ when $e < 30 \text{ a}$, and e^* is equal to zero for $e \geq 30$ for other solid cancers than breast cancer and thyroid cancer. For these two cancers, $e^* = (e - 30 \text{ a})/10 \text{ a}$ for all values of e . Attained age (in years) is t , and D is the organ or tissue equivalent dose. β_s , γ and η are fitting parameters of the model. For leukaemia the ERR and EAR models are of the form, given in equation (15) as:

$$\text{ERR}(t, e, D) \text{ or } \text{EAR}(t, e, D) = \beta_s D(1+\theta D) \cdot \exp[\gamma e^* + \delta \log((t-e)/25a) + \phi e^* \log((t-e)/25a)] \quad (15)$$

where $t - e$ is the time elapsed after the exposure and D is the equivalent dose in bone marrow. θ , δ and ϕ are fitting parameters. In the BEIR VII model, the site-specific EAR numbers take cancer incidence into account (Council, 2005).

The risk estimates for all organs and tissues is not provided by the Council (2005). The PCXMC employs the BEIR's "other solid cancers" model to compute the cancer mortality risk. It should be emphasized that the associated cancer numbers are those for all solid cancers after the individually regarded solid kinds of cancer have been excluded. When the distribution of dose in one's body is not homogeneous, it is difficult to determine the dose corresponding to those "other solid cancers". Due to its large mass, the dose would primarily correlate to the muscle tissue dose, which would likely be unreasonable if one were to employ the mean dose of all organs involved. A weighted average dosage ("weighted remainder") in the remaining organs and tissues has therefore been utilized in PCXMC. The level of weighting is calculated using the renormalized weighting factors from ICRP Publication 103, where their total is one. This entails the presumption that these organs' relative sensitivity levels are proportional to tissue weighting factors from ICRP 103 (ICRP, 2007).

The risk of cancer cannot be considered zero till after the period of latency. The BEIR VII makes a supposition that solid cancers have a 5-year latency phase. Leukaemia has a 2-year latency phase. These settings are utilized by PCXMC by default.

The estimated lifetime risks are derived from the excess risk numbers. The different quantities can be used by PCXMC to evaluate the lifetime risks. The three quantities are REID, LLE and LLE/REID.

The definitions of the quantities are given in the following equations as:

(Thomas et al., 1992)

$$\text{REID}_c(e, D) = \int_{\tau}^{\infty} [\mu_c(t|e, D) - \mu_c(t)] S(t|e, D) dt \quad (16)$$

and

$$\text{LLE}(e, D) = \int_{\tau}^{\infty} S(t|e)dt - \int_{\tau}^{\infty} S(t|e, D)dt \quad (17)$$

Suppose an individual involved was living at the age of exposure e and that the associated dose at that age was D , the rate of mortality due to the cause of death is given by the expression $\mu_c(t | e, D)$. In the concept of excess relative risk

$$\mu_c(t | e, D) = [1 + \text{ERR}_c(t, e, D)] \mu_c(t), \quad (18)$$

where the mortality rate at the background associated with the death cause c is denoted by $\mu_c(t)$. In the concept of excess absolute risk

$$\mu_c(t | e, D) = \text{EAR}_c(t, e, D) + \mu_c(t) \quad (19)$$

The conditional likelihood that the individual in question is still living at age t , considering a dose D at age e , is known as $S(t | e, D)$. The likelihood of an unexposed individual living to age t is $S(t | e)$. The risk models for $S(t | e, D)$, and mortality statistics as well as cancer mortality rates are used to compute these conditional survival functions. Specifically,

$$S(t|e, D) = \exp \left[- \int_e^t \mu(x|e, D) dx \right], \quad (20)$$

where $\mu(t | e, D)$ represents the mortality rate in its entirety. As a result, the software takes into consideration the decrease in S brought on by radiation exposure, and it also allows for the addition of site-specific REID estimates for various cancers. The total risk associated with the exposure in issue is represented by the sum. The integrals have a lower limit of $\tau=e+\lambda$, where λ is the latency period measured in years. Instead of infinity, PCXMC has set the maximum limit of integration to 120 years in these equations.

Cohort study methods were the source of the REID concept: The mortality rates of the exposed and unexposed groups are compared. If there is no statistically significant variation between the two groups, the null hypothesis is true. The loss of life expectancy refers to the disparity in life expectancy between an exposed person at age e and an unexposed person but was alive at the time. The average amount of time wasted due to an excess cancer death is explained by LLE/REID. In BEIR, these numbers were not taken into account (Council, 2005). When estimating LLE, PCXMC fails to use the DDREF idea; instead, it employs the relative risk model.

The BEIR VII group replace $S(t|e, D)$ by $S(t|e)$ in order to simplify the definition of REID. The lifetime attributable risk (LAR) was the name given to the resulting risk assessment (Council, 2005). Given the inherent uncertainties in the models, their numerical values are sufficiently similar to be read as being the same.

The factor values for dose and dose rate reduction DDREF equals 1.5 for solid cancers and 1 for leukemia have been recommended by the BEIR VII group. These settings are also applied by default in PCXMC. The risk estimates just account for the ionizing radiation's stochastic effect; thus, risk estimates should be carefully scrutinized if deterministic effects are possible.

The rates of mortality of particular sex and incidence of cancer are important input data for the computation. These data are usually given in five-year periods in PCXMC preset data sets. The Finnish mortality data were obtained on March 20, 2007, from the Finnish Cancer Registry (www.cancerregistry.fi), and the data from the incidence of cancer and mortality were obtained from the databank of Finland statistics (www.tilastokeskus.fi). The statistics on incidence

of cancer and mortality in Europe, North America, and Asia are obtained from ICRP publication 103 (ICRP, 2007). It is thought that radiation exposure is linked to chronic lymphocytic leukemia. Consequently, it is not included in the ICRP 103 leukaemia mortality statistics. All types of leukemia are included in the Finnish mortality and incidence statistics, which results in a slightly inflated leukemia risk. The uncertainty in the risk estimate for leukemia is much greater than this overestimation.

Chapter Summary

An interaction between a photon and a medium result in energy deposited in that medium. The three main photon interactions with matter are photoelectric effect, Compton scattering and coherent scattering. Photoelectric effect occurs when a photon impacts all its energy to an inner shell electron, thereby ejecting it in the process. The photon then disappears in the process. The difference between the incident X-ray energy and the binding energy of the electron is emitted as characteristics X-rays. Compton scattering occurs when an incident photon interacts with an outer shell electron. The photon impacts part of its energy to the electron in the process. The photon after the interaction scatters at angle θ and the electron recoils at an angle ϕ . Compton scattering results in scatter radiation to patients and operators of dental radiology facilities. Coherent scattering occurs when a photon with little energy is scattered from an atom with no energy loss. The wavelength of the incident photon is always equal to the wavelength of the scattered photon.

In radiation dosimetry and measurement, the common quantities used in determining doses to patients include exposure, air kerma and kerma area product. Other quantities include absorbed dose, equivalent dose, and effective dose. Once risk is directly related to the radiation dose received. Other risk factors are age at exposure, gender, and site of cancer.

Dental equipment factors directly impact the radiation doses to patients. They include kilovoltage, filtration and collimation. The kilovoltage determines the penetrability of the X-ray beam to produce the required image. The filtration removes low energy X-ray beams in preventing absorbed doses to patients. Collimation confines the X-ray beam to the specific body section to be imaged thereby avoiding exposing unintended tissues and organs.

The PCXMC 20Rotation could be used to evaluate the risk of cancer due to exposure to radiation during panoramic dental radiographies with very minimum uncertainties (0.1 %). The software utilises virtual phantoms of varied ages (1,5,10,15-year-olds, and adults). It allows for the inputs of patient's data and information, X-ray beam geometries and simulation parameters. The risk to patient is estimated based on the absorbed and effective doses.

CHAPTER THREE

METHODOLOGY

Introduction

The study areas, number and types of panoramic dental X-ray equipment studied, quality control test conducted, specific patient data collected, and the simulation software used in the computation of the cancer risks are presented in this section.

Panoramic Dental X-Ray Equipment

A total of six panoramic dental units from different vendors installed at six different dental facilities in Ghana were evaluated in this study. Five of the six were located within Accra and the other one installed in Kumasi. All of the six panoramic units were equipped with a digital system. Five of the digital systems used charge-coupled device (CCD) sensor chip and one was equipped with storage phosphor plates (PSP). The equipment information and the technical specifications are stated in Table 7.

Table 7: Panoramic Equipment Information and Technical Specifications

Type	Manufacturer	Model	Max. kV	Max. mA
DR*	Trident (Italy)	Kh-0.5-105	85	10
DR	Carestream (France)	CS81000SC	82	12
DR	Carestream (France)	OPX105	90	15
DR	Vatech (USA)	PHT-6500	90	10
DR	Gendex (U.S.A)	GX100-20DC	80	8
CR**	Siemens (Germany)	1117340V1010	90	12

DR*: Digital Radiography CR**: Computed Radiography

(Source: Field Data, 2021)

Magic Max Universal Multimeter for Performance Testing

The Magic Max Universal (IBA, 2013) is a piece of equipment used to perform acceptance testing and quality control of X-ray machine. The Magic Max Universal multimeter is a PC-based, USB-powered automatic precision instrument that measures and shows dose, dose rate, and dose per pulse; exposure time; non-invasive practical peak voltage, total filtration, and the first half-value-layer all at the same time. It has an easy-to-use software controls and displays the data. The Magic Max Universal has a compact design of sensors and electronics and is durable due to the solid-state design without motors or moving parts. The Magic Max Universal multimeter contains a unique six channel electrometer ASIC which converts the radiation induced currents in the detectors into electrical values. The data is gathered by a microcontroller and sent to the PC in real time via a high-speed USB interface, allowing for long-term waveform recording at the highest time resolution, comparable to high-performance oscilloscopes. The maximum dose surface product rate of $3000.00 \mu\text{Gym}^2/\text{s}$ should not be exceeded. It functions effectively within the temperature range of $15^\circ\text{C} - 35^\circ\text{C}$, pressure range of $800 \text{ hPa} - 1060 \text{ hPa}$, and a relative humidity less than 80% (without condensation) (IBA, 2013). Figure 7 shows the Magic Max universal tool.



Figure 7a: Magic Max kit



Figure 7b: XR Detector



Figure 7c: Base Unit



Figure 7d: Connection for Measurement

Figure 7: Magic Max Universal Tool

Performance Testing

Prior to measurements for the research study, the performance tests of all the panoramic dental equipment machines were carried out in accordance with international norms (IPEM, 2005; NSW EPA, 2001). The same protocols are used by the Nuclear Regulatory Authority, Ghana. The Magic Max Universal multimeter with the XR detector was used to measure and evaluate seven parameters which are kVp accuracy, kVp reproducibility, timer accuracy, timer

reproducibility, mA linearity, exposure reproducibility and Half Value Layer (HVL). The parameters which were measured for performance tests, and their acceptable criteria are shown in Table 8.

Table 8: Parameters for Performance Test and Acceptable Criteria

Parameter	Criterion
kVp Accuracy	within $\pm 5.00\%$
Timer Accuracy	within $\pm 10.00\%$
kVp Reproducibility	≤ 0.05
Timer Reproducibility	≤ 0.05
Exposure Reproducibility	≤ 0.05
mA Linearity	≤ 0.10
HVL	
For kVp < 70	≥ 1.5 mm Al
For kVp ≥ 70	≥ 2.5 mm Al

(Source: IPEM, 2005; NSW EPA, 2001)

Condition of Measurement for each Performance Parameters

kVp accuracy: The aim was to match the measured kVp to the generator setting.

Three variable kVp stations (60, 65, and 70) were chosen, and exposures at each station were carried out at a set mA, fixed time. The kVp accuracy was calculated using equation (19):

$$kVp \text{ accuracy} = \left(\frac{\text{Input kVp} - \text{Measured kVp}}{\text{Input kVp}} \right) 100\% \quad (21)$$

Timer Accuracy: The aim was to match exposure time with the selected time. At fixed kVp, fixed mA and exposure times of 15 s for the different panoramic units, measurements were taken. The timer accuracy was determined using equation (20):

$$\text{Timer accuracy} = \left(\frac{\text{Input time} - \text{Measured time}}{\text{Input time}} \right) 100\% \quad (22)$$

Time is in seconds.

kVp Reproducibility: The aim was to measure the kVp variation over a range of exposures at constant setting of the generator. At fixed kVps of 60, fixed mAs of 120, three exposures were made. The kVp reproducibility was calculated using equation (21):

$$\text{kVp reproducibility} = \left(\frac{(\max \text{ kVp} - \min \text{ kVp})}{(\max \text{ kVp} + \min \text{ kVp})} / 2 \right) 100\% \quad (23)$$

Timer Reproducibility: The aim was to measure the time variations over a range of exposures at constant settings of the generator. At fixed kVp of 65, fixed mA of 8 and a time of 15 s, three exposures were made. The timer reproducibility was calculated using equation (22):

$$\text{Timer reproducibility} = \left(\frac{(\max \text{ time} - \min \text{ time})}{(\max \text{ time} + \min \text{ time})} / 2 \right) 100\% \quad (24)$$

Exposure Reproducibility: The aim was to measure exposure variations over a range of exposures at constant settings of the generator. At fixed kVp of 60, fixed mA of 8 and a time of 15 s, three exposures were made. The exposure reproducibility was calculated using equation (23):

$$\text{Exposure reproducibility} = \left(\left(\frac{\max \text{ exposure} - \min \text{ exp}}{\max \text{ exp} + \min \text{ exp}} \right) / 2 \right) 100 \% \quad (25)$$

mA Linearity: The aim was to measure the radiation output's linearity over a range of mA settings. At fixed kVps of 50, 60, and 70, variable mA of 6, 7 and 8 respectively, three exposures each at the indicated kVps were made. The mA linearity was calculated using equation (24):

$$\text{mA Linearity} = \left(\left(\frac{\max \frac{\text{Kerma}}{\text{mA}} - \min \frac{\text{Kerma}}{\text{mA}}}{\text{aveg} \frac{\text{Kerma}}{\text{mA}}} \right) / 2 \right) 100 \% \quad (26)$$

Kerma is in mGy.

Half-Value Layer (HVL): The aim was to measure the beam quality by estimating the adequacy of filters. At 70 kVp and 8 mA, three exposures were made and the HVLs of each of the six equipment were recorded.

Patient Data Collection: The patient data collected from the six dental facilities (A, B, C, D, E, all within Accra and E in Kumasi) is shown in Table 9. The four standard age groups of five-, ten-, fifteen-year-olds, and adults (i.e., 30-year-olds) were considered in this study. In all, 406 patients' data were collected for the different age groups. The data were collected following the Institutional Review Board of the University of Cape approval with the identification number of "UCCIRB/CANS/2022/15".

Table 9: Patient Data for the Various Age Groups

		Age Group						Adult	
		5-year-olds		10-year-olds		15-year-olds		(30-year-olds)	
Number of Patients		84		94		104		124	
No. of Males	No. of Females	39	45	44	50	52	52	60	64
Mean Mass (kg) (\pm SD)		18.15 \pm 3.40		31.95 \pm 8.01		54.05 \pm 5.10		70.00 \pm 19.00	
Mean Height (cm) (\pm SD)		108.25 \pm 12.20		137.70 \pm 9.20		164.90 \pm 13.20		170.00 \pm 7.00	

(Source: Field Data, 2021)

Examination Factors and Dose Area Product Measurement

The examination factors which applied to actual patients within the four age categories during the panoramic radiographies were recorded. They were the kVp, time and mA.

The dose area product is calculated by multiplying the average radiation dose in the X-ray stream by the X-ray field area. The dose area product ($\text{mGy}\cdot\text{cm}^2$) is used to calculate the radiation exposure of a diagnostic X-ray unit. A DAP-meter consisting of a sizable area ion chamber (located right at the X-ray tube's exit section) and a portable electrometer (Germany's VacuDAP-0EM) was used to determine the DAP values. Whereas the examination factors relevant to the actual patients were utilized in the various X-ray machines for each dental radiography, the DAP measurements were performed without the patient present. Each measurement setting was performed three times and averaged to minimise errors. Figures 8 and 9 show the DAP meter and how the measurements were performed.



Figure 8: The DAP Meter (Image is from Field Work)



Figure 9: Set-Up for DAP Measurement (Image is from Field Work)

PCXMC Simulations for the various Dental Radiographies

An algorithm known as the Monte Carlo (MC) simulation predicts how X-ray photons will interact with a complicated medium like the human body (Tapiovaara & Siiskonen, 2008). This algorithm can be used in computer

software to determine the organ-absorbed dose and effective dose when the relevant physical and mechanical data are provided.

The software incorporates patient models (both paediatric and adult) with adjustable sizes, as well as a free X-ray examination method selection. The software also calculates the patient's estimated risk of dying from radiation-induced cancer using the BEIR VII committee's sex- and age-dependent risk model (Council, 2005).

The mathematical phantom models developed by Cristy and Eckerman served as the foundation for the anatomy data in the PCXMC (Eckerman et al., 1996). Hermaphrodite phantom models, which are adaptable to mimic the geometry of the patients, are used in this program to depict patients of various ages. The patient's arms were excluded to replicate the actual clinical exercise for patient dose calculation.

In the PCXMC 2.0 Rotation programme, the coordinates of a point within the phantom through which the X-ray beam is directed so that the positive z axis points upward, the x axis is to the left, and the y axis is to the back are designated as "Xref," "Yref," and "Zref". This is shown in Figure 10. The execution of the simulation needed the inputs of the patient's statistics, parameters of the beam, and geometry of irradiation. 180-degree rotation was one of the PCXMC 2.0 Rotation parameters.

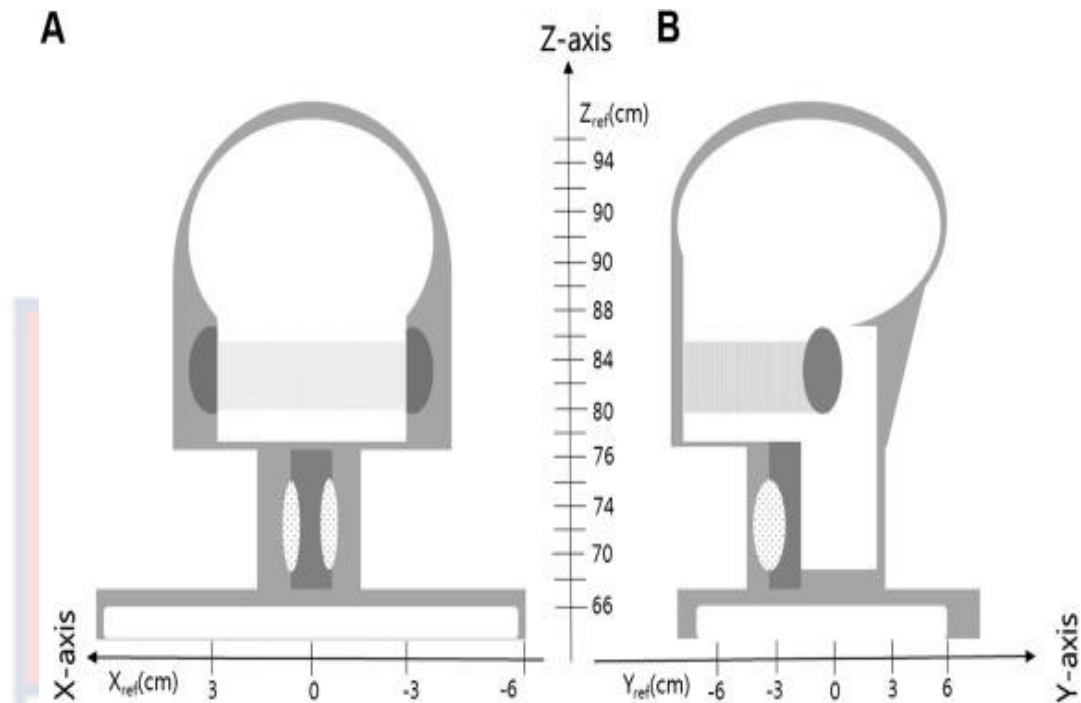


Figure 10: An Illustration of Geometry for the Purpose of Producing Rotational Data and the Consequent Calculations (Yeh & Chen, 2018).

Projections' geometry was impossible to model in its entirety at once.

In order to simulate, the scan was divided into 18 parts, from one ear to the other. The programme defined the radiation field's area, position's coordinates and the radiation beam's angle on the patient, the focus-reference distance, the quantity of photons simulated, and the highest energy for each segment. Therefore, at least 18 simulations and calculations were carried out to gather information about each process. The quantity of histories was specified to two hundred thousand (200, 000) for all simulations to obtain a statistical uncertainty of less than 0.1% in the outcomes. Figure 11 shows the PCXMC 2.0Rotation input interface.

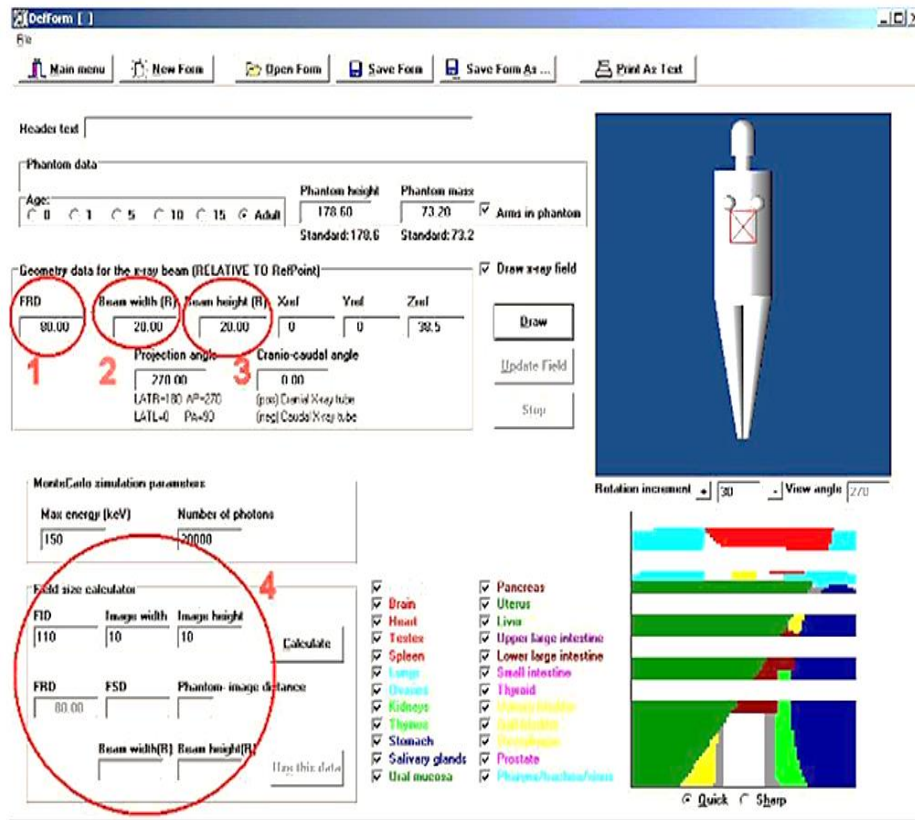


Figure 11: The PCXMC 20Rotation's Interface for Entering X-ray Examination Parameters (Tapiovaara & Siiskonen, 2008).

Computation of Organ and Effective Doses

In order to calculate the absorbed and effective doses, the programme needed accurate input values for the following factors: exposure dose, reference point, X-ray tube voltage, rotation angle, vertical angle of the central ray, focus-to-reference distance (FRD), X-ray beam width/height, and filtration.

The absorbed dose to the medium (D_{medium}) is given in equation (27) as:

$$D_{\text{medium}} = \frac{E_n}{M} \quad (27)$$

Where M is the mass of a medium that absorbs an energy of E_n

The equivalent dose H (unit: Sv) has been incorporated to account for the

relative biological effectiveness. Its definition is given in equation (28) as:

$$H = D \times W_r \quad (28)$$

Where D stands for the tissue's absorbed dose, W_r is radiation weighting factor.

For X-rays used in diagnostic radiography, the radiation weighting factor (W_r) is 1 (ICRP, 2007).

The effective dose is determined using equation (29)

$$E = \sum_i W_i H_i \quad (29)$$

where W_i denotes the weighting factor of the tissue, which represents the relative radio sensitivity of the specific organ, and H_i denotes the equivalent dose to organ i .

Computation of the Cancer Risk

The PCXMC 2.0 Rotation software and the BEIR VII study model were employed to determine the risk of getting cancer from ionizing radiation exposure. The BEIR VII group was tasked with creating the risk models for calculating an exposed person's cancer risk. The variables that affect an individual's risk include their sex, age at which the individual was exposed, and the dose from the radiation source (Council, 2005). The BEIR VII group developed the incidence of cancer and cancer mortality risk models. The lifelong cancer risk is then calculated using age-dependent mortality rates. Absolute and relative risk models for every cancer type was developed by the BEIR VII Committee.

The excess relative and absolute risk models with respect to ERR and

EAR for solid cancers are of the form given in equation (30) (Council, 2005):

$$ERR(t, e, D) \text{ or } EAR(t, e, D) = \beta_s D_{exp}(Ye^*) \left(\frac{t}{60a}\right)^\eta \quad (30)$$

where e is age at exposure in years and t is the attained age.

$e^* = (e - 30 a)/10 a$ when $e < 30 a$, and e^* is equal to zero for $e \geq 30 a$ for other solid cancers than breast cancer and thyroid cancer.

For these two cancers, $e^* = (e - 30 a)/10 a$ for all values of e .

t is the attained age (in years)

Organ or tissue equivalent dose is D .

The model's fitting parameters are β_s , γ and η

The ERR and EAR models for leukemia take the following form expressed in equation (31).

$$ERR(t, e, D) \text{ or } EAR(t, e, D) = \beta_s D (1 + \theta D) \cdot \exp [Ye^* + \delta \log \left(\frac{t-e}{25a}\right) + \phi e^* \log \left(\frac{t-e}{25a}\right)] \quad (31)$$

where $t - e$ is the time elapsed after the exposure

D denotes the equivalent dose in bone marrow

θ , δ and ϕ are fitting parameters

The additional risk of cancer from radiation, according to the absolute risk model, is independent to the cancer risk from the background. Excess risk values are used to calculate lifetime risk estimates. The lifetime risks in the PCXMC 2.0 Rotation programme are expressed as a function of the chance of

exposure-induced death (REID). It is evaluated using information on the patient's age, gender, and mortality rates (Euro-American). The programme demanded the patient's country of origin in order to perform the risk assessment. Thus, it was assumed that European-American statistics were similar to African statistic (Mantebea, 2015).

Most people believe that radiation exposure causes cancer in a stochastic manner, which is in line with the BEIR VII risk model. There is no threshold because the danger grows with dose in a linear-quadratic manner. The BEIR VII risk strategy influences the REID value. The risk models for leukemia, colon cancer, liver cancer, lung cancer, stomach cancer, breast cancer, and other cancers were examined in this research. The REID values of each cancer, with the exception of breast cancer, were given for both genders.

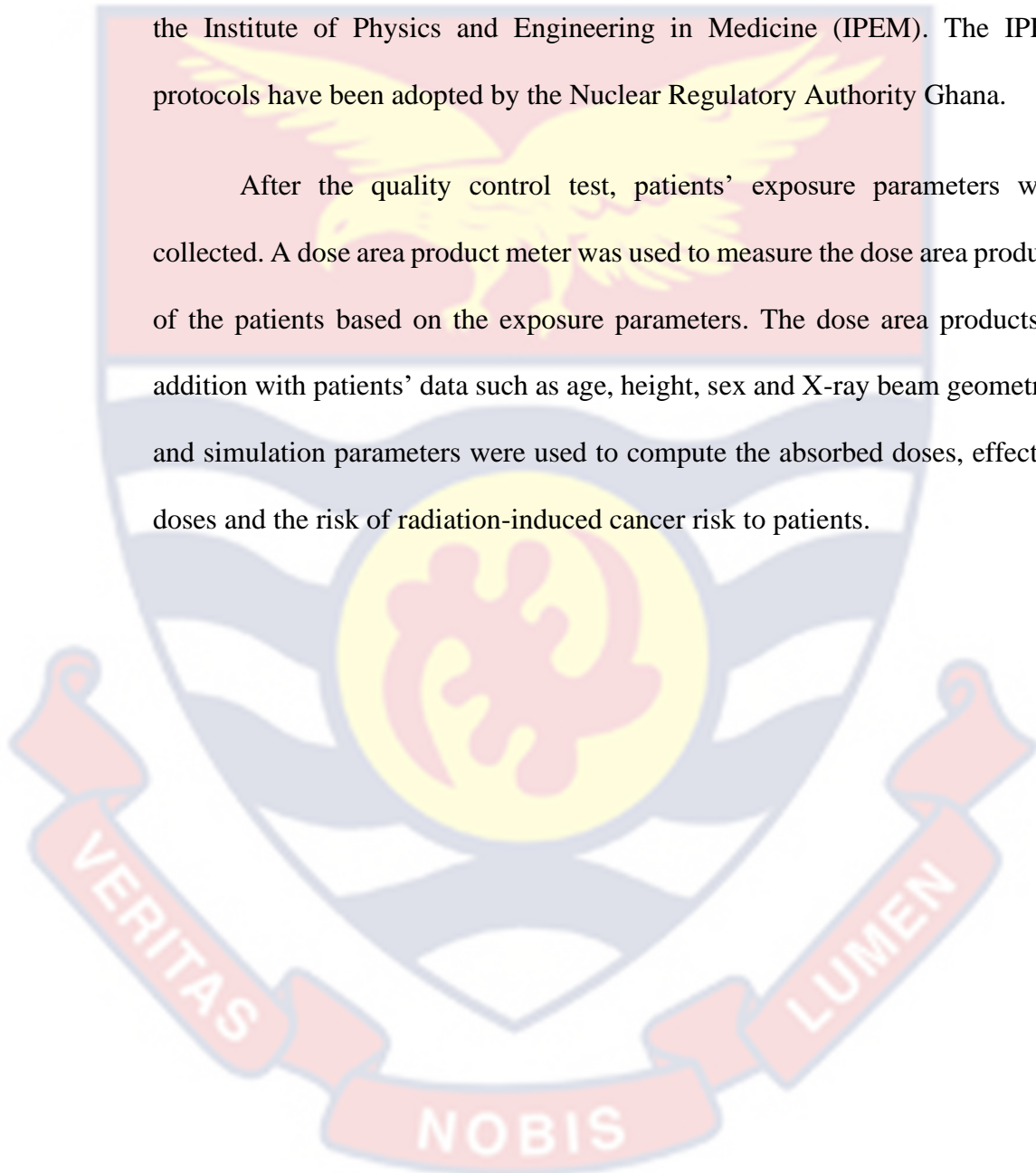
To calculate the risk, equivalent doses of vulnerable organs such as the breast, colon, lung, active bone marrow, liver, ovaries, prostate gland, stomach, thyroid gland, uterus, urinary bladder, and weighted remainder were used. The estimated dose for each of the 29 organs and tissues in the PCXMC phantom was determined for each projection.

Chapter Summary

Six panoramic dental X-ray equipment from six different dental facilities located within Accra and Kumasi were studied. Five of the equipment were in Accra and one in Kumasi. Five of the equipment were direct digital, with only one being indirect digital in nature. Before patients' data were collected, all the equipment were subjected to quality control test to ascertain whether or not they could be included in the study. The Magic Max multimeter was used in

performing the quality control test. The specific parameters that were tested for included the kV accuracy, timer accuracy, kVp reproducibility, timer reproducibility, exposure reproducibility, mA linearity and half value layer. The quality control parameters were benchmarked against acceptable criteria set by the Institute of Physics and Engineering in Medicine (IPEM). The IPEM protocols have been adopted by the Nuclear Regulatory Authority Ghana.

After the quality control test, patients' exposure parameters were collected. A dose area product meter was used to measure the dose area products of the patients based on the exposure parameters. The dose area products in addition with patients' data such as age, height, sex and X-ray beam geometries and simulation parameters were used to compute the absorbed doses, effective doses and the risk of radiation-induced cancer risk to patients.



CHAPTER FOUR

RESULTS AND DISCUSSION

Introduction

The results of the study are reported, analysed and discussed in this chapter.

Performance Tests

The results of the performance testing conducted on the equipment evaluated are shown in Table 10.

Table 10: Major Parameters Measured and their Acceptance Criteria

Equipment Model	Parameters measured						HVL (mm Al) @ 70 kV
	kVp acc. (%)	Timer Acc. (%)	mA Linearity	kV Repro.	Time Repro.	Exposure Repro.	
Kh-0.5-105	0.10	1.30	0.01	0.00	0.01	0.02	3.10
CS8100SC	1.80	0.44	0.00	0.01	0.00	0.02	2.99
OPX105	0.45	0.68	0.00	0.00	0.02	0.01	2.98
PHT-6500	1.46	0.90	0.02	0.01	0.01	0.00	3.24
GX100-20DC	0.85	1.92	0.01	0.03	0.01	0.01	3.14
1117340V1010	1.05	1.12	0.00	0.01	0.01	0.01	3.07
Acceptance criteria	± 5.00	± 10.00	0.10	0.05	0.05	005	≥ 2.50

(Source: Measured Data, 2021)

Table 10 shows the various parameters measured with reference to the performance tests conducted on the equipment. They include the kVp accuracy, timer accuracy, mA linearity, kV reproducibility, timer reproducibility, exposure reproducibility and half value layer. For an equipment to pass the kV accuracy test, it must measure a kV of within ± 5.00 % of set kV; timer accuracy must be

within $\pm 10.00\%$; mA linearity must be ≤ 0.10 ; the coefficient of variations (cov) for kV, time, exposure reproducibilities must be less than 5.00% and the half value layer (HVL) at 70 kV measured must be ≥ 2.50 mm Al. It could then be deduced that all the six-equipment evaluated passed the performance tests per the acceptance criteria, and this then justified the reason for including all the equipment in the study.

Dose Area Product

The results of the dose area product measurements for the different age categories per the equipment studied are shown in Table 11-14.

Table 11 shows the DAP values for the 5-year-olds. The mean values ranged from the least of 51.86 mGy.cm^2 to the highest of 56.60 mGy.cm^2 . In a similar study conducted by Chaparian and Dehghanzade (Chaparian & Dehghanzade, 2017), on a similar single digital panoramic machine, the DAP value obtained for the 5-year-olds was $53.77 \pm 11.89 \text{ mGy.cm}^2$. Comparing the values of this study with that of Chaparian and Dehghanzade (2017), percentage DAP differences observed were 1.36% , 3.55% , 1.23% , 5.26% , 2.34% and 4.33% for equipment models Kh-0.5-105, CS8100SC, OPX105, PHT-6500, GX100-20DC and 1117340V1010 respectively. The percentage difference observed for the overall mean DAP of this study and that of Chaparian and Dehghanzade (2017) was 1.82% . In another similar measurement performed to determine the DAP for 5-year-olds, Lee et. al obtained a mean value of 52.11 mGy.cm^2 (Lee et al., 2019). Comparing the values of Lee et. al (2019) with that obtained for this study with reference to the various panoramic equipment, 4.39% , 0.48% , 4.26% , 6.28% , 5.31% and 7.11% percentage differences were observed respectively

for the various models. The percentage difference observed for the overall mean DAP of this study and that of Lee et. al (2019) was 5.07 %. Both the DAP results of the present study involving the 5-year-olds when compared with that of Chaparian and Dehghanzade (2017) and Lee et al. (2019), showed some strong agreement and could, therefore, be said to be reliable. However, the percentage variations between the DAP values of this study and that of Chaparian and Dehghanzade (2017) and Lee et al. (2019) could be due to the different nature of the devices, measurement radiation conditions, as well as the techniques in measurements using the dose area product meter.

Table 11: kVp, mAs, and DAP (mGy.cm²) for the 5-year-old Group

Device Model	5-year-olds		DAP
	kVp	mAs	
Kh-0.5-105	63.05 ± 1.00	96.20 ± 12.00	54.50 ± 9.83
CS8100SC	62.01 ± 1.03	100.30 ± 18.60	51.86 ± 11.83
OPX105	65.0 ± 0.50	100.80 ± 12.00	54.43 ± 12.10
PHT-6500	65.02 ± 1.12	103.10 ± 9.00	56.60 ± 8.20
GX100-20DC	63.13 ± 0.30	99.43 ± 23.40	55.03 ± 10.82
1117340V1010	65.0 ± 1.21	105.10 ± 16.00	56.10 ± 9.00
Overall average	63.87 ± 0.86	100.82 ± 15.17	54.75 ± 10.30

(Source: Calculated Data, 2021)

The DAPs measured for the 10-year-olds from the panoramic radiographies are shown in Table 12. The mean values ranged from the least of 60.36 mGy.cm² to the highest of 66.06 mGy.cm². Chaparian and Dehghanzade (2017) obtained a value of 62.59 ± 17.39 mGy.cm² for the 10-year-olds. Now, comparing the mean DAP results of Chaparian and Dehghanzade (2017) with this study, the percentage differences were 1.50 %, 3.56 %, 5.54 %, 5.46 %, 1.12

% and 4.78 % for the respective equipment models. 2.11 % was obtained as the percentage difference of the overall mean DAP for this study and that of Chaparian and Dehghanzade (2017). The differences in the DAP values could be attributed to the radiation conditions under which the measurements were taken, the variations in the dental devices and the differences in techniques involved with the usage of the dose area product meters.

Table 12: kVp, mAs, and DAP (mGy.cm²) for the 10-year-olds

Device Model	10-year-olds		DAP
	kVp	mAs	
Kh-0.5-105	65.10 ± 0.10	123.50 ± 8.30	63.53 ± 14.10
CS8100SC	65.08 ± 1.12	132.92 ± 12.76	60.36 ± 12.65
OPX105	66.05 ± 2.01	143.00 ± 19.82	66.06 ± 13.01
PHT-6500	67.09 ± 1.70	138.50 ± 16.65	66.01 ± 9.60
GX100-20DC	65.07 ± 0.35	128.65 ± 2.10	61.89 ± 13.20
1117340V1010	67.00 ± 0.76	146.00 ± 22.32	65.58 ± 9.80
Overall average	65.90 ± 1.00	135.42 ± 13.66	63.91 ± 12.06

(Source: Calculated Data, 2021)

Shown in Table 13 are the DAP values with their respective standard deviations measured for the 15-year-old group. The values for the DAPs ranged from the least of 89.80 mGy.cm² to the highest of 93.39 mGy.cm². Comparing the DAP results of this study with that of Chaparian and Dehghanzade (2017) who had a value of 92.05 (± 10.20) mGy.cm², the percentage differences were 0.11 %, 2.44 %, 0.60 %, 2.28 %, 0.43 % and 1.46 % for the respective equipment models. The percentage difference observed for the overall mean DAP of this study and that of Chaparian and Dehghanzade (2017) was 0.39 %. The values obtained for this study when generally compared with that of Chaparian and

Dehghanzade (2017) show a fairly consistent trend, except that the slight differences could be due to differences in radiation conditions, variations in equipment and the variations in technique in using dose area product meters.

Table 13: kVp, mAs, and DAP (mGy.cm²) for the 15-year-olds

Device Model	15-year-olds		DAP
	kVp	mAs	
Kh-0.5-105	67.00 ± 0.00	142.05 ± 10.23	91.95 ± 3.60
CS8100SC	66.14 ± 0.10	148.58 ± 12.00	89.80 ± 8.20
OPX105	67.03 ± 0.05	138.00 ± 8.20	92.60 ± 8.30
PHT-6500	68.00 ± 0.04	132.15 ± 6.34	89.95 ± 1.66
GX100-20DC	67.12 ± 1.12	127.12 ± 2.50	92.45 ± 6.40
1117340V1010	68.05 ± 0.23	136.06 ± 6.50	93.39 ± 1.30
Overall average	67.23 ± 0.26	137.33 ± 7.63	91.69 ± 4.91

(Source: Calculated Data, 2021)

Table 14 shows the DAP values measured with their standard deviations for the adult group. The values ranged from the lowest of 93.54 mGy.cm² to the highest of 97.65 mGy.cm². Chaparian and Dehghanzade (2017) in their study involving the adult group obtained a value of 94.43 (± 13.46) mGy.cm². In comparing the mean values of the two studies, the respective DAP percentage differences were 3.40 %, 1.15 %, 3.12 %, 0.02 %, 1.20 % and 0.94 %. The percentage difference observed for the overall mean DAP of this study and that of Chaparian and Dehghanzade (2017) was 1.32 %. The mean values obtained for the DAPs with reference to the adult group for this study and that of Chaparian and Dehghanzade (2017) were fairly consistent. Honer et al. (2015) in their surveys for the adult group stated a mean DAP value of 94.0 mGy.cm²

which is fairly consistent with this study. The percentage differences in comparison with Honer et al. (2015) were respectively 3.88 %, 1.62 %, 3.60 %, 0.53 %, 1.66 % and 0.49 %. The percentage difference observed for the overall mean DAP of this study and that of Honer et al. (2015) was 1.79 %. The DAP differences for the adult study in comparison with Chaparian and Dehghanzade (2017) and Honer et al. (2015) may have come about as a result of the variation in dental devices, radiation conditions under which the measurements were taken and the variations in technique when using the dose area product meters.

Table 14: kVp, mAs, and DAP (mGy.cm²) for the Adults

Device Model	30-year-olds		DAP
	kVp	mAs	
Kh-0.5-105	71.23 ± 0.54	166.60 ± 2.50	97.65 ± 8.60
CS8100SC	70.09 ± 1.22	172.05 ± 0.05	95.52 ± 3.50
OPX105	70.00 ± 0.31	170.50 ± 1.24	97.38 ± 10.30
PHT-6500	71.10 ± 0.10	169.93 ± 3.50	94.45 ± 4.60
GX100-20DC	69.31 ± 0.44	170.00 ± 1.50	95.56 ± 2.05
1117340V1010	72.00 ± 1.20	173.45 ± 0.68	93.54 ± 11.30
Overall average	70.62 ± 0.64	170.43 ± 1.58	95.68 ± 6.73

(Source: Calculated Data, 2021)

By examining the DAP findings for the aforementioned age groups, it was feasible to infer that the DAP increased with age values for all examinations since the exposure situations, which are directly related to the DAP, increased with the age of patient.

Organ Absorbed and Effective Doses

Tables 15-20 display the results of the calculated organs absorbed and effective doses (\pm SD) for the different age groups and their associated panoramic equipment. The highest contribution of the organ absorbed doses for all the year groups were from the salivary glands, with the second highest being the oral mucosa. Extrathoracic and thyroid glands received higher doses compared to other organs, indicating that the irradiated region and its surroundings have higher organ absorbed doses. Considering Table 15, the 5-year-olds absorbed doses recorded for the salivary gland, oral mucosa, extrathoracic and thyroid gland were 282.65 μ Gy, 231.10 μ Gy, 159.45 μ Gy and 78.23 μ Gy respectively for equipment model Kh-0.5-105. The 10-year-olds organ absorbed doses recorded for the salivary gland, oral mucosa, extrathoracic and thyroid gland were 284.15 μ Gy, 221.20 μ Gy, 136.00 μ Gy and 65.22 μ Gy respectively for the same equipment model. 299.90 μ Gy, 220.00 μ Gy, 120.60 μ Gy and 44.56 μ Gy were respectively recorded for the 15-year-olds for the same equipment model. 329.47 μ Gy, 213.25 μ Gy, 113.57 μ Gy and 33.71 μ Gy were also recorded for adult group for the same model of equipment. This is the trend observed as presented in the rest of the Tables (i.e.16-20) for the various age groups and their respective equipment models. According to Ludlow et al. (2008) and Granlund et al. (2016), the salivary glands and oral mucosa encounter the highest radiation doses of any tissues during panoramic examinations as they commonly fall within the main radiation beam in panoramic radiography. Organs or tissues close to the primary beam recorded organ absorbed doses higher than those further away from the head and neck regions where the beam is much concentrated during panoramic radiographies.

The means and standard deviations of the effective doses for the panoramic radiographies shown in Tables 15-20 for the 5-, 10-, 15-year-olds and adult groups were $8.63 (\pm 1.65) \mu\text{Sv}$, $7.49 (\pm 1.640) \mu\text{Sv}$, $5.42 (\pm 0.560) \mu\text{Sv}$, and $5.14 (\pm 0.50) \mu\text{Sv}$ respectively for the equipment model Kh-0.5-105. For the equipment model CS8100SC, the values were $8.82 (\pm 1.55) \mu\text{Sv}$, $7.65 (\pm 1.50) \mu\text{Sv}$, $5.470 (\pm 0.61) \mu\text{Sv}$ and $5.05 (\pm 0.60) \mu\text{Sv}$ respectively. For the equipment model OPX105, the values were respectively $7.735 (\pm 1.74) \mu\text{Sv}$, $7.04 (\pm 1.56) \mu\text{Sv}$, $5.40 (\pm 0.55) \mu\text{Sv}$ and $5.05 (\pm 0.50) \mu\text{Sv}$. The values of $7.75 (\pm 1.57) \mu\text{Sv}$, $7.39 (\pm 1.35) \mu\text{Sv}$, $5.61 (\pm 0.68) \mu\text{Sv}$ and $5.01 (\pm 0.51) \mu\text{Sv}$ were respectively recorded for equipment model PHT-6500. The computed values for the equipment model GX100-20DC were $8.16 (\pm 1.70) \mu\text{Sv}$, $7.67 (\pm 1.73) \mu\text{Sv}$, $5.52 (\pm 0.48) \mu\text{Sv}$ and $5.008 (\pm 0.50) \mu\text{Sv}$ respectively. Lastly, the values of $7.49 (\pm 1.70) \mu\text{Sv}$, $7.20 (\pm 1.65) \mu\text{Sv}$, $5.72 (\pm .60) \mu\text{Sv}$ and $5.00 (\pm 0.52) \mu\text{Sv}$ were respectively recorded for equipment model 1117340V1010. The effective doses decreased with increasing ages for almost all examinations, which are consistent with the results of Chaparian and Dehghanzade (2017) and Zenone (Zenone et al., 2012). This may be explained by the reality that, as opposed to conventional radiography, where the radiation field size can be adjusted based on the size of the patient, the radiation field size in all dental radiographies for all age groups is uniform. Therefore, it is expected that further organs and tissues would be exposed in younger age groups.

Chaparian and Dehghanzade (2017) conducted a similar study for the 5-,10-, 15-year-olds and adult group. The values obtained for the effective doses were $7.72 (\pm 1.66) \mu\text{Sv}$, $6.09 (\pm 1.64) \mu\text{Sv}$, $5.52 (\pm 0.59) \mu\text{Sv}$ and $5.04 (\pm 0.70) \mu\text{Sv}$ respectively. In another study conducted by Lecomber (Lecomber et al.,

2001) and Danforth (Danforth & Clark, 2000), the mean effective doses obtained were 2.00-9.00 μSv and 3.85 μSv respectively. The results of the of studies of Chaparian and Dehghanzade (2017), Lecomber et al. (2001) and Danforth and Clark (2000) are generally in agreement with this study. The variations in findings between this study and others may be due to the inclusion of the presently used tissue weighting factors (ICRP, 2007) in the computations of the organ or tissue doses in this study, as against some previous studies doing the calculations based on the old tissue weighting factors (ICRP, 1991).

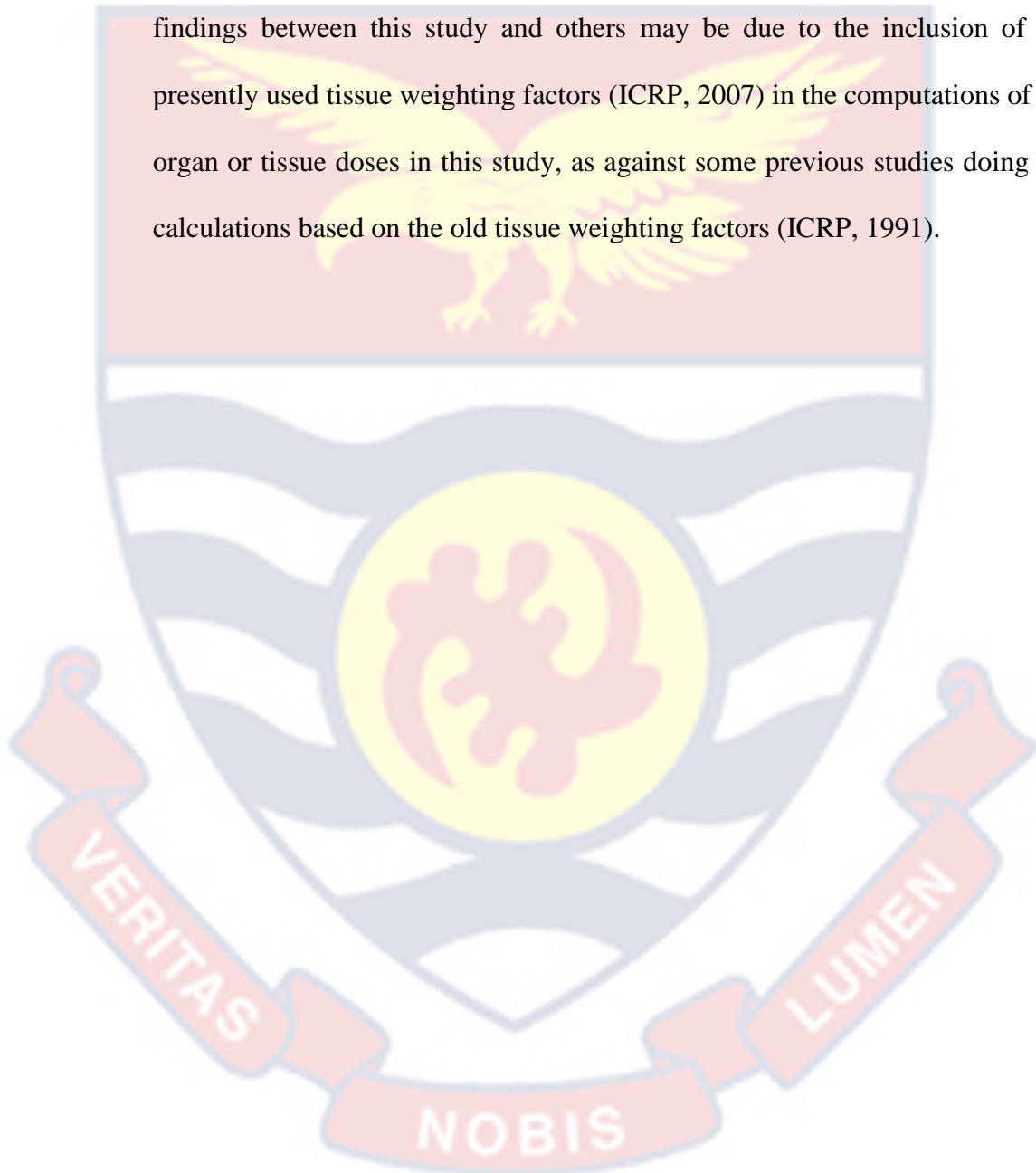


Table 15: Organ Absorbed and Effective Dose (\pm SD) from Kh-0.5-105**Panoramic Equipment**

Organ	Absorbed dose (μ Gy)			
	5-year-olds	10-year-olds	15-year-olds	30-year-olds
Active bone marrow	11.91	11.62	11.32	1.43
Adrenals	0.12	0.11	0.11	0.00
Brain	17.90	17.00	16.20	14.79
Breasts	0.17	0.20	0.20	0.27
Colon (Large intestine)	0.00	0.00	0.00	0.00
Extrathoracic airways	159.45	136.00	120.60	113.57
Gall bladder	0.09	0.07	0.01	0.00
Heart	0.56	0.44	0.29	0.14
Kidneys	0.05	0.04	0.02	0.00
Liver	0.22	0.18	0.13	0.09
Lungs	2.25	1.15	1.20	1.07
Lymph nodes	45.04	45.02	45.00	44.97
Muscle	9.76	8.86	6.11	6.29
Oesophagus	2.07	1.88	1.80	0.80
Oral mucosa	231.10	221.20	220.00	213.25
Pancreas	0.26	0.20	0.10	0.01
Salivary glands	282.65	284.15	299.90	329.47
Skeleton	56.50	54.61	51.13	45.34
Skin	25.81	20.01	20.00	14.12
Small intestine	0.01	0.00	0.00	0.00
Spleen	0.14	0.12	0.09	0.02
Stomach	0.09	0.08	0.03	0.02
Thymus	3.82	2.12	2.00	0.47
Thyroid	78.23	65.22	44.56	33.71
Effective dose (μ Sv)	8.63 (\pm 1.65)	7.49 (\pm 1.64)	5.42 (\pm 0.56)	5.14 (\pm 0.50)

(Source: Simulation, 2021)

Table 16: Organ Absorbed and Effective Dose (\pm SD) from CS8100SC**Panoramic Equipment**

Organ	Absorbed dose (μ Gy)			
	5-year-olds	10-year-olds	15-year-olds	30-year-olds
Active bone marrow	11.81	11.72	11.42	1.42
Adrenals	0.13	0.12	0.11	0.00
Brain	18.90	17.00	16.80	14.19
Breasts	0.17	0.20	0.20	0.27
Colon (Large intestine)	0.00	0.00	0.00	0.00
Extrathoracic airways	159.56	139.10	131.60	112.32
Gall bladder	0.09	0.07	0.01	0.00
Heart	0.60	0.43	0.30	0.13
Kidneys	0.05	0.04	0.03	0.00
Liver	0.21	0.18	0.14	0.08
Lungs	2.15	1.17	1.10	1.08
Lymph nodes	45.14	45.01	45.01	44.97
Muscle	9.97	8.97	7.00	6.17
Oesophagus	2.09	1.90	1.70	0.70
Oral mucosa	241.00	220.21	217.00	214.45
Pancreas	0.27	0.21	0.11	0.01
Salivary glands	292.15	294.00	297.91	357.51
Skeleton	57.40	55.50	53.03	46.24
Skin	25.82	21.00	20.10	14.22
Small intestine	0.01	0.004	0.00	0.00
Spleen	0.14	0.13	0.10	0.02
Stomach	0.20	0.08	0.04	0.02
Thymus	3.92	2.22	2.00	0.47
Thyroid	79.21	65.22	43.44	35.61
Effective dose (μ Sv)	8.82 (± 1.55)	7.65 (± 1.50)	5.47 (± 0.61)	5.05 (± 0.40)

(Source: Simulation, 2021)

Table 17: Organ Absorbed and Effective Dose (\pm SD) from OPX105**Panoramic Equipment**

Organ	Absorbed dose (μ Gy)			
	5-year-olds	10-year-olds	15-year-olds	30-year-olds
Active bone marrow	11.82	11.7	11.52	1.41
Adrenals	0.21	0.12	0.10	0.00
Brain	18.20	17.10	15.10	14.68
Breasts	0.17	0.20	0.20	0.269
Colon (Large intestine)	0.00	0.00	0.00	0.00
Extrathoracic airways	161.00	146.10	123.90	123.46
Gall bladder	0.08	0.06	0.01	0.00
Heart	0.51	0.45	0.30	0.13
Kidneys	0.05	0.04	0.02	0.00
Liver	0.22	0.19	0.14	0.09
Lungs	2.35	1.75	1.10	1.08
Lymph nodes	45.15	45.10	45.09	44.97
Muscle	9.66	7.78	6.33	6.15
Oesophagus	2.02	1.76	1.70	0.60
Oral mucosa	235.10	223.10	218.00	214.15
Pancreas	0.27	0.21	0.11	0.00
Salivary glands	291.11	296.00	298.80	348.44
Skeleton	58.40	55.47	52.15	45.44
Skin	25.52	21.11	20.01	14.22
Small intestine	0.01	0.01	0.01	0.00
Spleen	0.14	0.12	0.07	0.02
Stomach	0.10	0.08	0.04	0.01
Thymus	3.89	2.24	2.00	0.45
Thyroid	75.32	66.31	43.48	34.90
Effective dose (μ Sv)	7.74 (\pm 1.74)	7.04 (\pm 1.56)	5.40 (\pm 0.55)	5.05 (\pm 0.50)

(Source: Simulation, 2021)

Table 18: Organ Absorbed and Effective Dose (\pm SD) from PHT-6500**Panoramic Equipment**

Organ	Absorbed dose (μ Gy)			
	5-year-olds	10-year-olds	15-year-olds	30-year-olds
Active bone marrow	11.83	11.59	11.44	1.41
Adrenals	0.26	0.13	0.10	0.00
Brain	17.80	17.01	16.1010	14.68
Breasts	0.18	0.20	0.21	0.28
Colon (Large intestine)	0.00	0.00	0.00	0.00
Extrathoracic airways	157.00	146.10	121.01	114.44
Gall bladder	0.08	0.07	0.00	0.00
Heart	0.52	0.43	0.28	0.14
Kidneys	0.05	0.04	0.023	0.00
Liver	0.23	0.19	0.14	0.08
Lungs	2.15	1.25	1.18	1.00
Lymph nodes	45.22	45.18	45.11	44.92
Muscle	9.93	7.17	7.01	6.14
Oesophagus	2.01	1.75	1.62	0.60
Oral mucosa	234.00	224.21	217.00	211.14
Pancreas	0.25	0.22	0.17	0.01
Salivary glands	290.33	296.15	299.01	349.93
Skeleton	55.53	54.73	52.01	45.54
Skin	25.90	21.11	20.10	14.32
Small intestine	0.01	0.00	0.00	0.001
Spleen	0.14	0.17	0.09	0.02
Stomach	0.10	0.08	0.05	0.04
Thymus	3.74	2.17	2.01	0.40
Thyroid	77.24	64.65	46.43	32.64
Effective dose (μ Sv)	7.75 (\pm 1.57)	7.34 (\pm 1.35)	5.61 (\pm 0.68)	5.01 (\pm 0.51)

(Source: Simulation, 2021)

Table 19: Organ Absorbed and Effective Dose (\pm SD) from GX100-20DC**Panoramic Equipment**

Organ	5-year-olds	Absorbed dose (μ Gy)		
		10-year-olds	15-year-olds	30-year-olds
Active bone marrow	11.86	11.58	11.43	1.42
Adrenals	0.30	0.20	0.13	0.00
Brain	17.61	17.10	16.00	14.29
Breasts	0.18	0.20	0.20	0.28
Colon (Large intestine)	0.00	0.00	0.00	0.00
Extrathoracic airways	158.04	139.00	126.00	112.58
Gall bladder	0.07	0.06	0.01	0.00
Heart	0.50	0.43	0.31	0.13
Kidneys	0.05	0.03	0.03	0.00
Liver	0.23	0.18	0.14	0.09
Lungs	2.00	1.19	1.06	1.04
Lymph nodes	45.18	45.12	45.09	44.88
Muscle	9.68	7.89	6.44	6.17
Oesophagus	2.04	1.78	1.71	0.71
Oral mucosa	237.00	221.11	216.00	214.21
Pancreas	0.261	0.20	0.11	0.01
Salivary glands	290.49	293.01	299.01	344.83
Skeleton	56.50	54.61	51.13	45.34
Skin	25.87	25.01	20.00	14.00
Small intestine	0.01	0.01	0.00	0.00
Spleen	0.14	0.13	0.10	0.03
Stomach	0.09	0.08	0.06	0.03
Thymus	3.74	2.22	2.01	0.50
Thyroid	74.54	53.23	43.58	34.63
Effective dose (μ Sv)	8.16 (\pm 1.70)	7.67 (\pm 1.73)	5.52 (\pm 0.48)	5.01 (\pm 0.50)

(Source: Simulation, 2021)

Table 20: Organ Absorbed and Effective Dose (\pm SD) from 1117340V1010**Panoramic Equipment**

Organ	Absorbed dose (μ Gy)			
	5-year-olds	10-year-olds	15-year-olds	30-year-olds
Active bone marrow	11.91	11.62	11.42	1.40
Adrenals	0.22	0.12	0.20	0.00
Brain	17.70	17.30	16.40	14.57
Breasts	0.17	0.20	0.20	0.28
Colon (Large intestine)	0.001	0.00	0.00	0.00
Extrathoracic airways	151.25	133.30	120.61	113.00
Gall bladder	0.08	0.054	0.01	0.00
Heart	0.54	0.47	0.30	0.20
Kidneys	0.05	0.03	0.02	0.00
Liver	0.23	0.19	0.14	0.08
Lungs	2.44	1.26	1.19	1.09
Lymph nodes	45.20	45.13	45.10	44.71
Muscle	9.57	8.97	6.32	6.01
Oesophagus	2.00	1.76	1.62	0.70
Oral mucosa	233.10	222.00	218.00	213.11
Pancreas	0.25	0.24	0.13	0.08
Salivary glands	293.33	297.35	298.00	366.68
Skeleton	57.10	54.82	50.02	40.05
Skin	25.771	20.04	20.01	14.33
Small intestine	0.01	0.01	0.00	0.00
Spleen	0.15	0.13	0.08	0.08
Stomach	0.10	0.09	0.06	0.03
Thymus	3.77	2.34	2.11	0.43
Thyroid	75.12	54.73	46.66	34.62
Effective dose (μ Sv)	7.49 (\pm 1.70)	7.20 (\pm 1.65)	5.72 (\pm 0.60)	5.00 (\pm 0.52)

(Source: Simulation, 2021)

Risk of Exposure-Induced Cancer Death (REID)

The REID values for the various age categories with respect to the different panoramic equipment are shown in Figures 12-17.

Figure 12 shows the REID for the male and female age groups with respect to the equipment model Kh-0.5-105 in terms of number per million. The REID values for the males were 2.04 (\pm 0.23), 3.06 (\pm 0.14), 4.31 (\pm 0.21) and 6.45 (\pm 0.12) per ten million for the adult, 15-, 10- and 5-year old groups respectively and that of the females were 2.62 (\pm 0.09), 3.96 (\pm 0.14), 6.41 (\pm 0.15) and 8.32 (\pm 0.10) per ten million for the adult, 15-, 10- and 5-year old groups respectively.

The REIDs for the equipment model CS8100SC is presented in Figure 13. The values computed for the males were 2.51 (\pm 0.20), 3.50 (\pm 0.09), 5.60 (\pm 0.22) and 7.45 (\pm 0.06) per ten million for the adult, 15-, 10- and 5-year old groups respectively and that of the females were 3.62 (\pm 0.09), 5.40 (\pm 0.20), 7.34 (\pm 0.12) and 9.02 (\pm 0.08) per ten million for the adult, 15-, 10- and 5-year old groups respectively.

Shown in Figure 14 is the REIDs with reference to equipment model OPX105. For the males, the values were 2.03 (\pm 0.02), 4.01 (\pm 0.31), 7.43 (\pm 0.11) and 8.50 (\pm 0.18) per ten million for the adult, 15-, 10- and 5-year old groups respectively and for the females, the REID values were 4.12 (\pm 0.08), 6.40 (\pm 0.23), 9.30 (\pm 0.07) and 11.02 (\pm 0.20) per ten million for the adult, 15-, 10- and 5-year old groups respectively.

Figure 15 shows the REID values for the model PHT-6500. They are 2.65 (\pm 0.19), 4.05 (\pm 0.17), 4.98 (\pm 0.06) and 7.99 (\pm 0.07) per ten million for the adult, 15-, 10- and 5-year old groups respectively whereas that of the females

were 3.90 (± 0.09), 5.95 (± 0.14), 6.65 (± 0.05) and 10.52 (± 0.12) per ten million for the adult, 15-, 10- and 5-year old groups respectively.

Considering equipment model GX100-20DC, 1.95 (± 0.07), 2.49 (± 0.10), 3.38 (± 0.05), and 8.45 (± 0.14) per ten million were obtained for the adult, 15-, 10- and 5-year-old groups respectively and that of females were 3.09 (± 0.07), 4.98 (± 0.10), 5.45 (± 0.03) and 10.68 (± 0.06) as shown in Figure 16.

Figure 17 shows the REID values for the equipment model 1117340V1010. The values obtained were 3.21 (± 0.09), 4.78 (± 0.41), 6.12 (± 0.15) and 9.85 (± 0.24) per ten million respectively for adult, 15-, 10- and 5-year old groups and that of the females were 4.09 (± 0.12), 5.92 (± 0.18), 7.36 (± 0.27) and 11.05 (± 0.16) per ten million respectively for adult, 15-, 10- and 5-year old groups.

Figures 12–17 show that for both sexes, REID values decline with growing age at exposure. The overall cancer risk is higher in children than in adults, and in female patients than in male patients in all panoramic radiographies. Children are more susceptible to the negative effects or danger of radiation exposure because many of their cells continue to divide throughout their growth periods. In addition, because of their smaller bodies than adults, children at younger ages receive greater doses of scatter radiation to their surrounding tissues and organs. In similar study by Chaparian and Dehghanzade (2017), the REID values obtained for the various age groups was 2.1 to 7.32 per ten million. In another study by Horner et al. (2015), the REID value was 2 to 9 per ten million. The findings of this research and those of Chaparian and Dehghanzade (2017) and Horner et al. (2015) were largely in agreement. The differences in panoramic devices and radiation conditions between this research and those of Chaparian

and Dehghanzade (2017), Horner et al. (2015), and other studies may be the cause of the discrepancy. The various techniques used to calculate the cancer risk may also account for the difference in REID values between this research and the others. In contrast to other studies, which simply multiplied the effective dose by constant coefficients to determine the cancer risk, this study's risk evaluation was based on the BEIR VII publication models (Council, 2005). In certain studies, the risks were calculated for adults only, irrespective of the gender. This made the complete comparison of the results of those studies with this study impossible. Some of those studies failed to state the type of dental examinations. Those studies used general terminologies such as dental radiography without specifically mentioning the type of dental modality. In order to deal with this problem, only studies that had clearly stated the type of dental radiography were compared with this study.

The differences between the REID values (per ten million) of the six-equipment evaluated could as well be attributed to the variable nature of the panoramic devices.

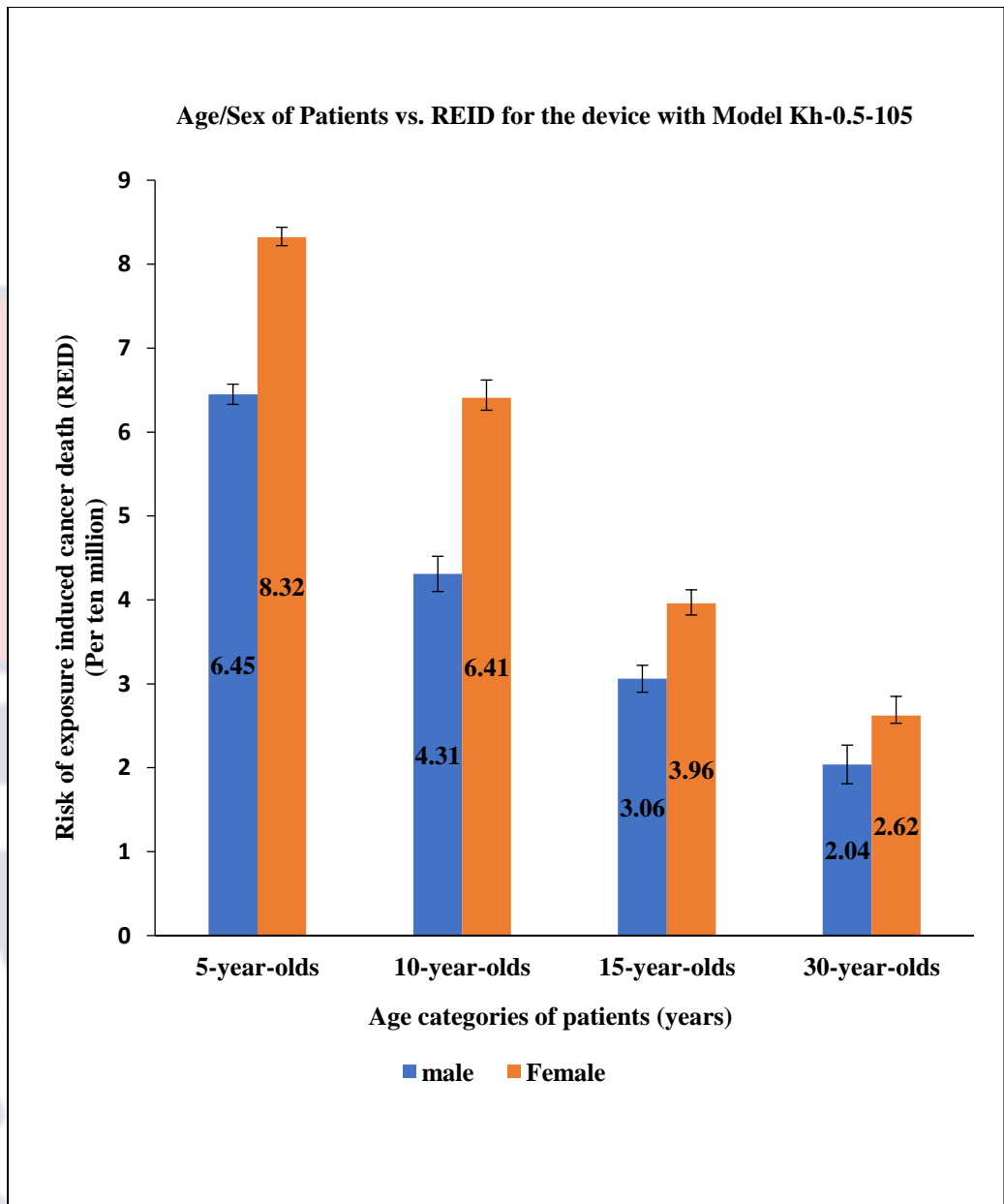


Figure 12: REID Values from Device Model Kh-0.5-105

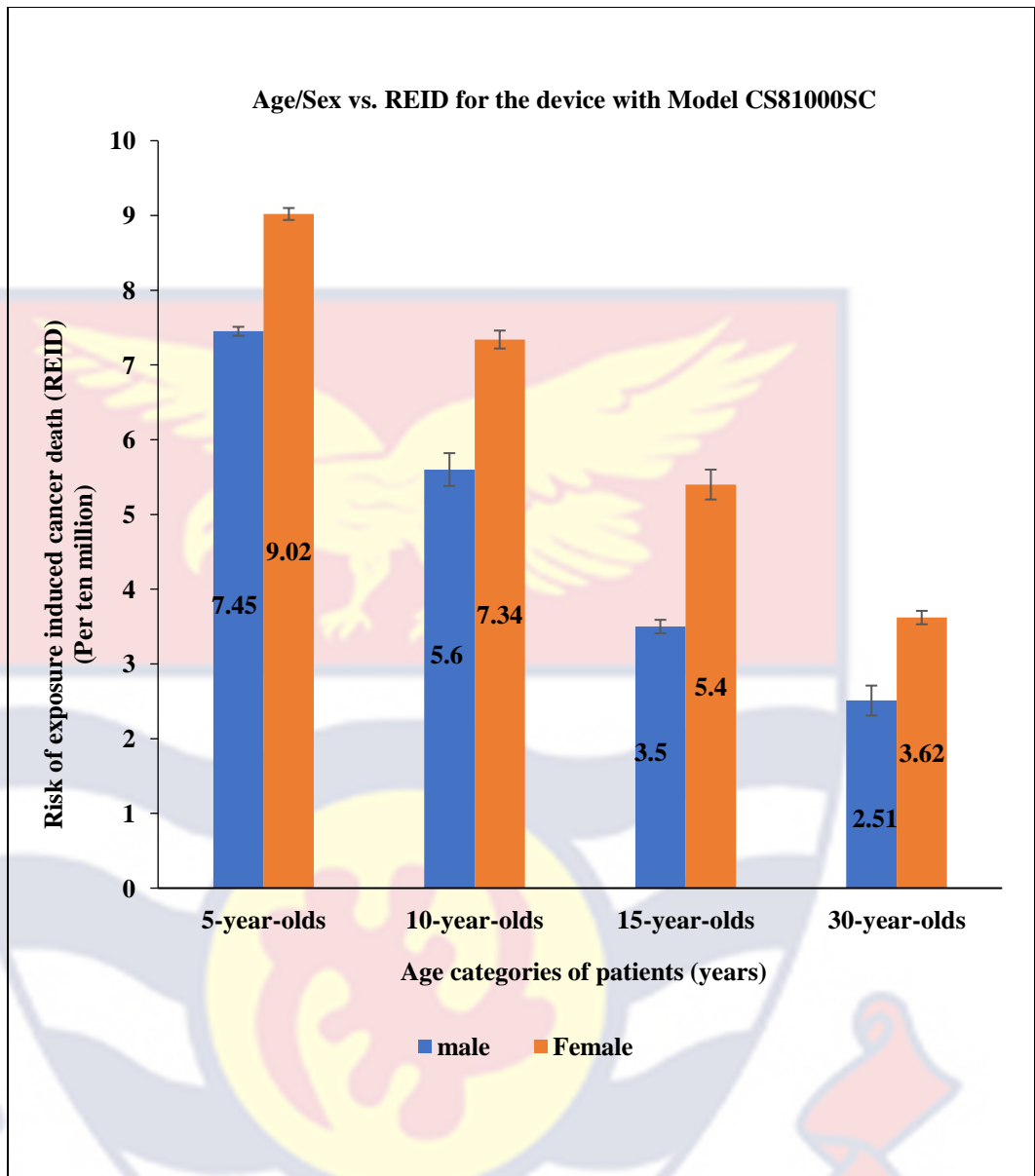


Figure 13: REID Values from Device Model CS8100SC

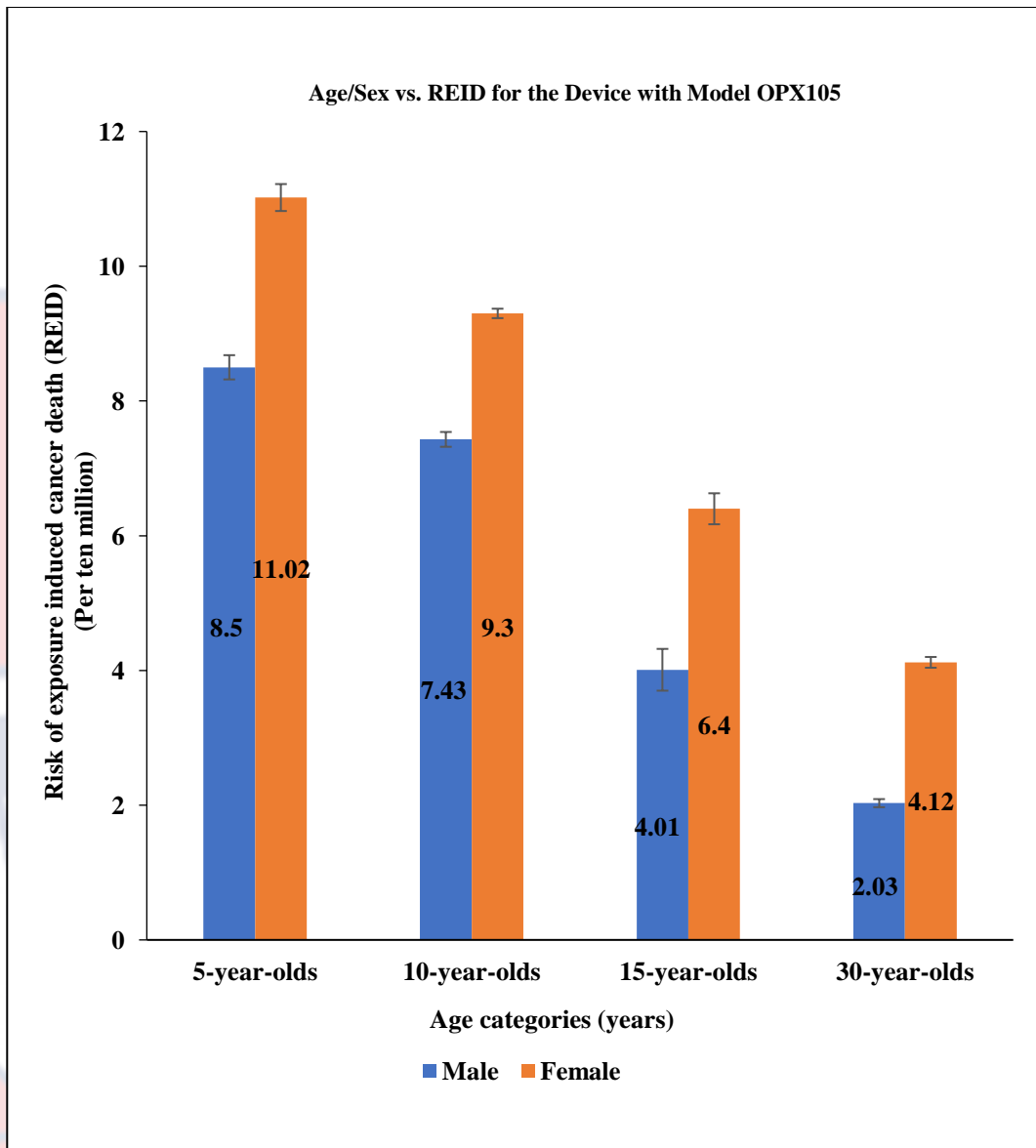


Figure 14: REID Values from Device Model OPX105

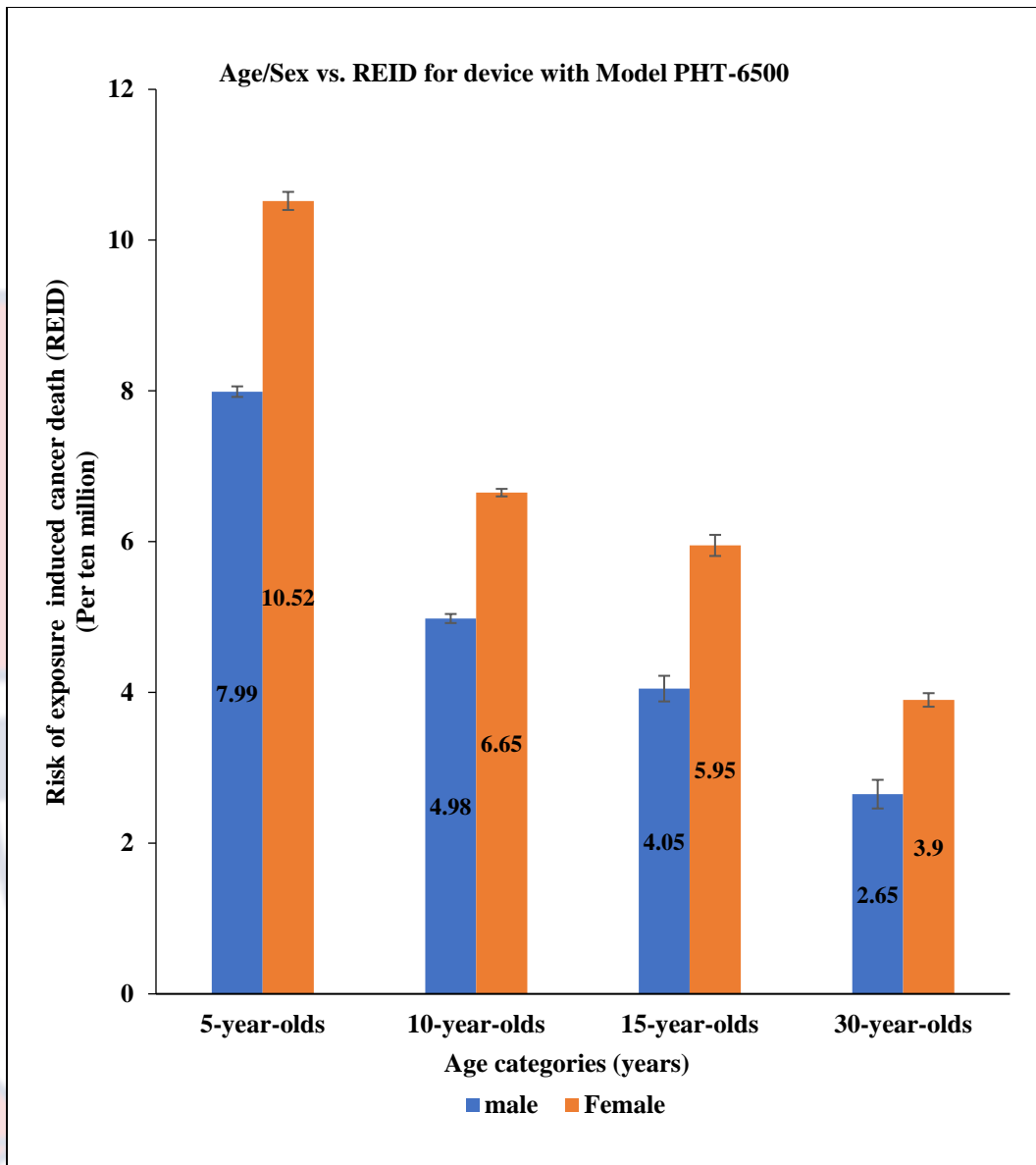


Figure 15: REID Values from Device Model PHT-6500

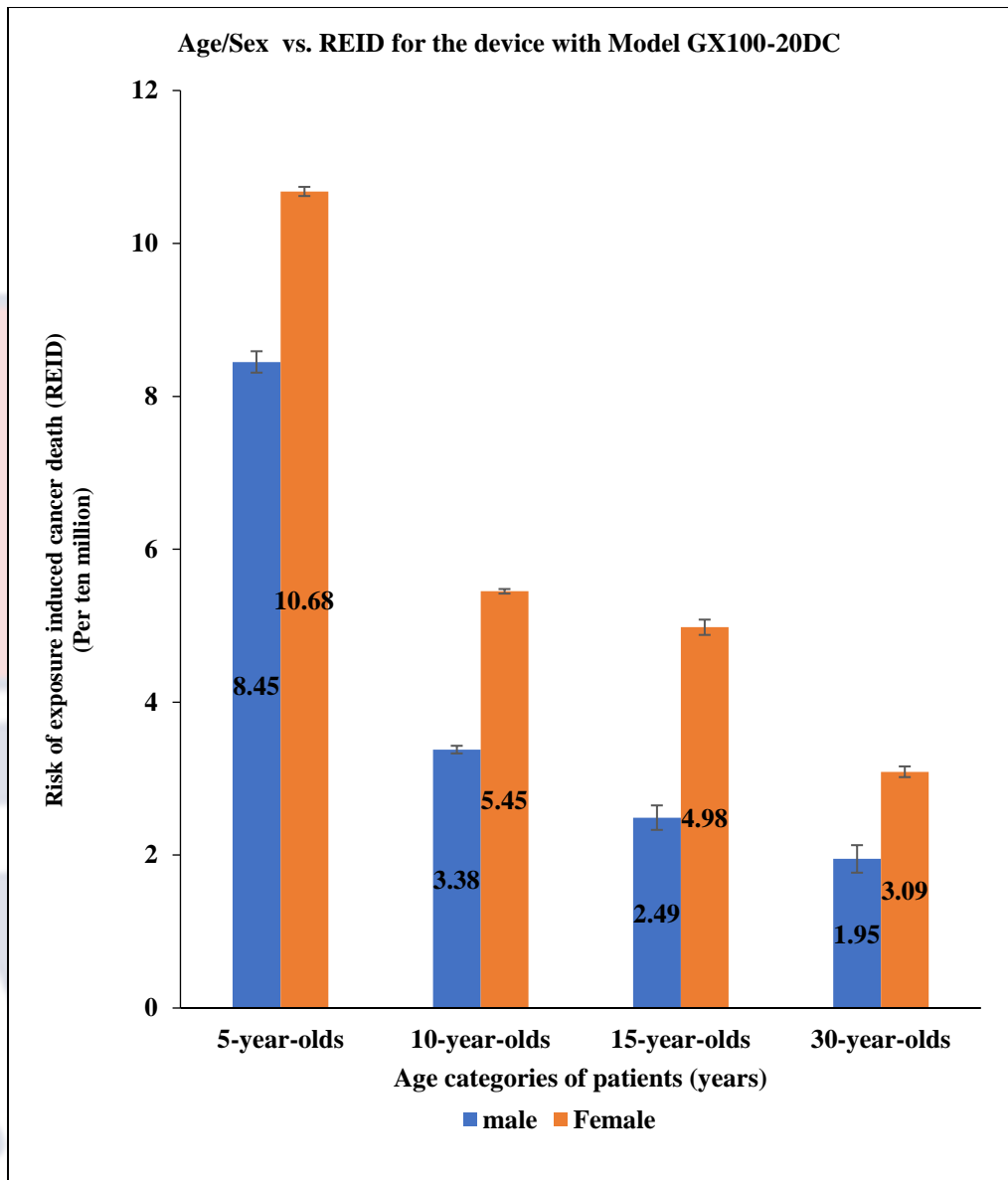


Figure 16: REID Values from Device Model GX100-20DC

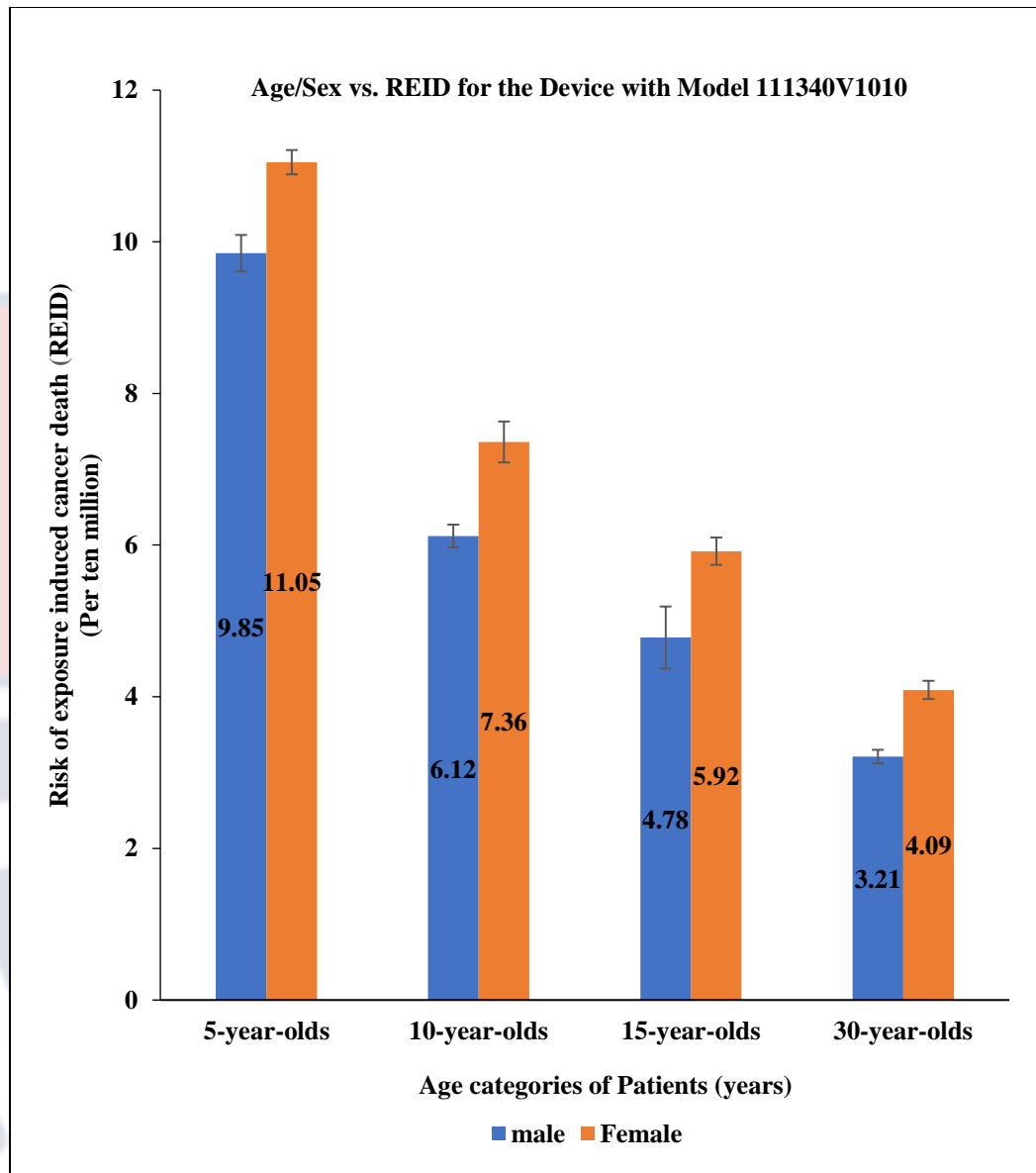


Figure 17: REID Values from Device Model 1117340V1010

Individual/Organ Specific Radiogenic Cancers

Figures 18 to 23 a-e show graphs of the five individual radiogenic cancers for both genders from the different panoramic equipment.

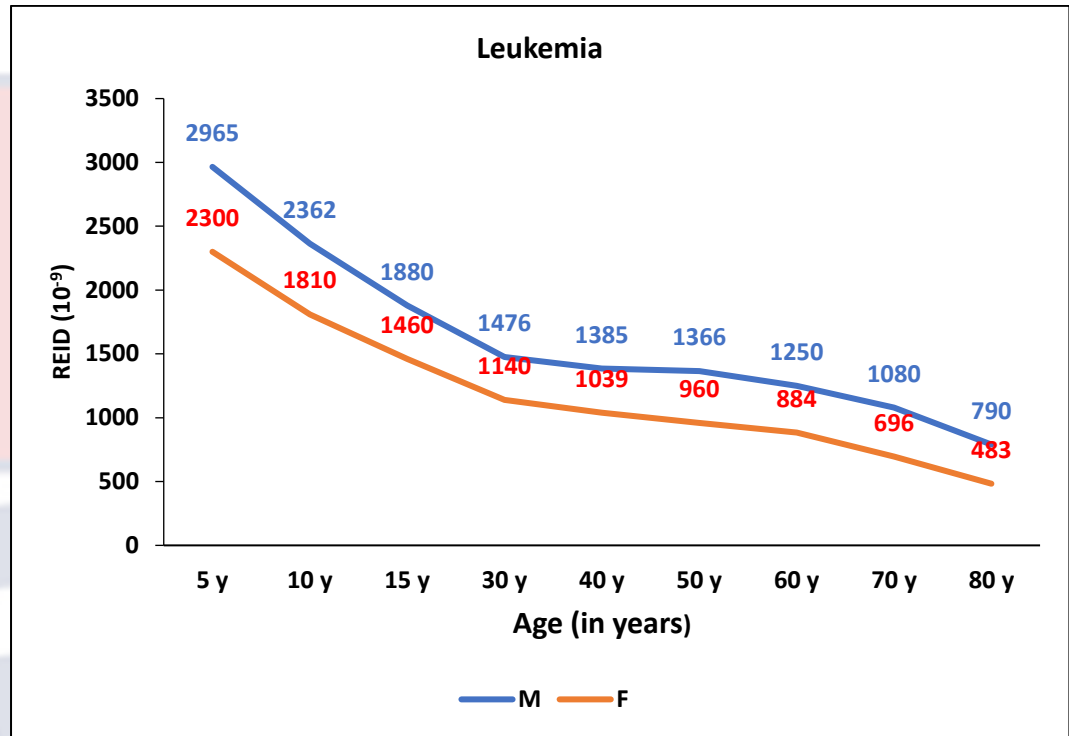


Figure 18a: The REID Values for Leukemia from the Kh-0.5-105 Panoramic Equipment Model.

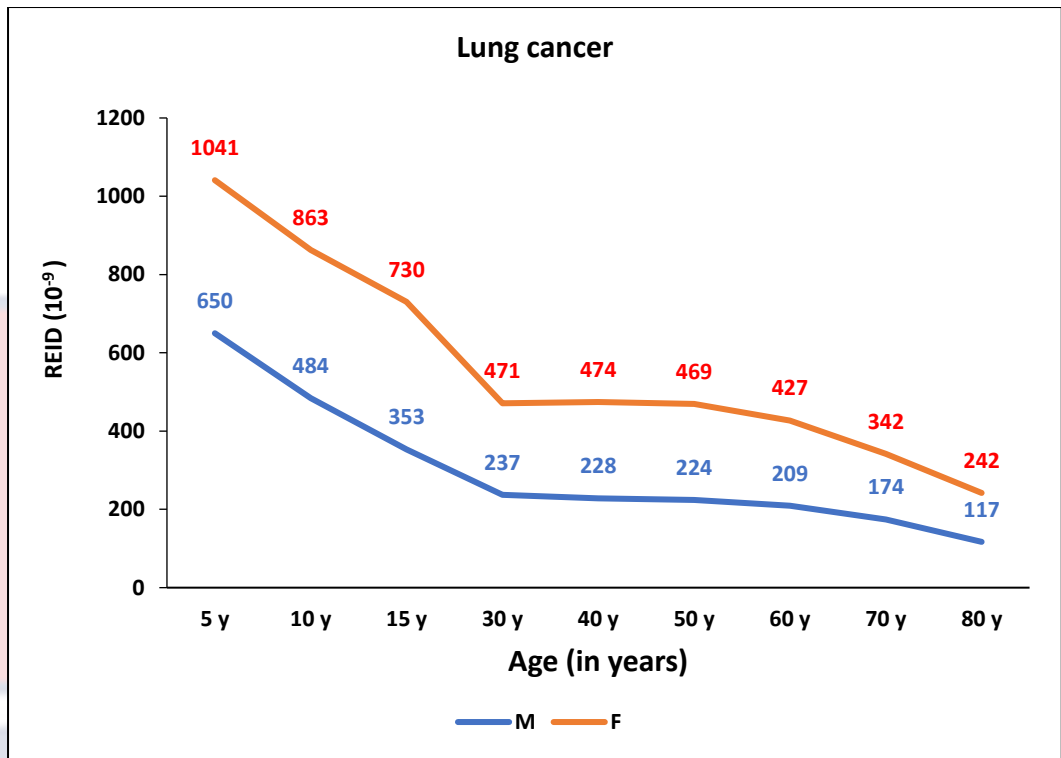


Figure 18b: The REID Values for Lung Cancer from the Kh-0.5-105 Panoramic Equipment Model

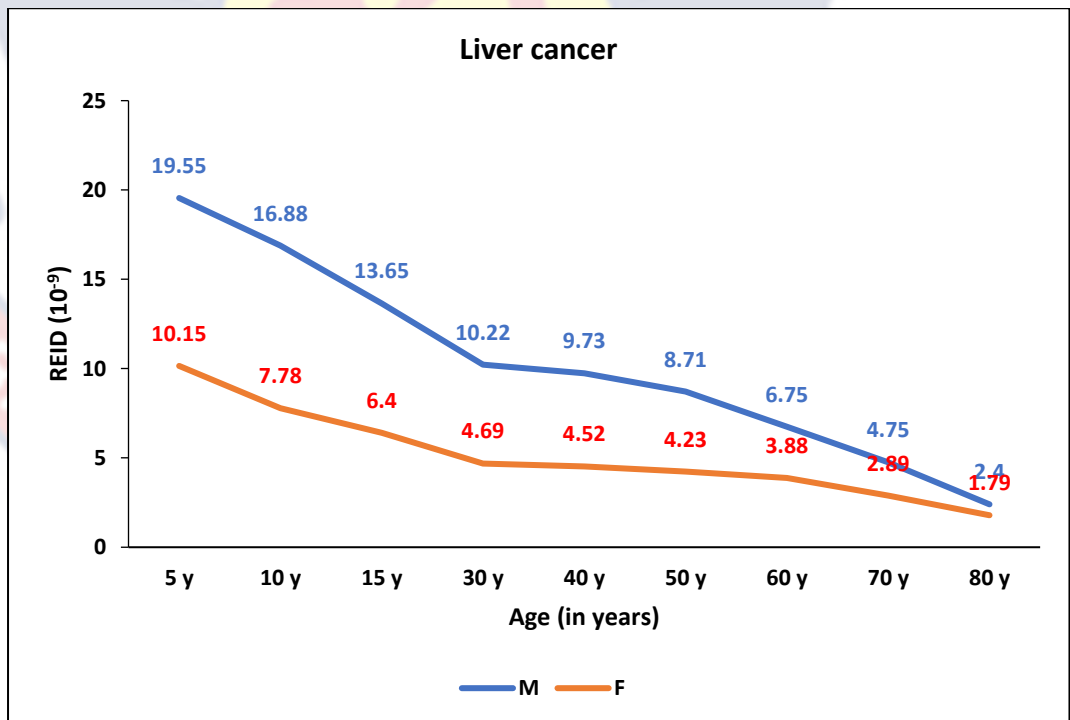


Figure 18c: The REID Values for Liver Cancer from the Kh-0.5-105 Panoramic Equipment Model

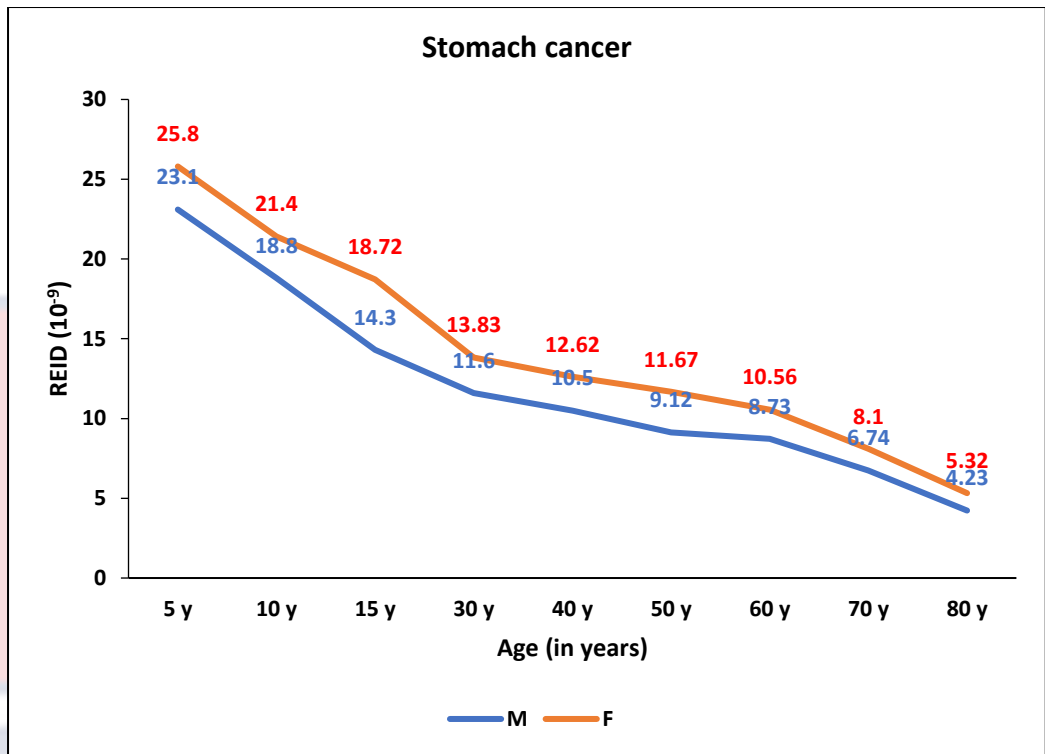


Figure 18d: The REID Values for Stomach Cancer from the Kh-0.5-105 Panoramic Equipment Model

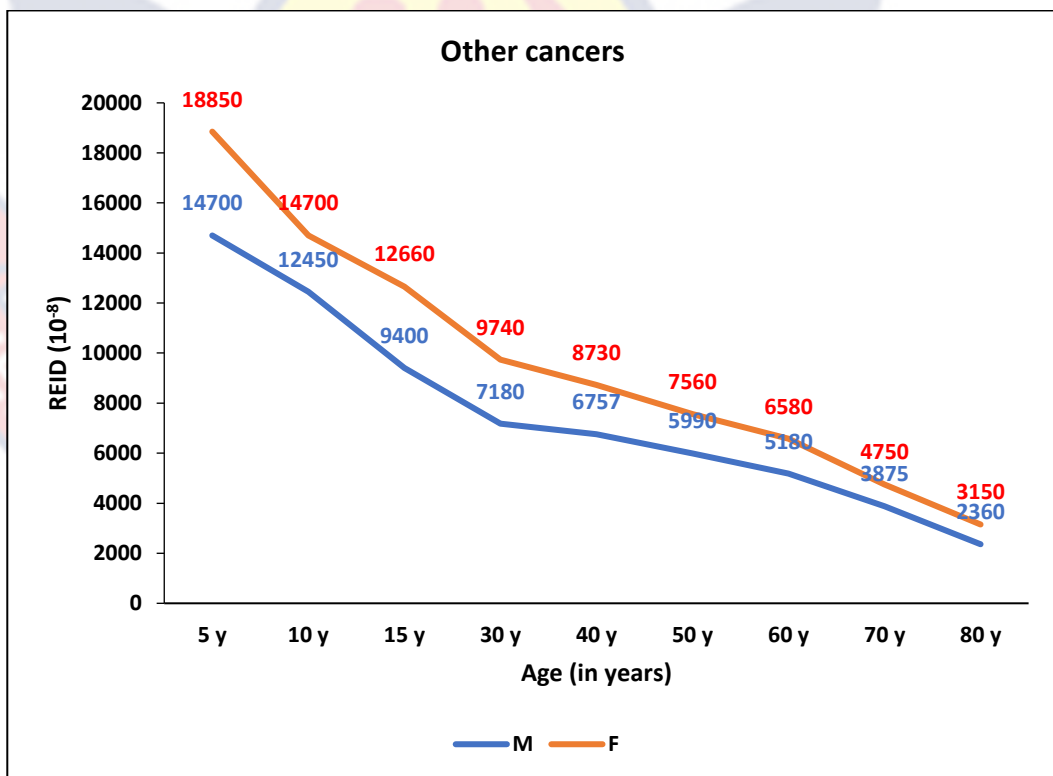


Figure 18e: The REID Values for Other Cancers from the Kh-0.5-105 Panoramic Equipment Model

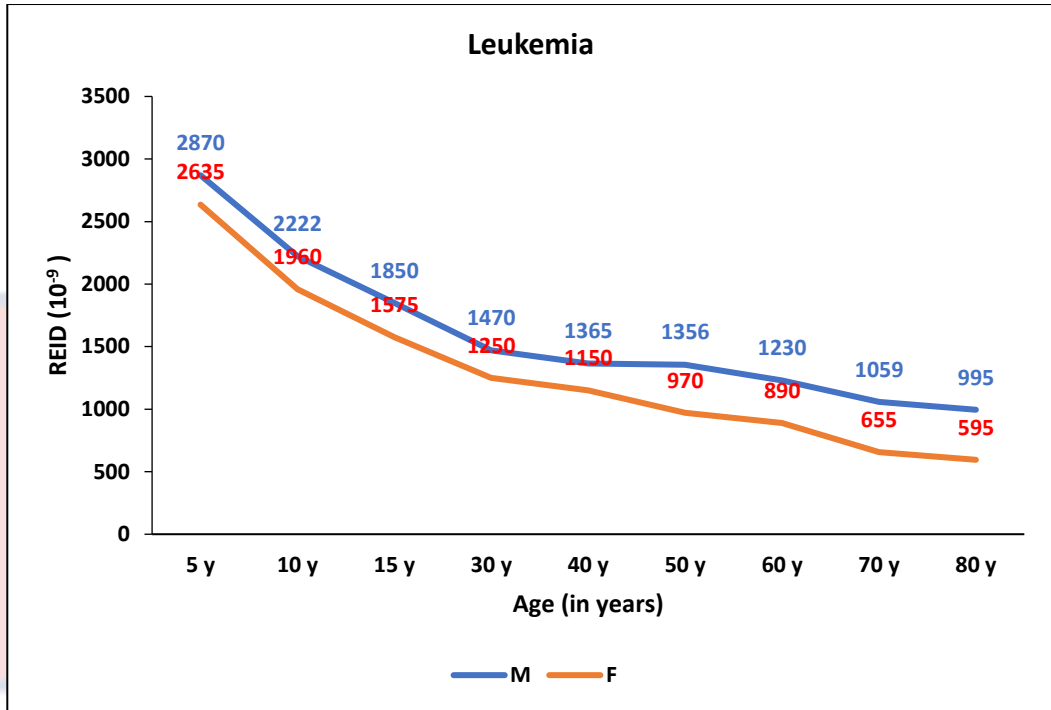


Figure 19a: The REID Values for Leukemia from the CS8100SC Panoramic Equipment Model

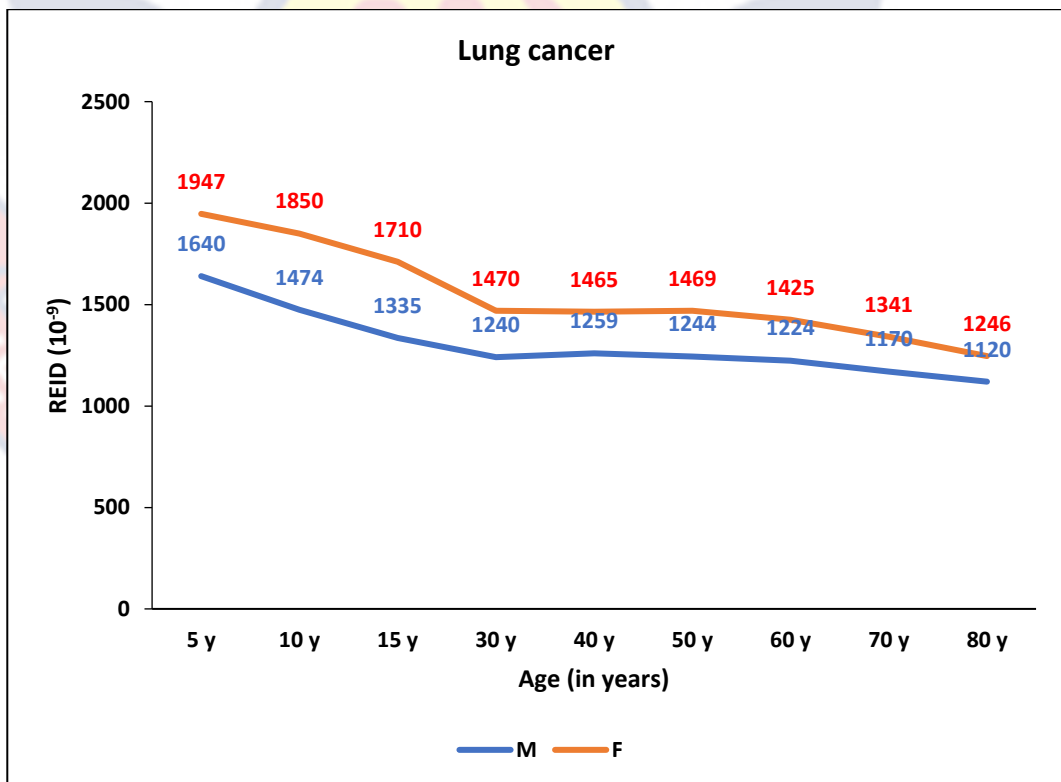


Figure 19b: The REID Values for Lung Cancer from the CS8100SC Panoramic Equipment Model.

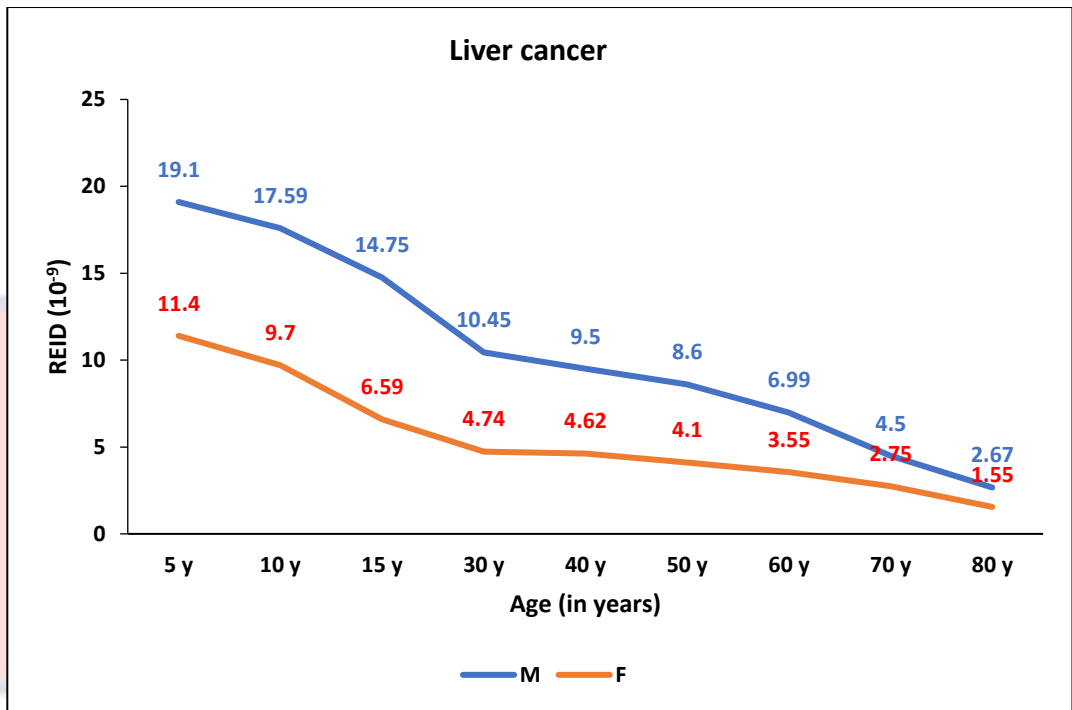


Figure 19c: The REID Values for Liver Cancer from the CS8100SC Panoramic Equipment Model

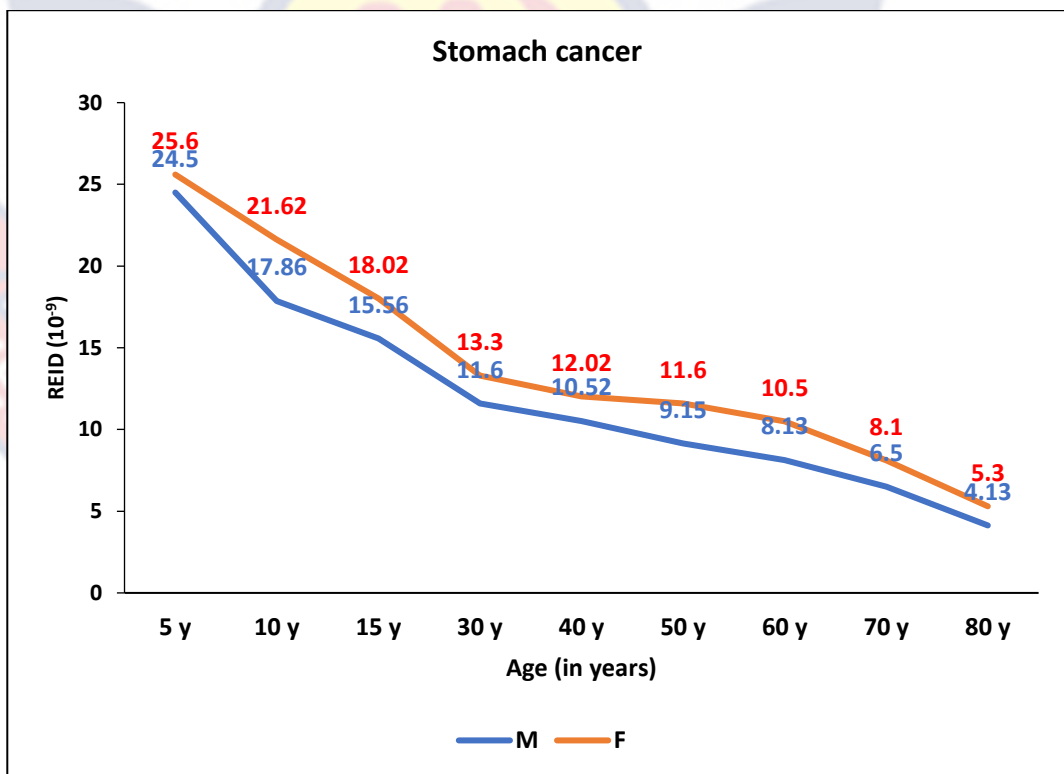


Figure 19d: The REID Values for Stomach Cancer from the CS8100SC Panoramic Equipment Model.

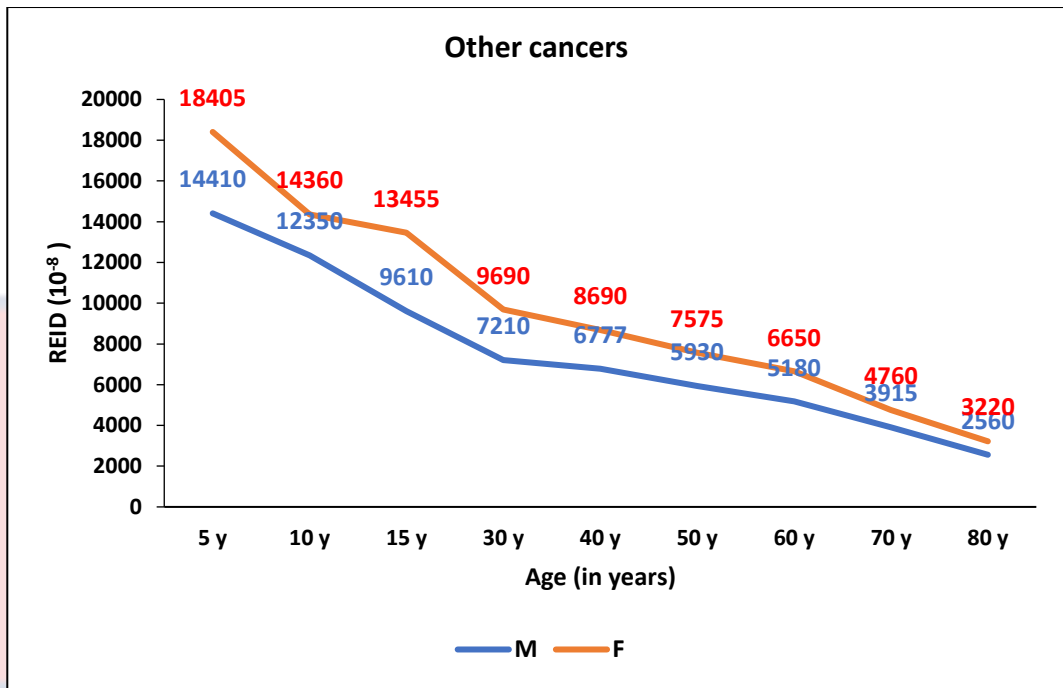


Figure 19e: The REID Values for Other Cancers from the CS8100SC Panoramic Equipment Model

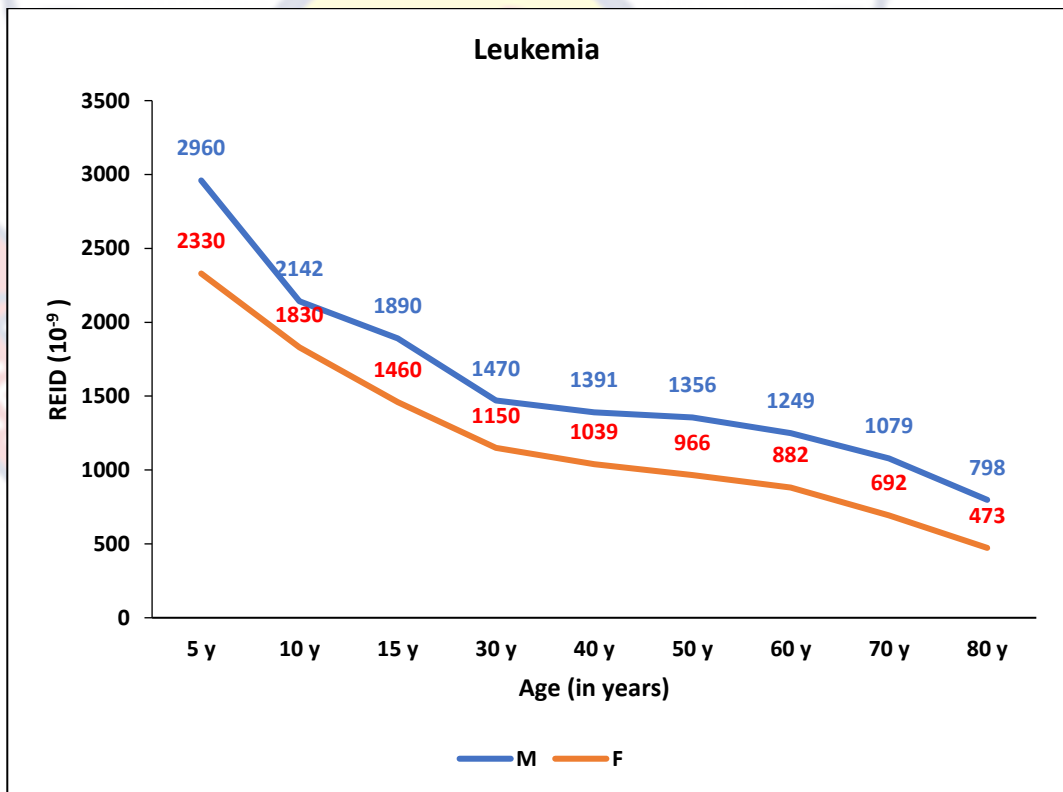


Figure 20a: The REID Values for Leukemia from the OPX105 Panoramic Equipment Model

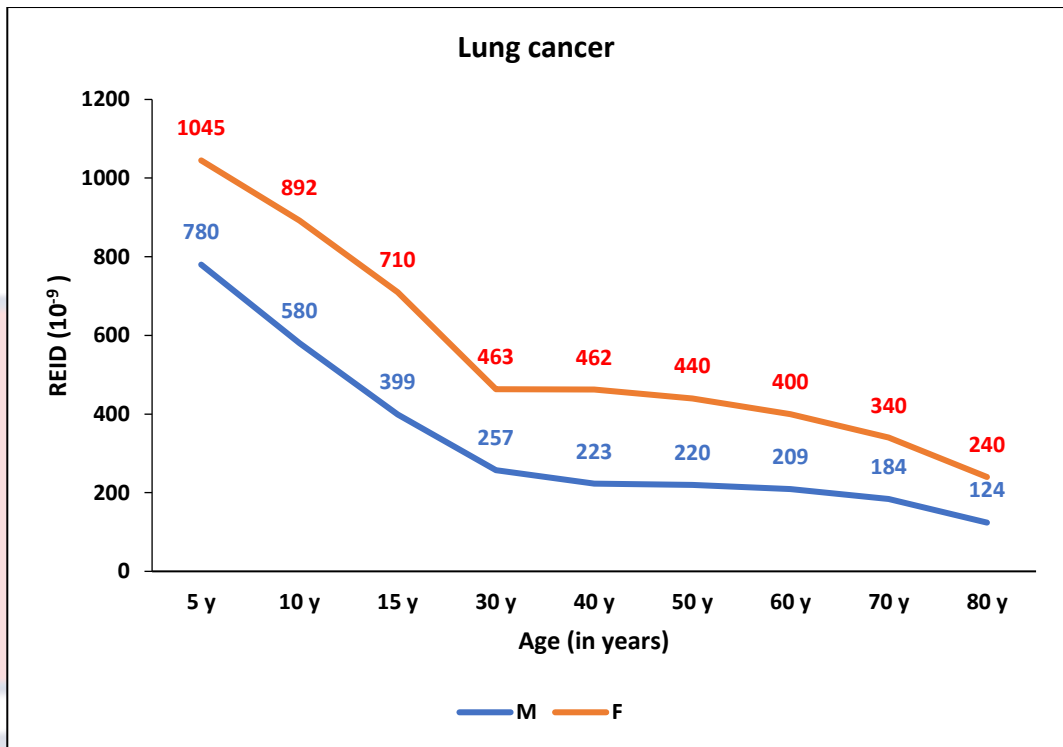


Figure 20b: The REID Values for Lung Cancer from the OPX105 Panoramic Equipment Model

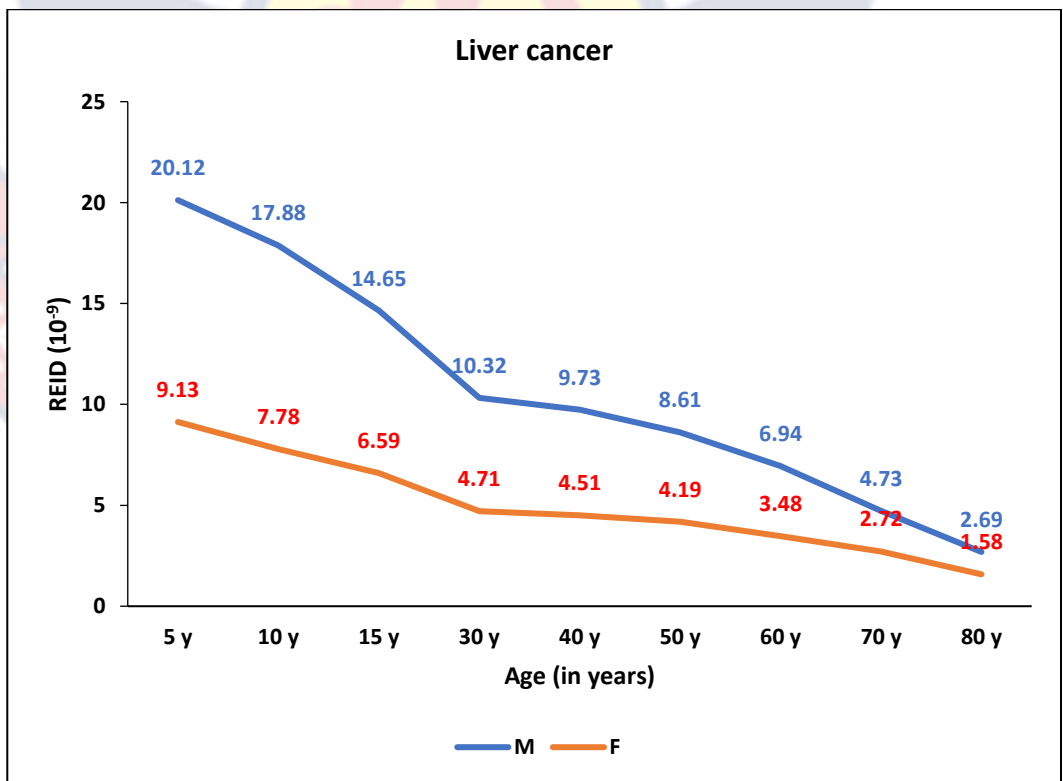


Figure 20c: The REID Values for Liver Cancer from the OPX105 Panoramic Equipment Model

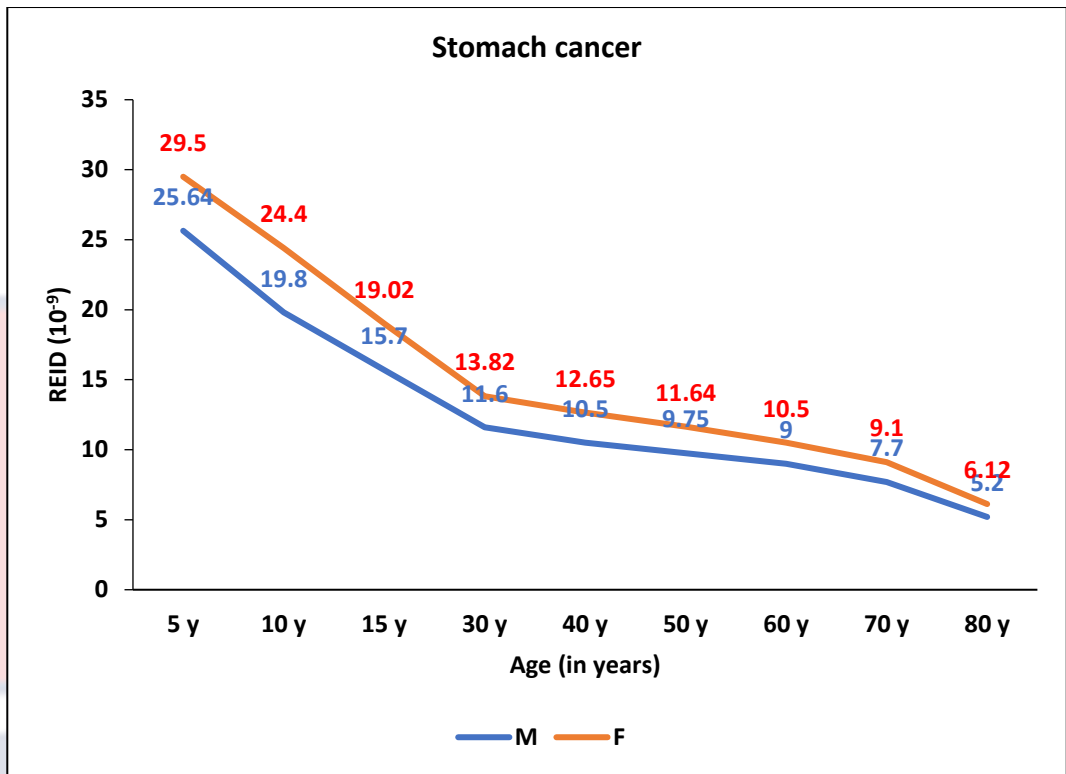


Figure 20d: The REID Values for Stomach Cancer from the OPX105 Panoramic Equipment Model

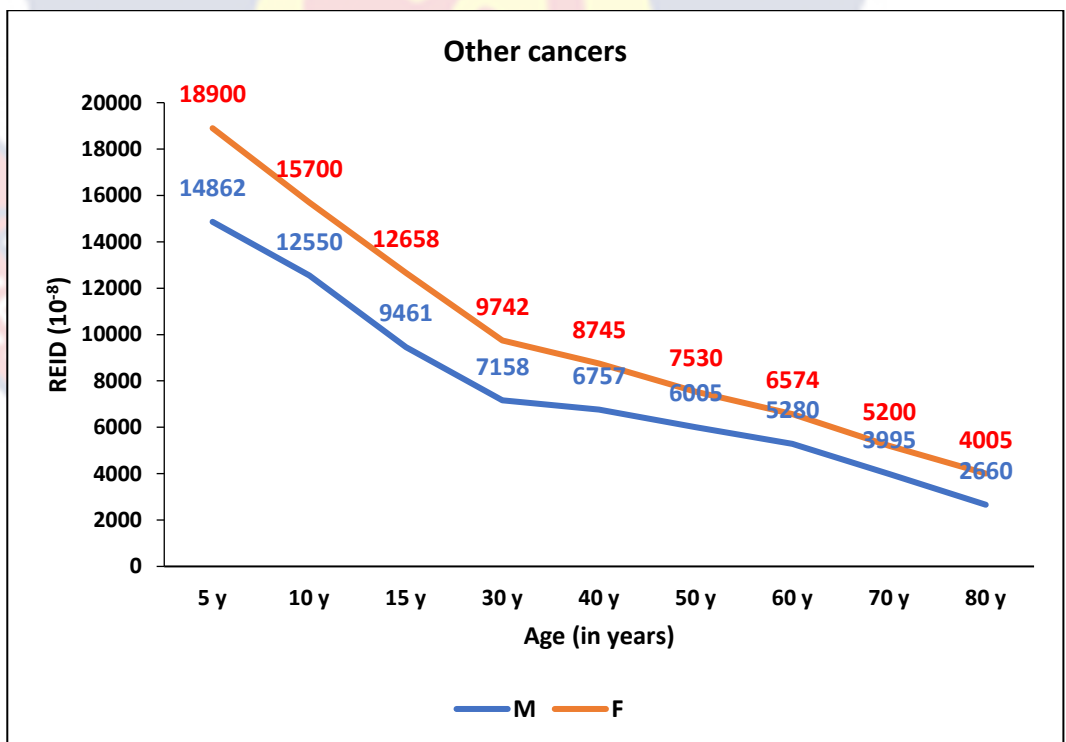
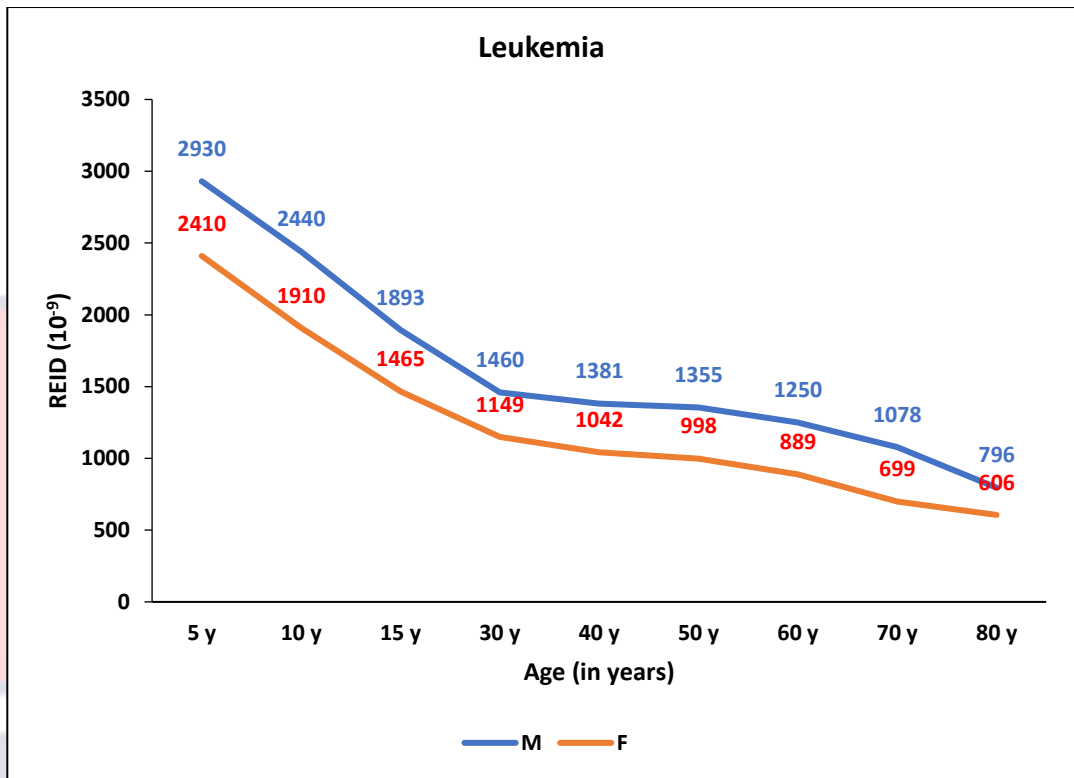
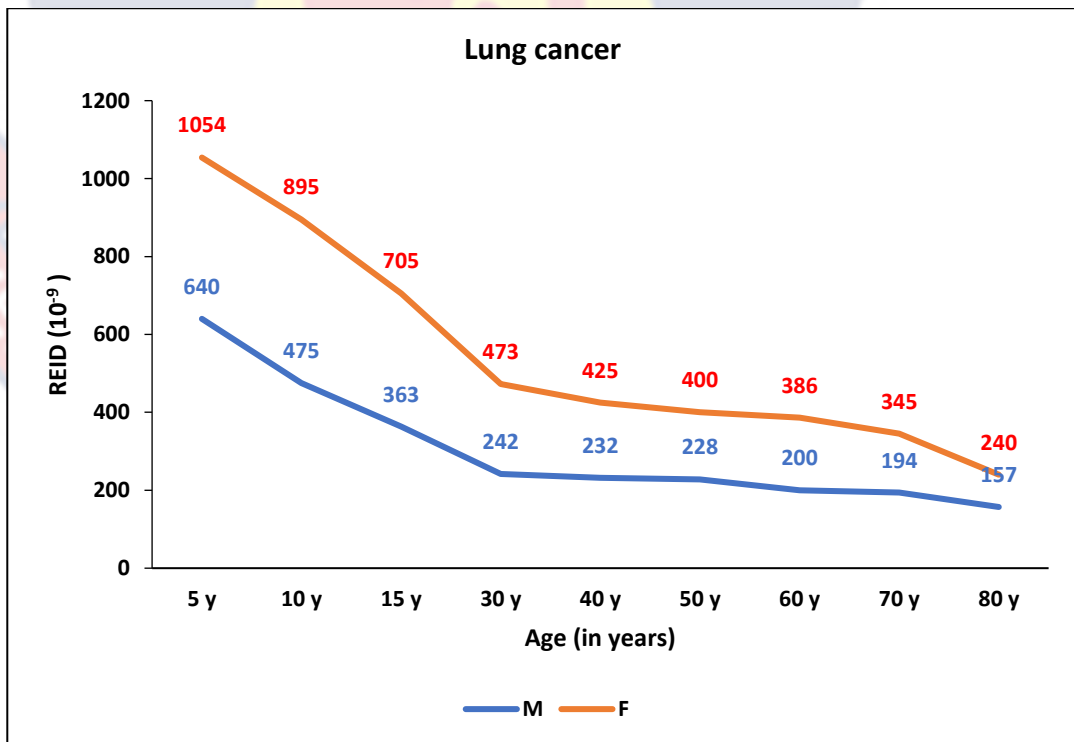


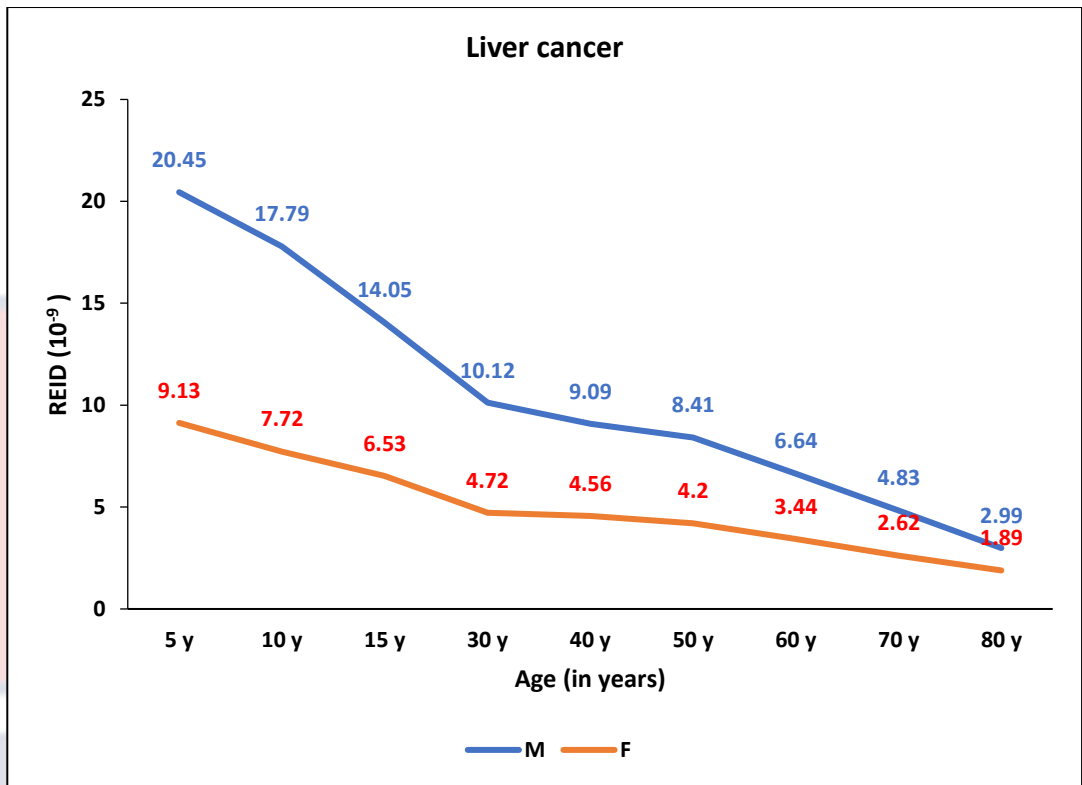
Figure 20e: The REID Values for Other Cancers from the OPX105 Panoramic Equipment Model



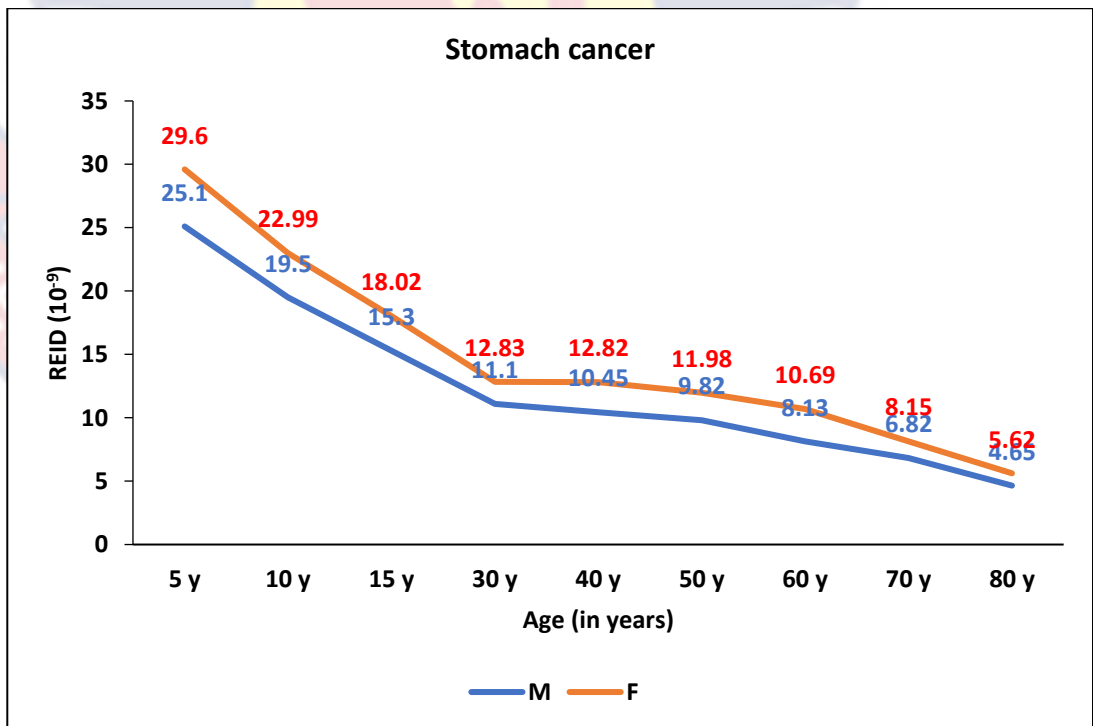
Figures 21a: The REID Values for Leukemia from the PHT-6500 Panoramic Equipment Model



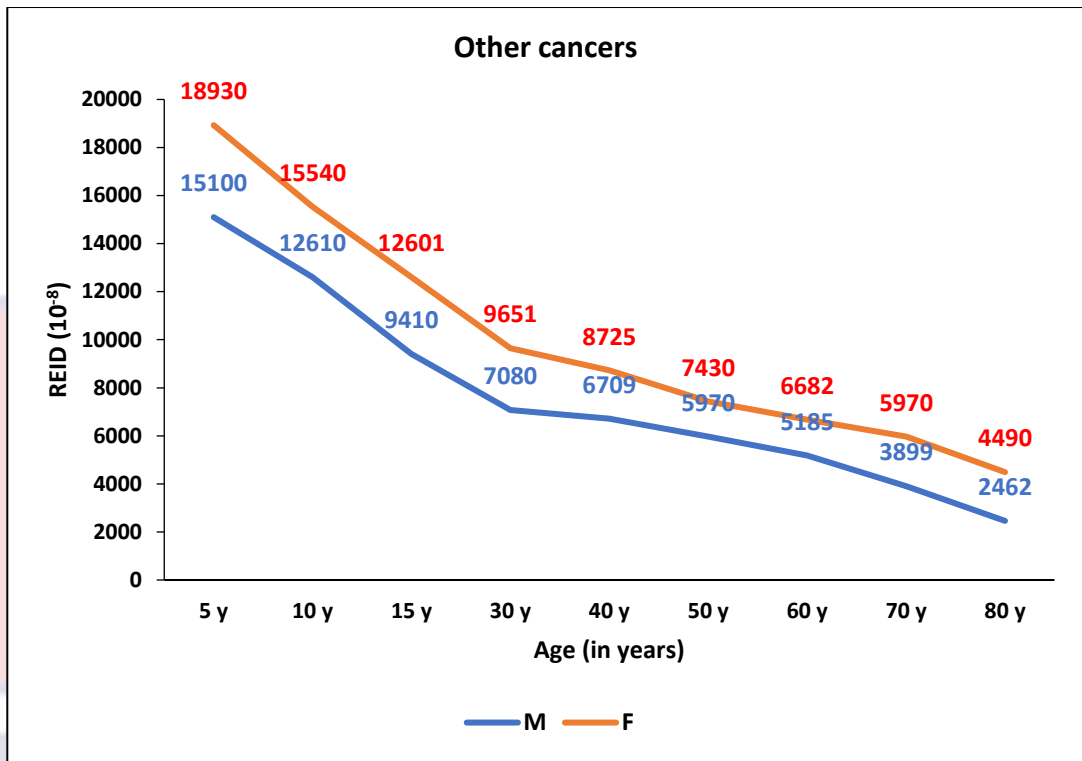
Figures 21b: The REID Values for Lung Cancer from the PHT-6500 Panoramic Equipment Model



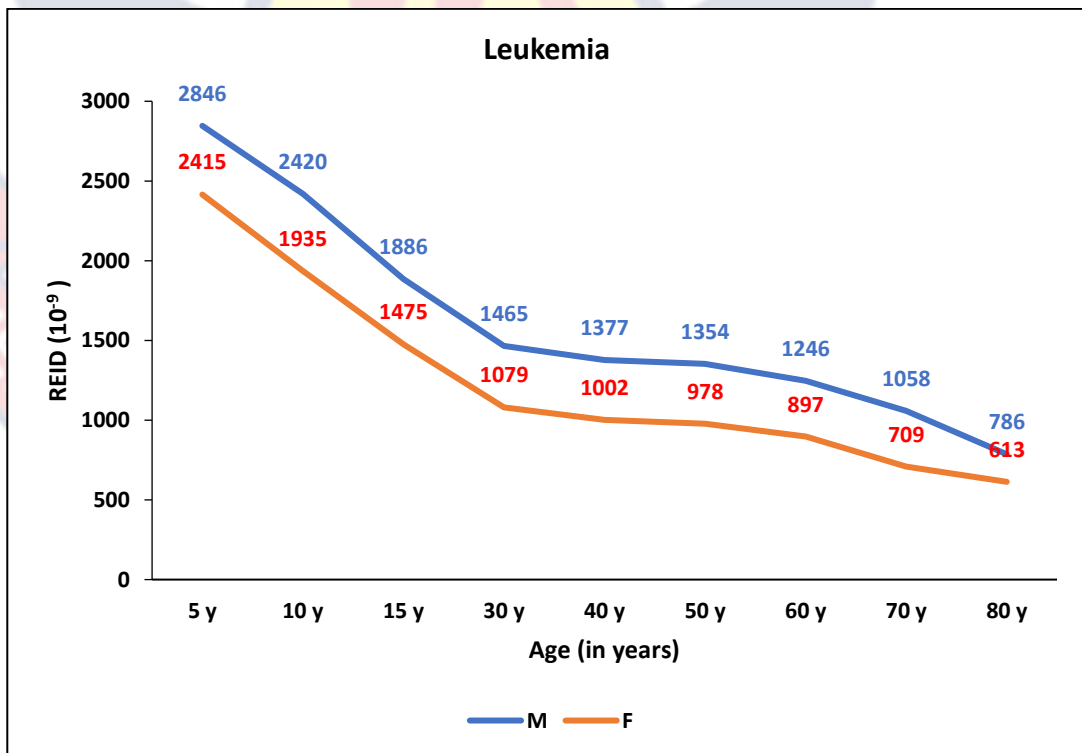
Figures 21c: The REID Values for Liver Cancer from the PHT-6500 Panoramic Equipment Model



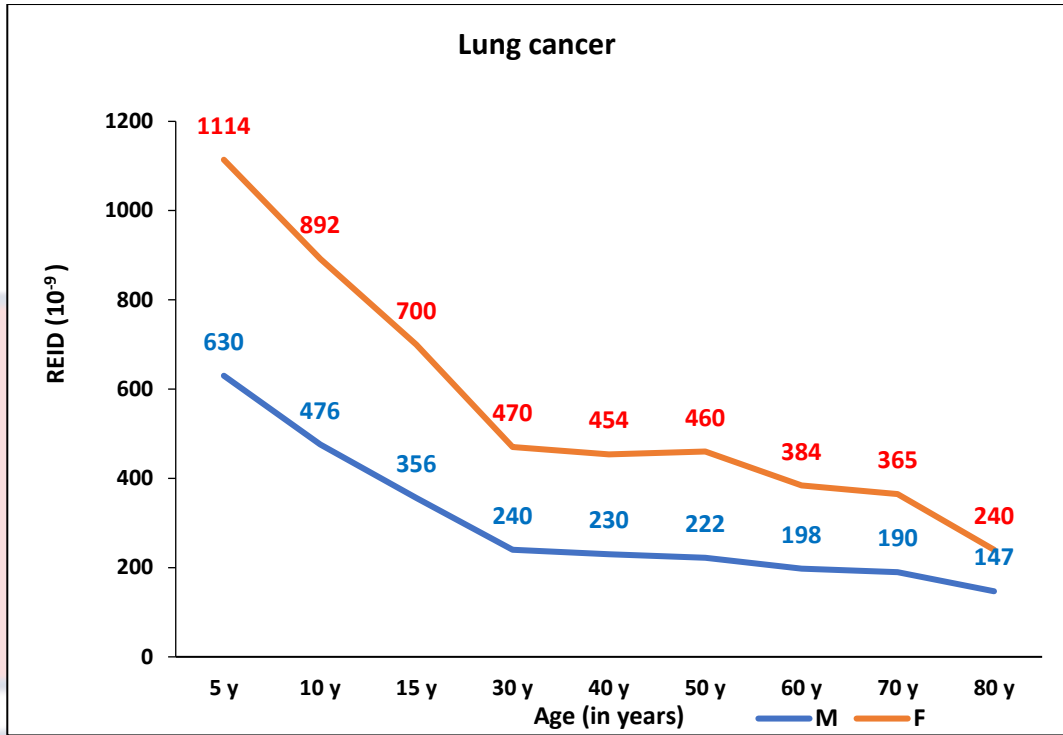
Figures 21d: The REID Values for Stomach Cancer from the PHT-6500 Panoramic Equipment Model



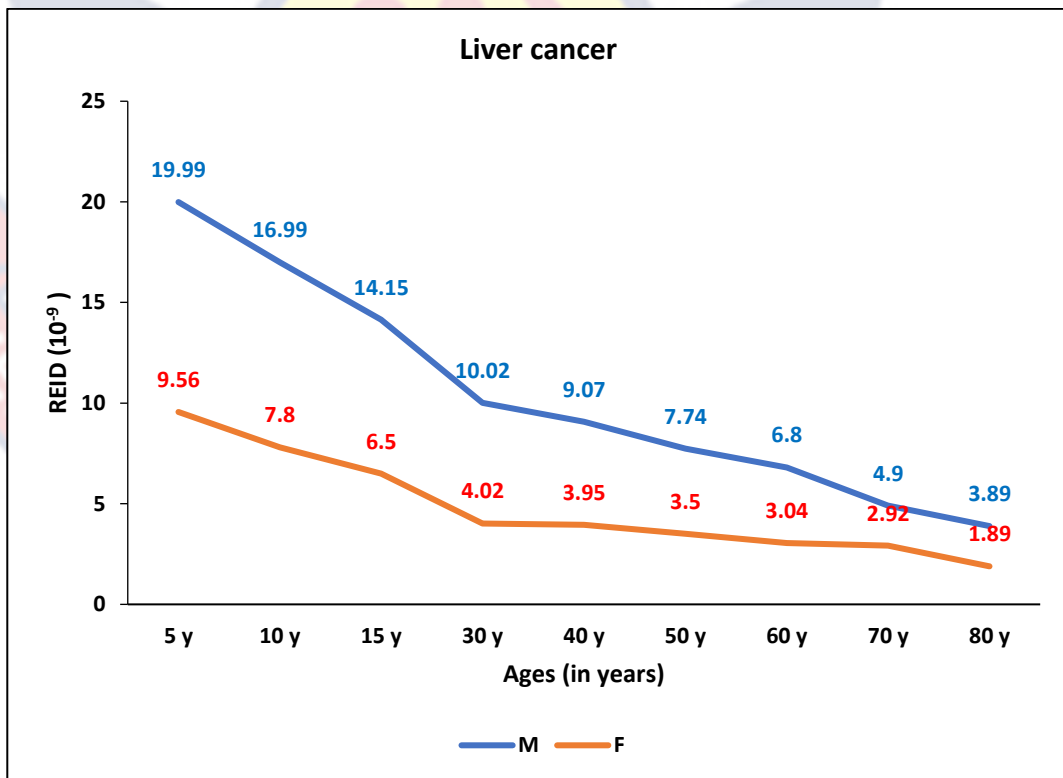
Figures 21e: The REID Values for Other Cancers from the PHT-6500 Panoramic Equipment Model



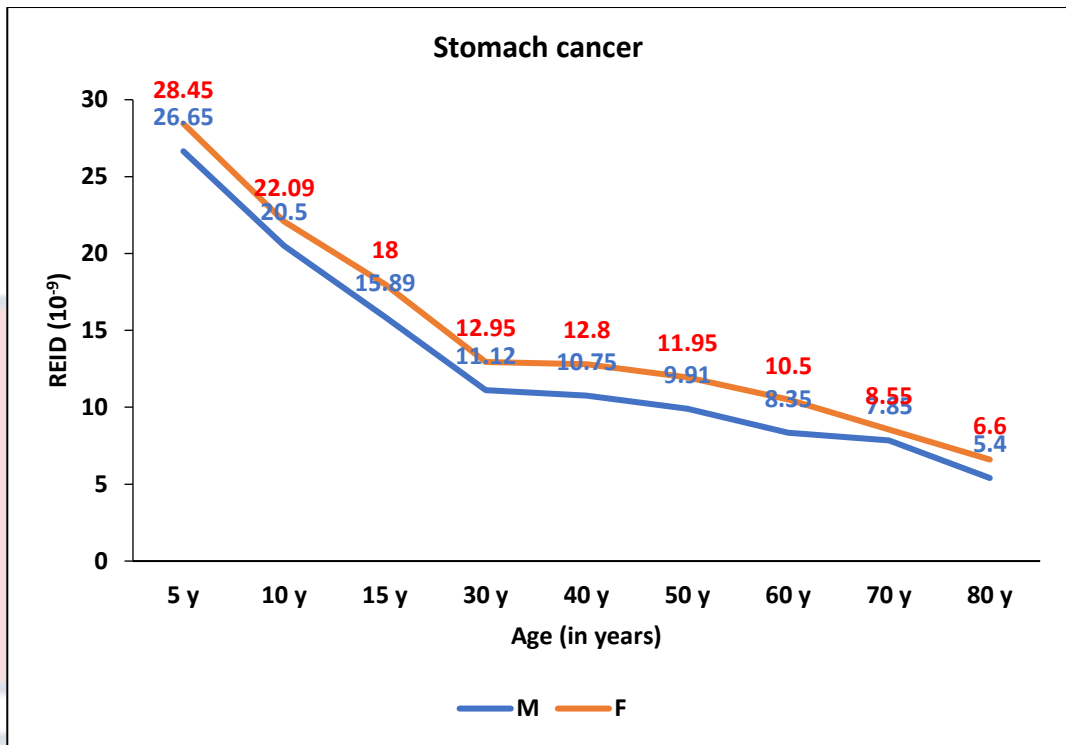
Figures 22a: The REID Values for Leukemia from the GX100-20DC Panoramic Equipment Model



Figures 22b: The REID Values for Lung Cancer from the GX100-20DC Panoramic Equipment Model.

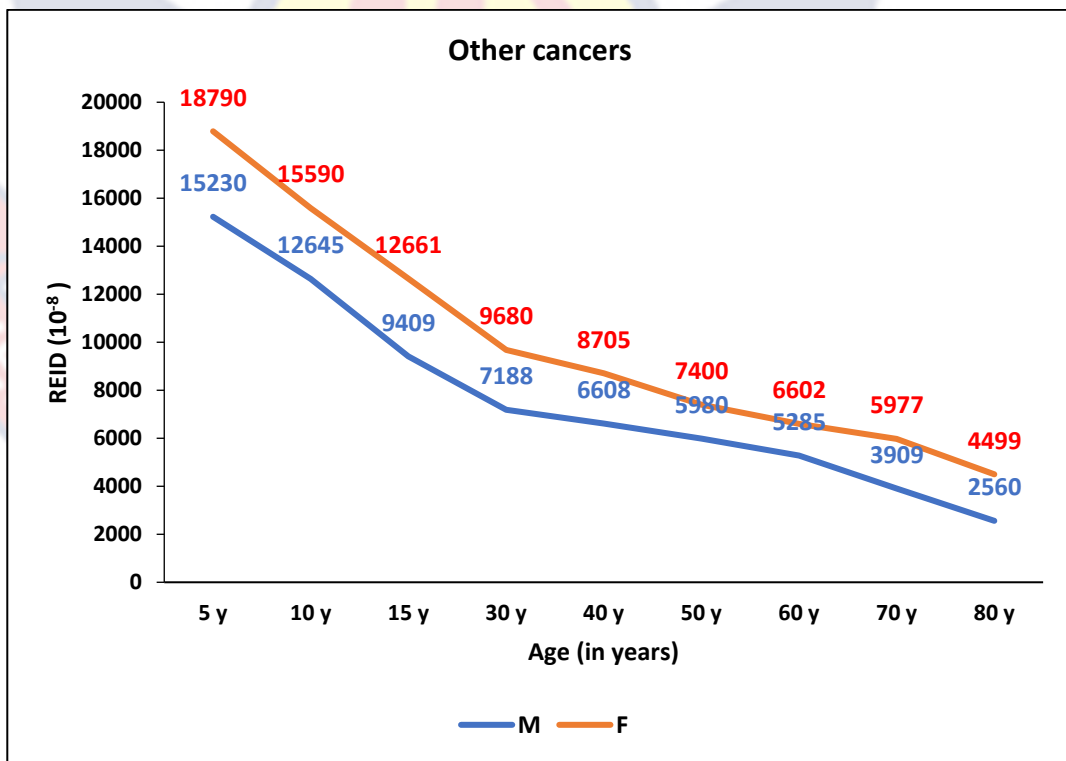


Figures 22c: The REID Values for Liver Cancer from the GX100-20DC Panoramic Equipment Model



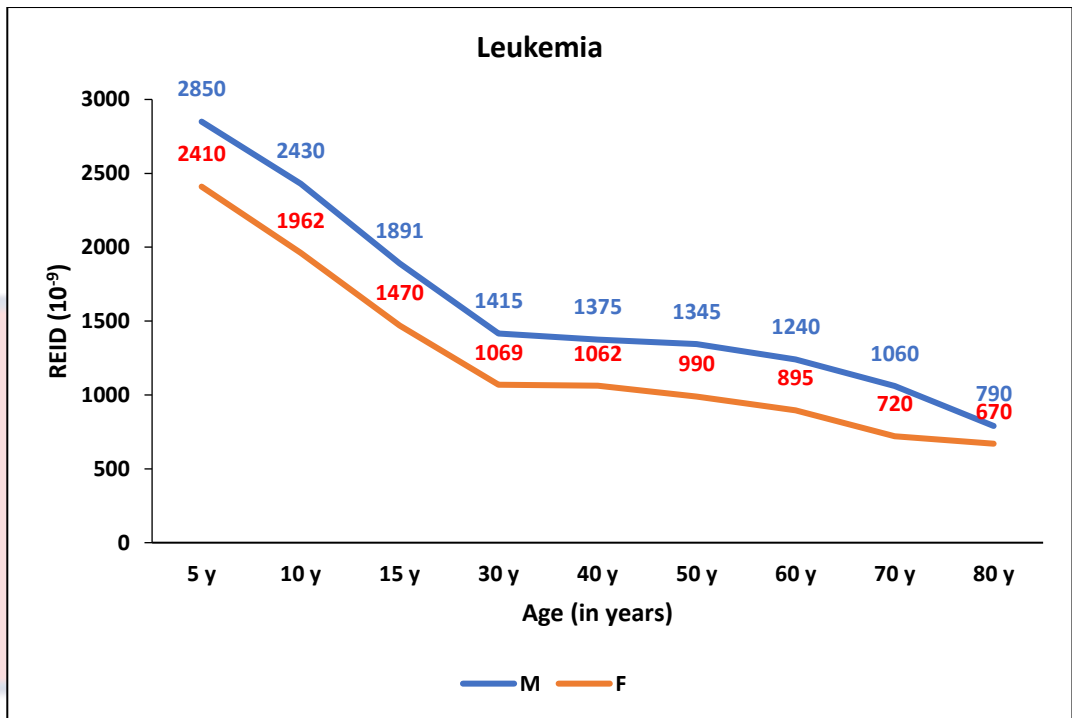
Figures 22d: The REID Values for Stomach Cancer from the GX100-20DC

Panoramic Equipment Model

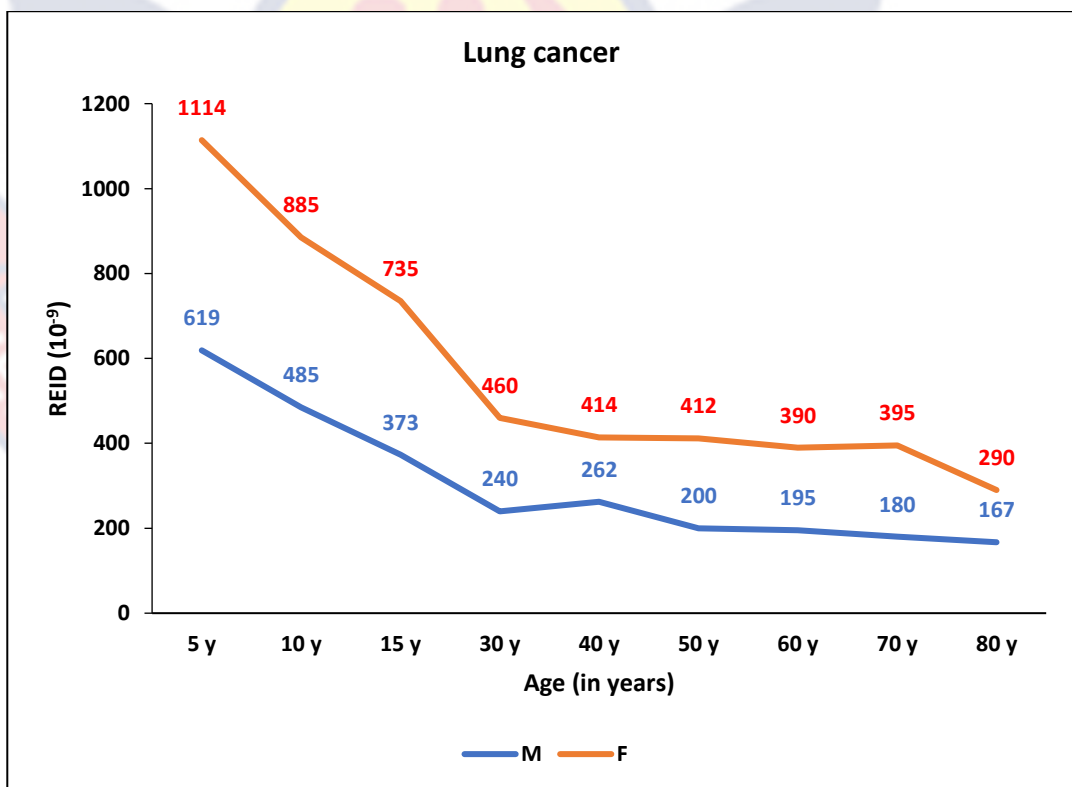


Figures 22e: The REID Values for Other Cancers from the GX100-20DC

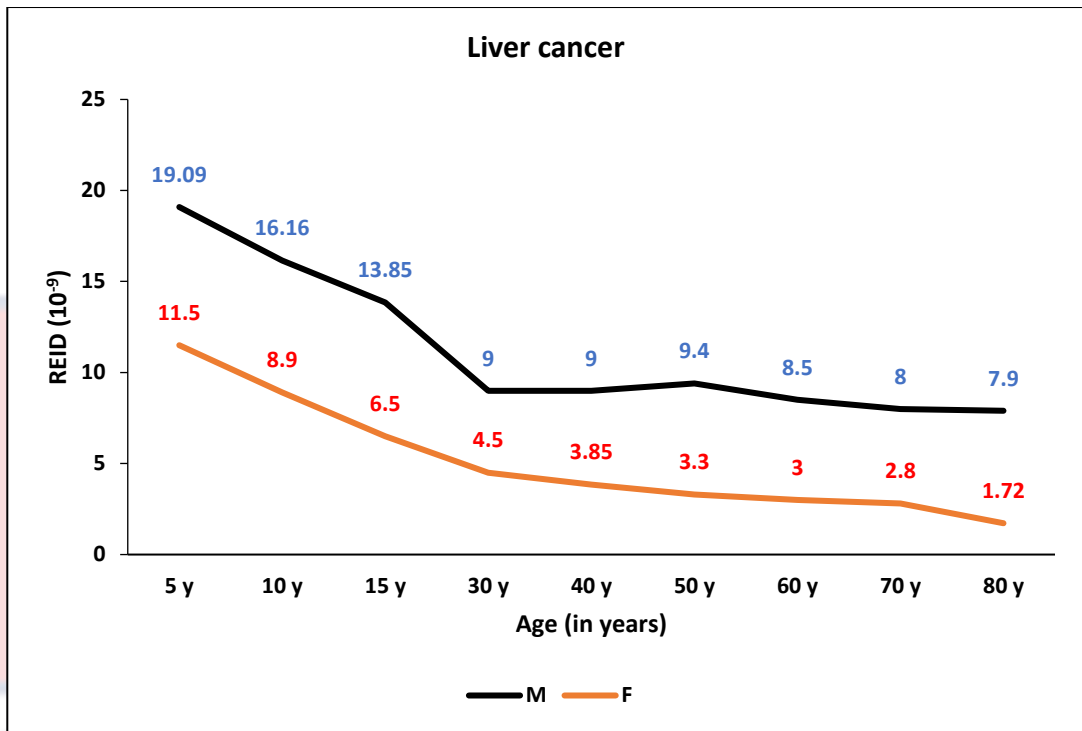
Panoramic Equipment Model



Figures 23a: The REID Values for Leukemia from the 1117340V1010 Panoramic Equipment Model

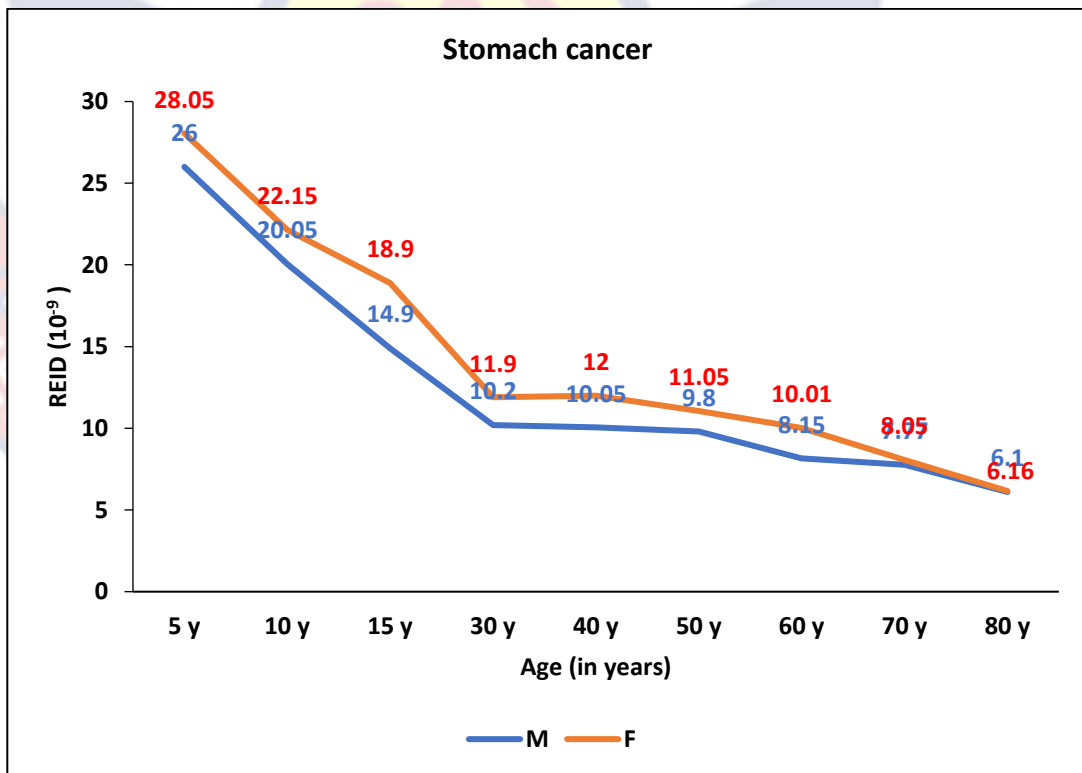


Figures 23b: The REID Values for Lung Cancer from the 1117340V1010 Panoramic Equipment Model



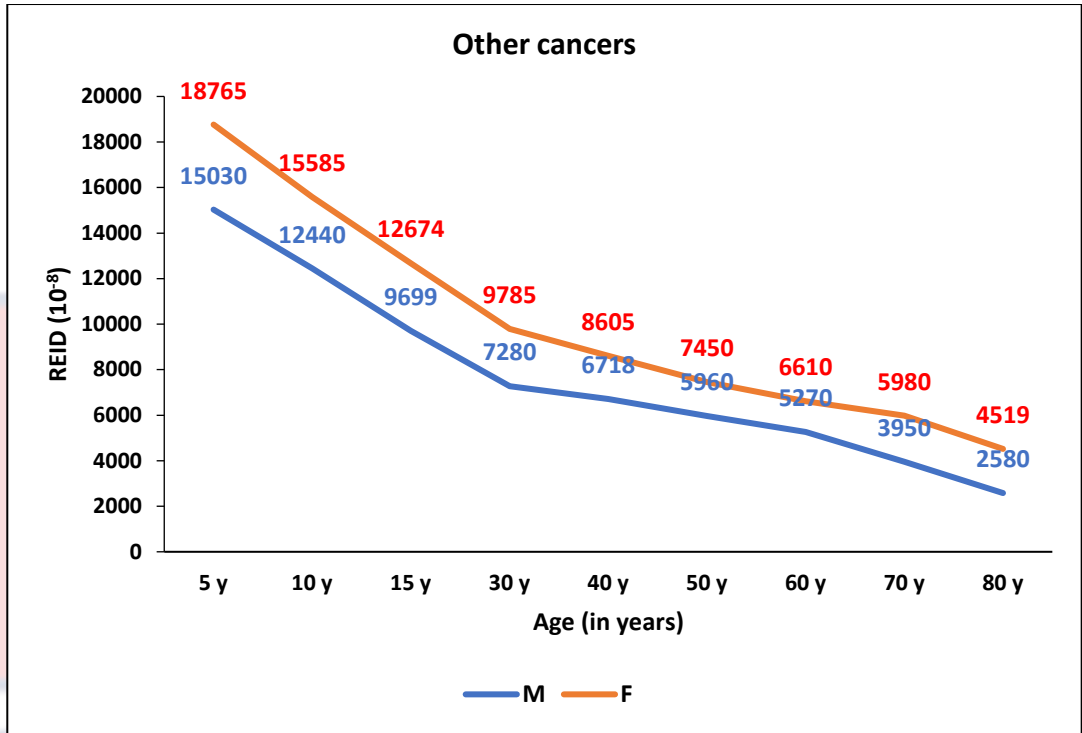
Figures 23c: The REID Values for Liver Cancer from the 1117340V1010

Panoramic Equipment Model



Figures 23d: The REID Values for Stomach Cancer from the 1117340V1010

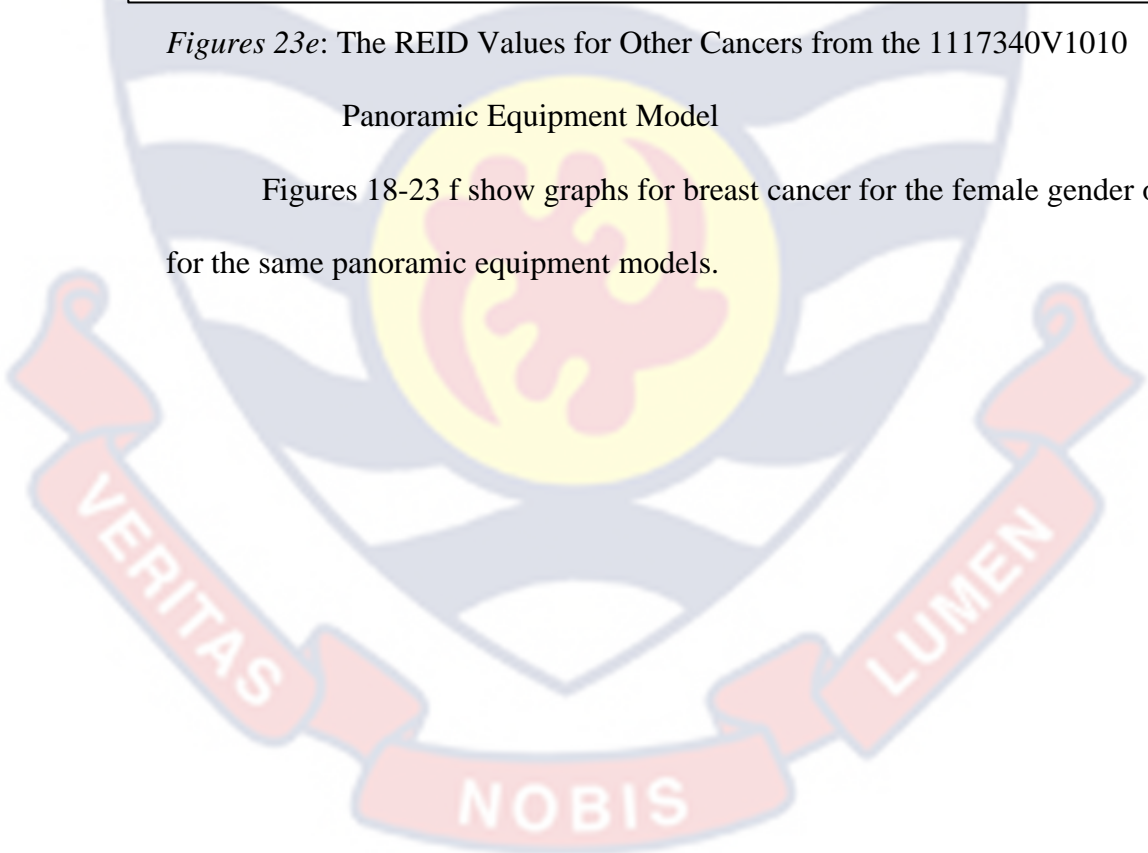
Panoramic Equipment Model



Figures 23e: The REID Values for Other Cancers from the 1117340V1010

Panoramic Equipment Model

Figures 18-23 f show graphs for breast cancer for the female gender only for the same panoramic equipment models.



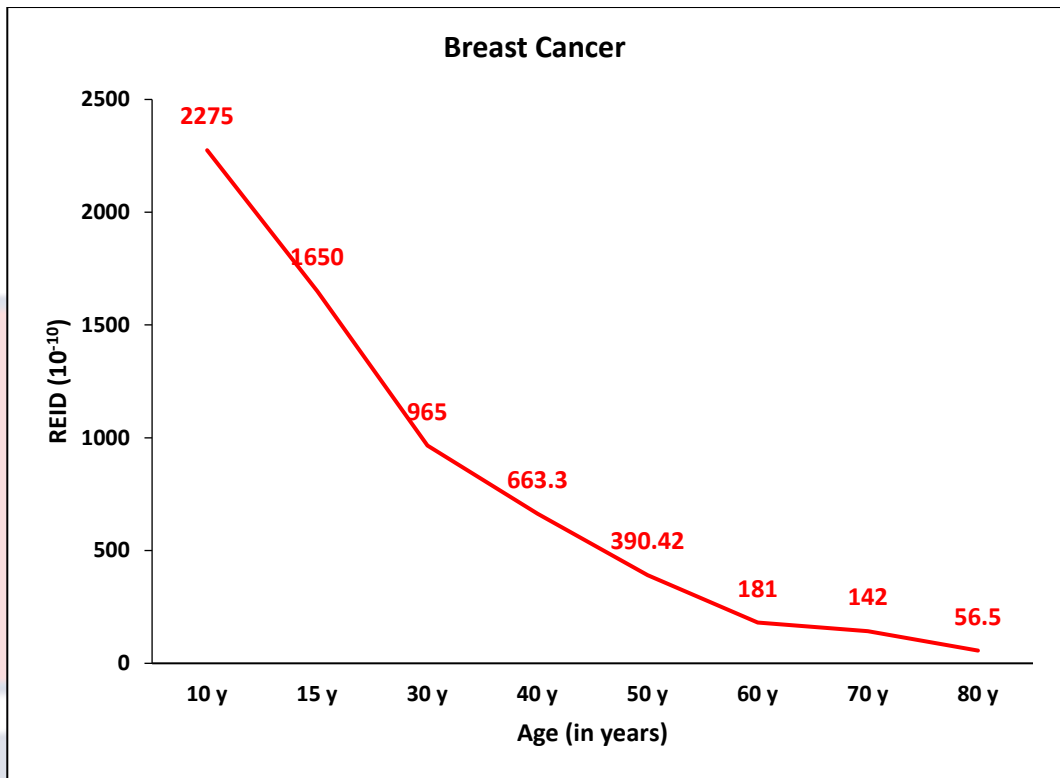


Figure 18f: REID for Breast Cancer from the Kh-0.5-105 Panoramic Equipment Model.

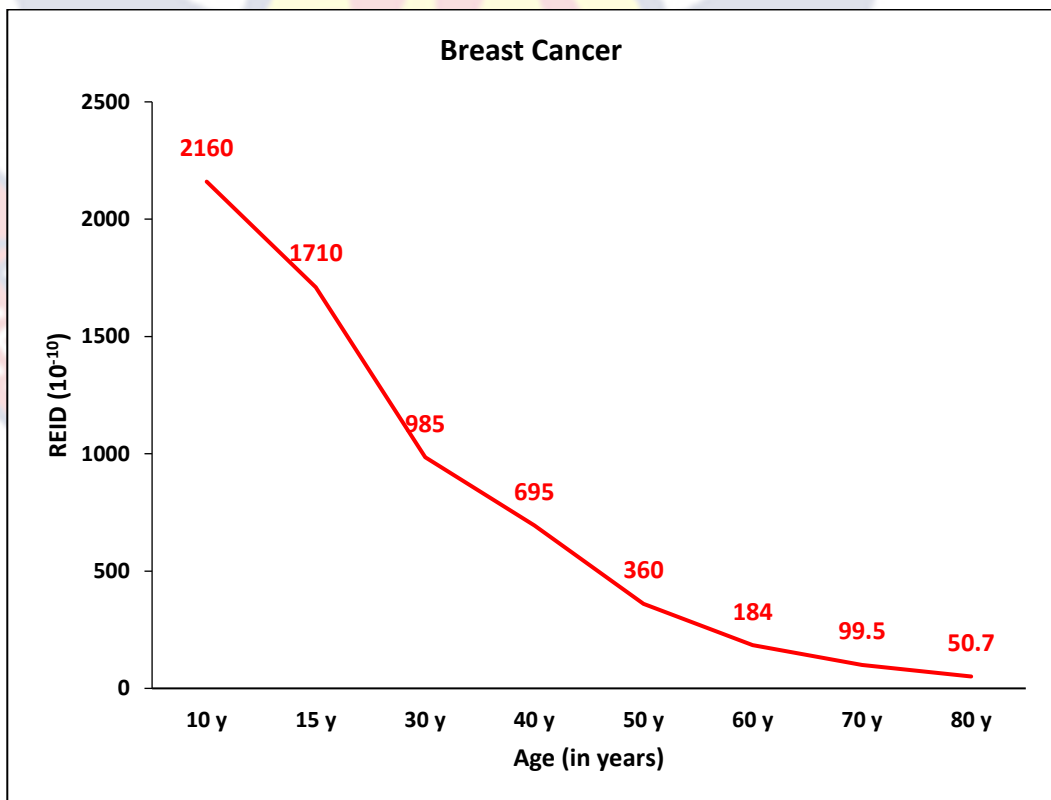
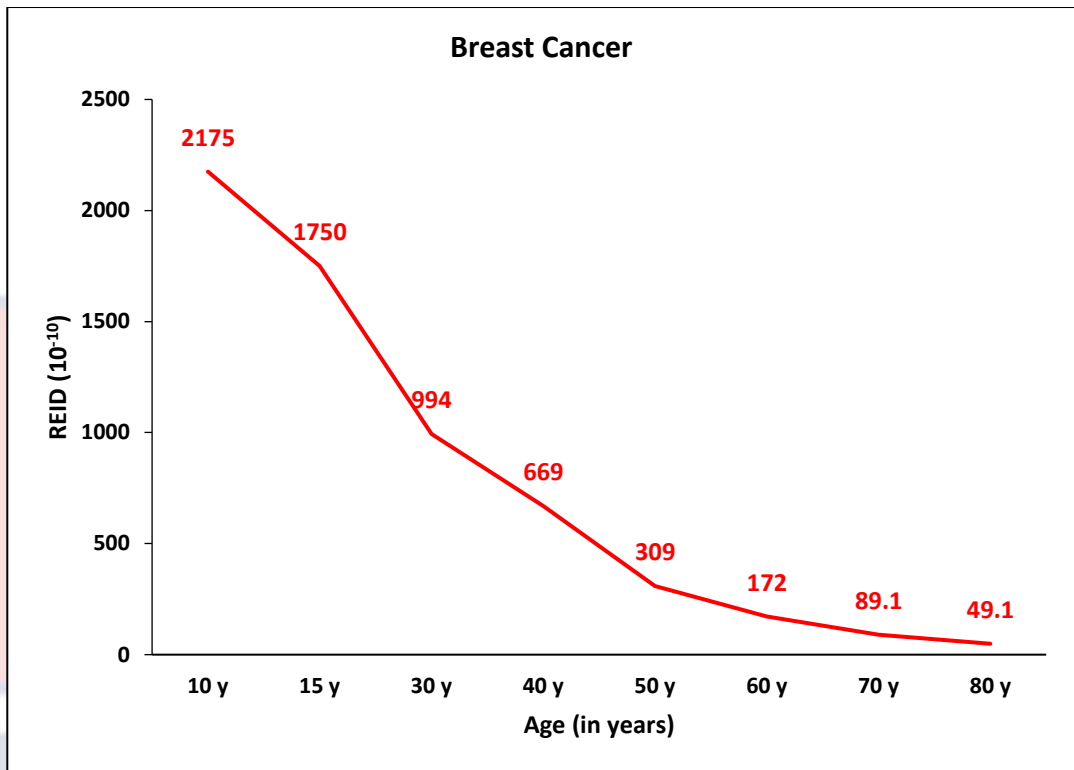
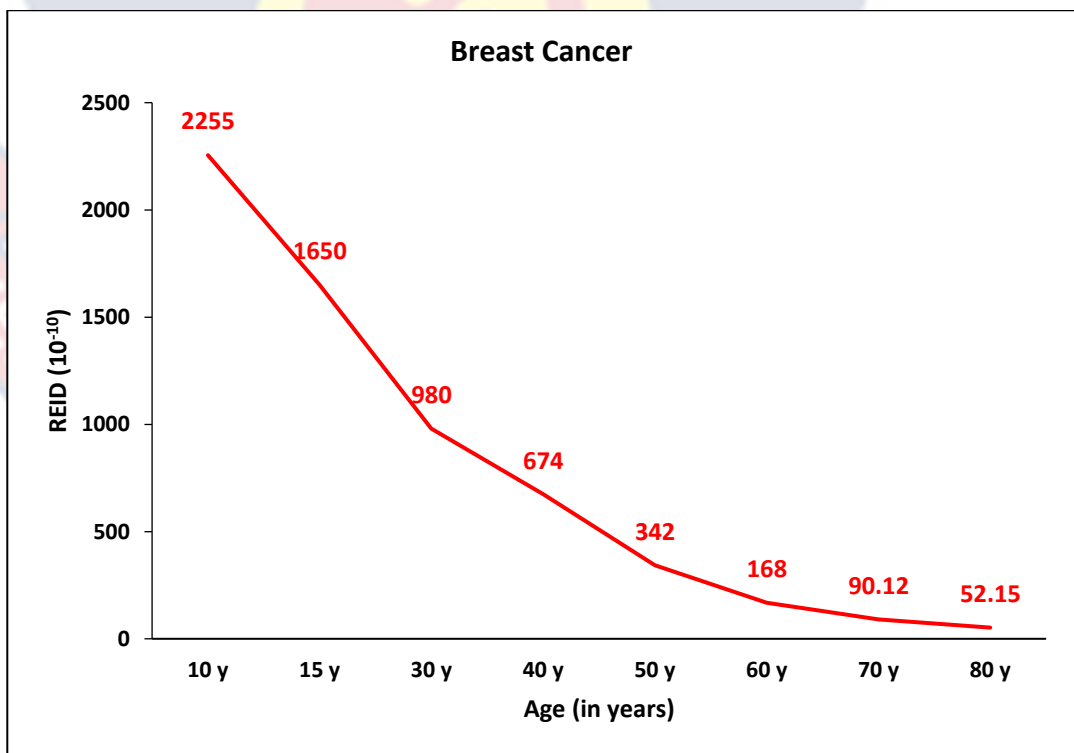


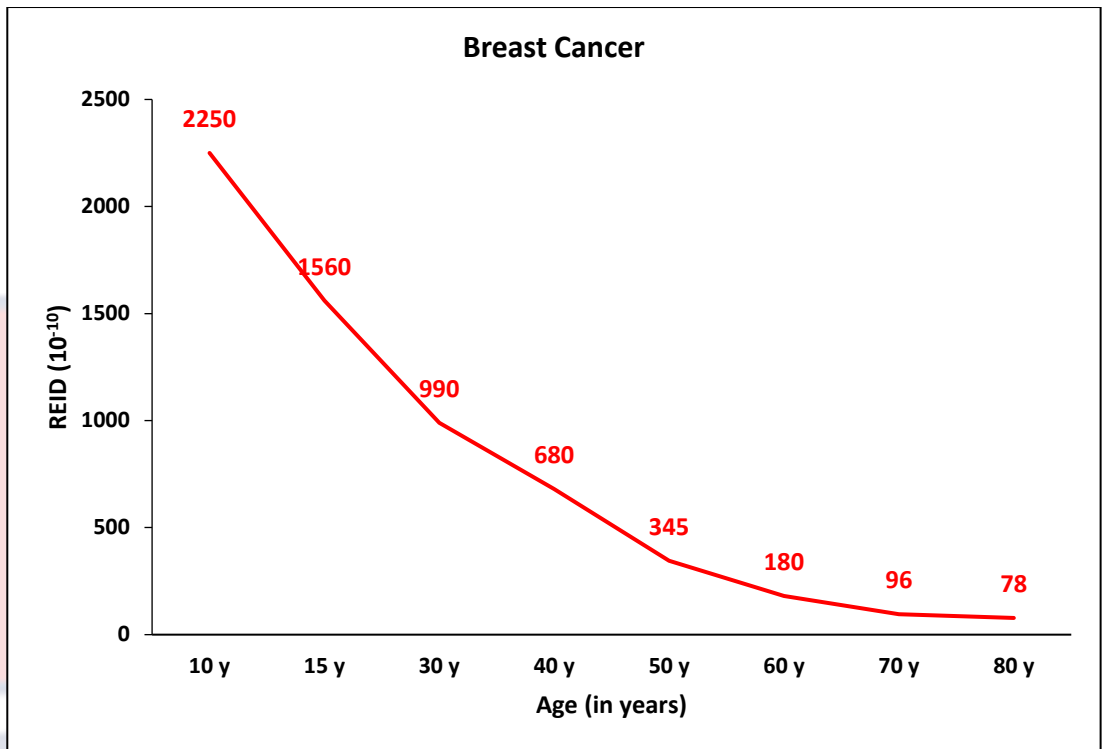
Figure 19f: REID for Breast Cancer from the CS8100SC Panoramic Equipment Model



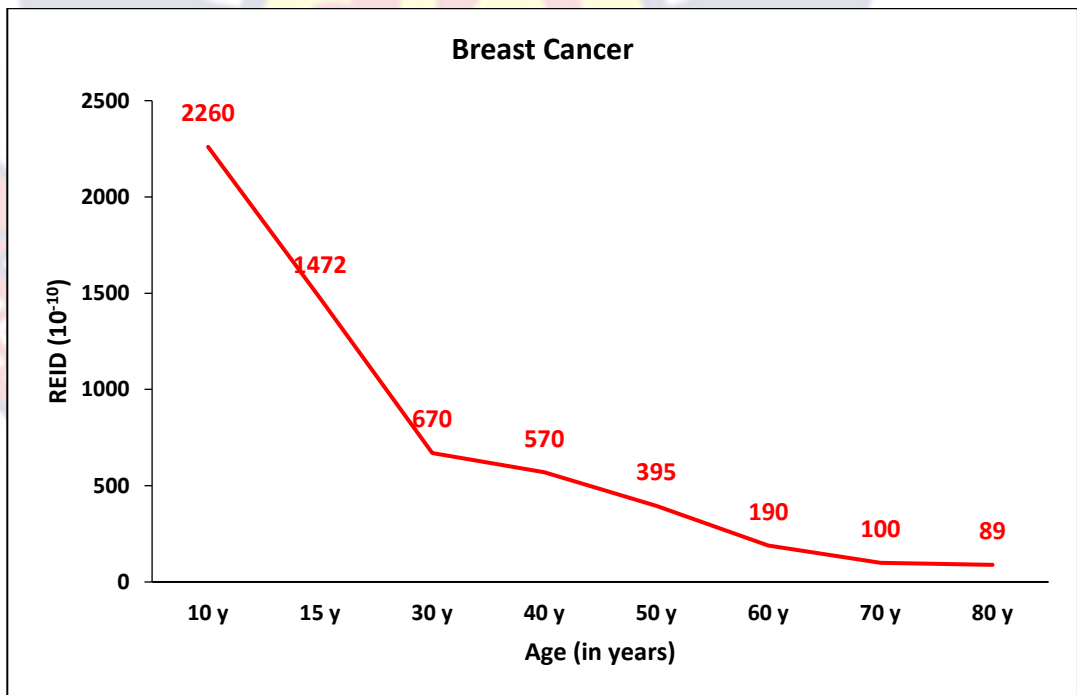
Figures 20f: REID for Breast Cancer from the OPX105 Panoramic Equipment Model



Figures 21f: REID for Breast Cancer from the PHT-6500 Panoramic Equipment Model



Figures 22f: REID for Breast Cancer from the GX100-20DC Panoramic Equipment Model



Figures 23f: REID for Breast Cancer from the 1117340V1010 Panoramic Equipment Model.

The red bone marrow, lung, stomach, liver and breast are tissues and organs that are extremely sensitive to radiation and, as a result, are extremely vulnerable to cancer development. According to ICRP (2007) the tissue weighting factors (W_T) for the organs and tissues are 0.12, 0.12, 0.12, 0.04 and 0.12 respectively. The tissue weighting factor is a relative estimate of the chance of stochastic effects caused by irradiation of that particular tissue. It explains the varying radiosensitivity of organs and tissues to ionising radiation. Higher radiosensitivity is shown by cells that are actively dividing and are less differentiated. While dividing, hematopoietic stem cells in the bone marrow, for example, differentiate into numerous blood cells. Cancer incidences are higher in immature (undifferentiated) hematopoietic cells that have divided (proliferated) from stem cells as a consequence of a tiny amount of radiation than in differentiated cells because they are more sensitive to radiation. As a result, the supply of blood cells is halted, and the quantity of different types of cells in the blood decreases.

Males were found to have higher REID for leukemia and liver cancer than females; however, females had higher risks for stomach cancer, lung cancer, and other cancers. In general, the risks for all cancer types were found to be higher in children than adults for all cancer types for both genders, with the exception of breast cancer, which is more common in women. The REID values for the five individual cancers did not decline monotonically with increasing age at exposure, with only a minor change after 30 years of age. Beyond thirty years, the decrease of radiation risk became smoother. The risks of developing radiation-induced breast cancer peaked at the age of 10 and steadily declined with increasing age at exposure (Figures 18-23 f). Girls between the ages of 10 and 20 experience rapid

cell proliferation in the breast tissue, which enhances the breast's sensitivity to radiation (Yeh & Chen, 2018). Women under the age of 20 have a higher chance of developing breast cancer linked to radiation exposure than those exposed at older ages. According to Preston (Preston et al., 2002), there is no measurably increased chance of breast cancer in women over the age of 50. According to previous studies (Russo & Russo, 1997); (Moolgavkar et al., 1980), the in-utero, puberty, and pregnancy phases indicate increased susceptibility to mammary carcinogenesis because they are times of increased cell proliferation.

In Figure 18a for instance, the mean REID values obtained for leukaemia for the 5-, 10, 15- year-olds and adult males were respectively 2965×10^{-9} , 2362×10^{-9} , 1880×10^{-9} and 1476×10^{-9} and that of the females were 2300×10^{-9} , 1810×10^{-9} , 1460×10^{-9} and 1140×10^{-9} respectively. Comparing the REID values for the two genders for all the age groups confirm that the risk in males is higher than females. Jih-Kuei and Chia-Hui (2018) estimated the individual radiogenic cancers from dental cone-beam computed tomography examination in orthodontics patients, and the findings revealed that leukemia is more common in males than females across all age groups examined, and in children than adults across both genders. According to Jackson (Jackson et al., 1999), leukaemia is prevalent in males at almost every age. In Figure 18 b, the REID values for lung cancer in males were 650×10^{-9} , 484×10^{-9} , 353×10^{-9} and 237×10^{-9} for the respective age categories whereas that of the females were 1041×10^{-9} , 863×10^{-9} , 730×10^{-9} , 353×10^{-9} respectively for the same age categories. Jih-Kuei and Chia-Hui (2018) in their study on the dental CT established that lung cancer risk is higher in females than in males. It is known that women experience more lung cancer than males do (Fidler-Benaoudia et al., 2020). Figure 18 c shows that the

REID values for liver carcinoma were higher in men than in women. The male REID values for liver cancer were 19.55×10^{-9} , 16.88×10^{-9} , 13.65×10^{-9} , 10.22×10^{-9} and that of the female were 10.15×10^{-9} , 7.78×10^{-9} , 6.4×10^{-9} and 4.69×10^{-9} for the respective age brackets. Jih-Kuei and Chia-Hui (2018) in their study on dental cone beam computed tomography similarly had the REID values for the liver cancer being higher within the male population than in the female group. A study was conducted and which established that males were more likely than women to develop liver cancer (Manieri et al., 2019). The stomach and the other cancers were observed to be higher in females than in males as shown in Figures 18 d-e. The specific cancer types and the observed trends were in conformity with that of Jih-Kuei and Chia-Hui (2018) who performed similar REID estimation on cone-beam dental CT equipment. The differences between the organ/tissue specific REID values from the equipment of this study are as a result of variations of the equipment studied. The differences between the organ/tissue specific REID values of this study and the other study by Jih-Kuei and Chia-Hui (2018) are due to different methods employed in obtaining the cancer risk, radiation conditions as well as variations in the dental X-ray equipment.

According to the ICRP (ICRP, 1991), an individual's risk in relation to age are as follows: at ages less than ten years, the multiplication factor is three; between the ages of ten and twenty, the multiplication factor is two; between the ages of twenty and thirty, the multiplication factor is one and half; between the ages of thirty and fifty, the multiplication factor is 0.5; between the ages of fifty and eighty, the multiplication factor is 0.3; and at age eighty and above, the risk is negligible. For both sexes, the multiplication risk is averaged. Women are always at a greater relative risk than men. Beyond the age of eighty, the risk is

negligible because the patient's life span will be surpassed due to the latent time between exposure and manifestation of tumour. On the contrary, the prospective life span of younger people is probable to exceed the latent period because their organs and tissues are more radiosensitive at the early stages of their life. The younger ones are inherently more vulnerable to radiation because there are more dividing cells in the growing children. Additionally, due to their smaller bodies than adults, which receive higher doses of the scattered radiation, nearby organs could potentially be exposed to an increased risk.

According to the Linear No-threshold (LNT) risk assessment model, any amount of radiation exposure could result in cancer in the exposed person due to the stochastic biological effects of ionizing radiation (Council, 2005). Since any amount of radiation has the potential of inducing cancer in the exposed individual, patients must be protected from both the primary and the scattered radiation during panoramic dental radiographies.

Chapter Summary

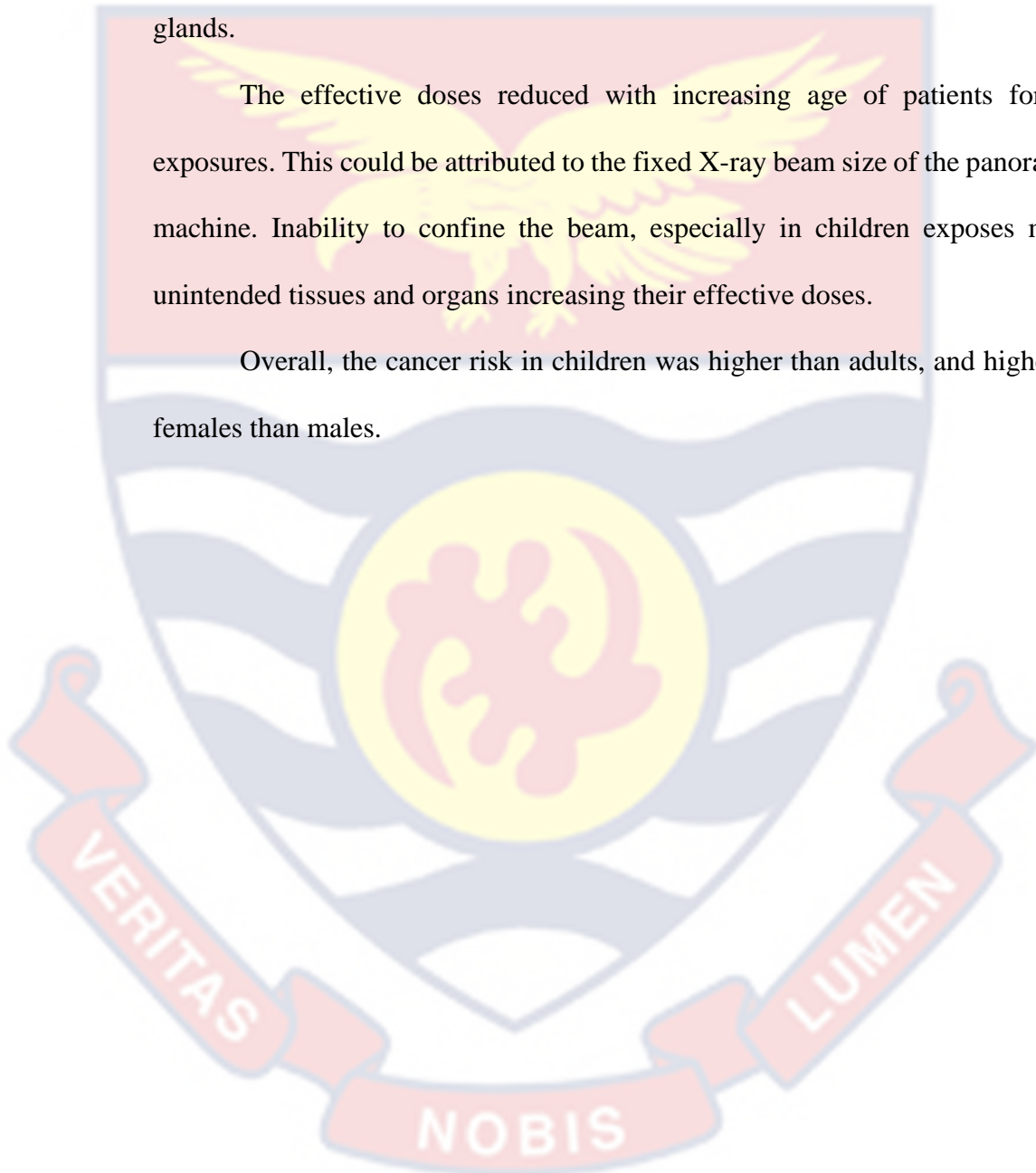
All the six equipment subjected to the quality control procedures passed the tests (i.e., kVp accuracy, timer accuracy, mA linearity, kV reproducibility, timer reproducibility, exposure reproducibility, HVL) and were therefore included in the study.

The dose area products (DAP) results showed that for all examinations, DAP increased with increasing age since the exposure parameters are directly proportional to the ages of patients.

The organs and tissues around the head and neck regions that are in close proximity to the X-ray beam during the panoramic procedures received higher doses compared to those that were bit far off. The mostly affected organs and tissues included the salivary glands, oral mucosa, extra-thoracic and thyroid glands.

The effective doses reduced with increasing age of patients for all exposures. This could be attributed to the fixed X-ray beam size of the panoramic machine. Inability to confine the beam, especially in children exposes more unintended tissues and organs increasing their effective doses.

Overall, the cancer risk in children was higher than adults, and higher in females than males.



CHAPTER FIVE

SUMMARY, CONCLUSIONS AND RECOMMENDATIONS

Overview

This study was conducted with the purpose of estimating the risk of exposure-induced cancer death (REID) to patients of varied age groups (5,10, 15-year-old and adult) during panoramic dental radiography procedures. The REIDs were estimated based on the ages, masses, heights gender of patients, inputs doses (DAPs), exposure parameters, geometries of the X-ray beam and simulation parameters. As part of the procedures leading to the estimation of the cancer risks, the dose-area products were initially determined for the different age groups using examination protocols for the patients. The DAPs, exposure factors and PCXMX 2.0Rotation simulation software were used to compute the absorbed and effective doses. The cancer risks were evaluated based on the ages and genders of the patients.

Summary

The inputs doses have direct relationship with the examination protocols of patients. This is due to the fact that the exposure protocols increase with increasing age of patients.

The absorbed doses were found to higher in tissues and organs that were either directly in X-ray beam or close to it.

The age of exposure of an individual directly impacts the effective dose.

The REIDs were higher in youngsters than adults and generally in females than males.

Conclusions

Judging from the findings of this study, the overall radiation exposure-induced cancer risk and the individual radiogenic cancers to patients during dental panoramic X-ray examinations are higher in children than adults and in female patients than males for most cancers. The REID values declined with advancing age for all kinds of cancer exposures. The REID values will guide dental practitioners in their requests for dental examinations by weighing the benefits of the diagnosis and treatment against the risk of the radiation-induced cancer to patients. The average cancer risk as a result of the exposure could serve as a guide in assessing the benefits and risks due to each examination for the age groups. This is especially essential for children since their organs and tissues are constantly developing and dividing, making them more vulnerable to the effects of ionising radiation exposure. Situations where radiographers unnecessarily repeat examinations due to lack of co-operation from the children has the potential to proportionally increase their cancer risks. It is, therefore, important that awareness is created about these REID values from the various dental radiographies to justify the need for such examinations before patients are made to undertake them. Although estimates of overall and individual cancer risks as a function of gender and age are low, there is a concern about the risks posed by dental panoramic X-rays due to their widespread use in dental examinations.

Recommendations

Retakes of panoramic dental radiographies must be avoided, particularly with younger children and female patients due to the sensitive nature of their organs and tissues. Any small amount of radiation has the potential to induce cancer to the exposed individual. Issues such as lack of cooperation from the

children to be imaged, not properly setting up the patient before exposure is taken and the bad state of image receptors must be corrected before the individual is exposed.

Referral dental practitioners must justify dental panoramic X-ray examination before making a requisition. The dentist must weigh the benefits against the risk of exposure and if there is an alternative means of obtaining the image for diagnosis or treatment which does not use ionising radiation, the patient must be encouraged to resort to that technology. Examples of the alternative means are the ultra-sound, MRI among others.

Organs and tissues that are directly in the main beam and will probably be exposed to scattered radiation throughout the dental radiographic process, as well as those that are susceptible to cancer incidence and mortality, must always be shielded. Particular attention must be paid to those around the head, neck and chest regions. The radiosensitive organs include the thyroid, lung, red bone marrow, breast, liver, oesophagus and stomach. Routinely wearing thyroid shields and lead aprons during procedures can keep these organs safe from the main and scattered beam.

The mean REID values derived from this research should be used as a guide to evaluate the risks and benefits for each age group. This raises awareness of the cancer risks associated with various dental panoramic X-ray examinations, which is required for justifications of these examinations.

The Nuclear Regulatory Authority, Ghana, must perform risk assessments on similar equipment imported into the country in future to ascertain the level of risk each one of them poses to patients.

Varying panoramic dental X-ray units' field of view (FOV) settings can offer varying coverage of anatomy of the radiosensitive organs in the head, neck, and chest regions.



REFERENCES

- Aps, J. (2013). Theoretical assessment of the thyroid gland's radiation dose from radiographs taken in dento-alveolar trauma in pediatric patients. *Pediatric and Neonatal Care*, 1(1). <https://research-repository.uwa.edu.au/en/publications/theoretical-assessment-of-the-thyroid-glands-radiation-dose-from->
- Avendano, B., Frederiksen, N. L., Benson, B. W., & Sokolowski, T. W. (1996). Effective dose and risk assessment from detailed narrow beam radiography. *Oral Surgery, Oral Medicine, Oral Pathology, Oral Radiology, and Endodontics*, 82(6), 713–719. [https://doi.org/10.1016/s1079-2104\(96\)80448-3](https://doi.org/10.1016/s1079-2104(96)80448-3)
- Beutel, J., Kundel, H. ., & Van Metter, R. . (2014). Handbook of Medical Imaging, Volume 1. Physics and Psychophysics. *Handbook of Medical Imaging, Volume 1. Physics and Psychophysics*. <https://doi.org/10.1117/3.832716>
- Birch, R., & Marshall, M. (1979). Computation of bremsstrahlung X-ray spectra and comparison with spectra measured with a Ge(Li) detector. *Physics in Medicine and Biology*, 24(3), 505–517. <https://doi.org/10.1088/0031-9155/24/3/002>
- Bohay, R. N., Kogon, S. L., & Stephens, R. G. (1994). A survey of radiographic techniques and equipment used by a sample of general dental practitioners. *Oral Surgery, Oral Medicine, and Oral Pathology*, 78(6), 806–810. [https://doi.org/10.1016/0030-4220\(94\)90100-7](https://doi.org/10.1016/0030-4220(94)90100-7)

Bouchet, L. G., Bolch, W. E., Weber, D. A., Atkins, H. L., & Poston, J. W. (1999).

MIRD Pamphlet No. 15: Radionuclide S values in a revised dosimetric model of the adult head and brain. Medical Internal Radiation Dose. *Journal of Nuclear Medicine : Official Publication, Society of Nuclear Medicine*, 40(3), 62S-101S.

Brenner, D. J., Doll, R., Goodhead, D. T., Hall, E. J., Land, C. E., Little, J. B., Lubin, J. H., Preston, D. L., Preston, R. J., Puskin, J. S., Ron, E., Sachs, R. K., Samet, J. M., Setlow, R. B., & Zaider, M. (2003). Cancer risks attributable to low doses of ionizing radiation: assessing what we really know. *Proceedings of the National Academy of Sciences of the United States of America*, 100(24), 13761–13766.

<https://doi.org/10.1073/PNAS.2235592100>

Büermann, L., Grosswendt, B., Kramer, H.-M., Selbach, H.-J., Gerlach, M., Hoffmann, M., & Krumrey, M. (2006). Measurement of the x-ray mass energy-absorption coefficient of air using 3 keV to 10 keV synchrotron radiation. *Physics in Medicine and Biology*, 51(20), 5125–5150.

<https://doi.org/10.1088/0031-9155/51/20/004>

Button, T. M., Moore, W. C., & Goren, A. D. (1999). Causes of excessive bitewing exposure: results of a survey regarding radiographic equipment in New York. *Oral Surgery, Oral Medicine, Oral Pathology, Oral Radiology, and Endodontics*, 87(4), 513–517. [https://doi.org/10.1016/S1079-2104\(99\)70254-4](https://doi.org/10.1016/S1079-2104(99)70254-4)

Carestream Health, I. (2007). *Dental Radiography Series Radiation safety in dental radiography*. Retrieved June 19, 2022 from

<http://www.kodakdental.com/>

Cederberg, R. A., Frederiksen, N. L., Benson, B. W. & Sokolowski, T. W.

(1997). Effect of the geometry of the intraoral position-indicating device on effective dose. *Oral Surgery, Oral Medicine, Oral Pathology, Oral Radiology, and Endodontics*, 84(1), 101–109.

[https://doi.org/10.1016/s1079-2104\(97\)90304-8](https://doi.org/10.1016/s1079-2104(97)90304-8)

Chaparian, A., & Dehghanzade, F. (2017). Evaluation of radiation-induced cancer risk to patients undergoing intra-oral and panoramic dental radiographies using experimental measurements and Monte Carlo calculations. *International Journal of Radiation Research*, 15(2), 197–205.

<https://doi.org/10.18869/acadpub.ijrr.15.2.197>

Chen, T. R., Tyan, Y. S., Teng, P. S., Chou, J. H., Yeh, C. Y., T W E, Shao, C.

H., & Tung, C. J. (2011). Population dose from medical exposure in Taiwan for 2008. *Medical Physics*, 38(6), 3139–3148.

<https://doi.org/10.1118/1.3592936>

Council, N. R. (2005). Health Risks from Exposure to Low Levels of Ionizing Radiation: BEIR VII Phase 2. *Health Risks from Exposure to Low Levels of Ionizing Radiation: BEIR VII Phase 2*, 1–406.

<https://doi.org/10.17226/11340>

Cristy, M., & Eckerman, K. (1987). *Specific absorbed fractions of energy at various ages from internal photon sources. I. Methods. Report ORNL/TM-8381/VI. Oak Ridge: Oak Ridge National Laboratory.*

Cristy M. (1980). *Mathematical phantoms representing children of various ages for use in estimates of internal dose, NUREG/CR-1159,.*

<https://www.osti.gov/biblio/5308345>

- Czajka, J., Rushton, V. E., Shearer, A. C., & Horner, K. (1996). Sensitometric and image quality performance of “rapid” intraoral film processing techniques. *The British Journal of Radiology*, *69*(817), 49–58. <https://doi.org/10.1259/0007-1285-69-817-49>
- Danforth, R. A., & Clark, D. E. (2000). Effective dose from radiation absorbed during a panoramic examination with a new generation machine. *Oral Surgery, Oral Medicine, Oral Pathology, Oral Radiology, and Endodontics*, *89*(2), 236–243. <https://doi.org/10.1067/moe.2000.103526>
- Dentistry, P. (2015). *Panoramic Imaging*. <https://pocketdentistry.com/10-panoramic-imaging/>. Retrieved March 12, 2022, from <https://pocketdentistry.com/>
- Dula, K., Mini, R., Lambrecht, J. T., Stelt, P. F., Schneeberger, P., Clemens, G., Sanderink, H., & Buser, D. (1997). Hypothetical mortality risk associated with spiral tomography of the maxilla and mandible prior to endosseous implant treatment. *European Journal of Oral Sciences*, *105*(2), 123–129. <https://doi.org/10.1111/j.1600-0722.1997.tb00190.x>
- Dula, K., Mini, R., van der Stelt, P. F., & Buser, D. (2001). The radiographic assessment of implant patients: decision-making criteria. *The International Journal of Oral & Maxillofacial Implants*, *16*(1), 80–89.
- Dula, K., Sanderink, G., Van Der Stelt, P. F., Mini, R., & Buser, D. (1998). Effects of dose reduction on the detectability of standardized radiolucent lesions in digital panoramic radiography. *Oral Surgery, Oral Medicine, Oral Pathology, Oral Radiology, and Endodontology*, *86*(2), 227–233. [https://doi.org/10.1016/S1079-2104\(98\)90130-5](https://doi.org/10.1016/S1079-2104(98)90130-5)
- Eckerman, K., Cristy, M., & Ryman, J. (1996). *The ORNL mathematical phantom*

series. Retrieved February 6, 2021, from <http://homer.ornl.gov/vlab/mird2.pdf>.

FARDT. (2019). *It's Just A Little Radiation! Fayetteville AR Dental Technology*. Retrieved September 10, 2022, from

<https://www.greenwaydentalcare.com/2019/09/dont-worry-so-much-its-just-a-little-radiation/>

Fidler-Benaoudia, M. M., Torre, L. A., Bray, F., Ferlay, J., & Jemal, A. (2020). Lung cancer incidence in young women vs. young men: A systematic analysis in 40 countries. *International Journal of Cancer*, *147*(3), 811–819. <https://doi.org/10.1002/ijc.32809>

Frederiksen, N. L., Benson, B. W., & Sokolowski, T. W. (1994). Effective dose and risk assessment from film tomography used for dental implant diagnostics. *Dento Maxillo Facial Radiology*, *23*(3), 123–127. <https://doi.org/10.1259/dmfr.23.3.7835511>

Frederiksen, N. L., Benson, B. W., & Sokolowski, T. W. (1995). Effective dose and risk assessment from computed tomography of the maxillofacial complex. *Dento Maxillo Facial Radiology*, *24*(1), 55–58. <https://doi.org/10.1259/dmfr.24.1.8593910>

Geist, J. R., & Brand, J. W. (2001). Sensitometric comparison of speed group E and F dental radiographic films. *Dento Maxillo Facial Radiology*, *30*(3), 147–152. <https://doi.org/10.1038/sj/dmfr/4600595>

Gijbels, F., Bou Serhal, C., Willems, G., Bosmans, H., Sanderink, G., Persoons, M., & Jacobs, R. (2001). Diagnostic yield of conventional and digital cephalometric images: a human cadaver study. *Dento Maxillo Facial Radiology*, *30*(2), 101–105. <https://doi.org/10.1038/sj/dmfr/4600585>

- Gijbels, F., Jacobs, R., Sanderink, G., De Smet, E., Nowak, B., Van Dam, J., & Van Steenberghe, D. (2002). A comparison of the effective dose from scanography with periapical radiography. *Dento Maxillo Facial Radiology*, 31(3), 159–163. <https://doi.org/10.1038/sj/dmfr/4600683>
- Gori, C., Rossi, F., Stecco, A., Villari, N., & Zatelli, G. (2000). Dose Evaluation and Quality Criteria in Dental Radiology. *Radiation Protection Dosimetry*, 90(1), 225–227. <https://doi.org/10.1093/oxfordjournals.rpd.a033125>
- Granlund, C., Thilander-Klang, A., Ylhan, B., Lofthag-Hansen, S., & Ekestubbe, A. (2016). Absorbed organ and effective doses from digital intra-oral and panoramic radiography applying the ICRP 103 recommendations for effective dose estimations. *The British Journal of Radiology*, 89(1066). <https://doi.org/10.1259/BJR.20151052>
- Hagemann, K., Vollmer, D., Niegel, T., Ehmer, U., & Reuter, I. (2000). Prospective study on the reproducibility of cephalometric landmarks on conventional and digital lateral headfilms. *Journal of Orofacial Orthopedics = Fortschritte Der Kieferorthopadie : Organ/Official Journal Deutsche Gesellschaft Fur Kieferorthopadie*, 61(2), 91–99. <https://doi.org/10.1007/BF01300351>
- Hall, E. J. (2002). Lessons we have learned from our children: cancer risks from diagnostic radiology. *Pediatric Radiology*, 32(10), 700–706. <https://doi.org/10.1007/S00247-002-0774-8>
- Hall, E. J., & Brenner, D. J. (2008). Cancer risks from diagnostic radiology. *British Journal of Radiology*, 81(965), 362–378. <https://doi.org/10.1259/BJR/01948454>

- Hallquist, A., Hardell, L., Degerman, A., Wingren, G., & Boquist, L. (1994). Medical diagnostic and therapeutic ionizing radiation and the risk for thyroid cancer: a case-control study. *European Journal of Cancer Prevention : The Official Journal of the European Cancer Prevention Organisation (ECP)*, 3(3), 259–267. <https://doi.org/10.1097/00008469-199403030-00004>
- Hayakawa, Y., Fujimori, H., & Kuroyanagi, K. (1993). Absorbed doses with intraoral radiography. *Oral Surgery, Oral Medicine, Oral Pathology*, 76(4), 519–524. [https://doi.org/10.1016/0030-4220\(93\)90022-V](https://doi.org/10.1016/0030-4220(93)90022-V)
- Helmrot, E., Carlsson, G. A., & Eckerdal, O. (1994). Effects of contrast equalization on energy imparted to the patient: a comparison of two dental generators and two types of intraoral film. *Dento Maxillo Facial Radiology*, 23(2), 83–90. <https://doi.org/10.1259/dmfr.23.2.7835508>
- Hintze, H. (1993). Radiographic screening examination: frequency, equipment, and film in general dental practice in Denmark. *Scandinavian Journal of Dental Research*, 101(1), 52–56. <https://doi.org/10.1111/J.1600-0722.1993.TB01647.X>
- Horn-Ross, P. L., Ljung, B. M., & Morrow, M. (1997). Environmental factors and the risk of salivary gland cancer. *Epidemiology (Cambridge, Mass.)*, 8(4), 414–419. <https://doi.org/10.1097/00001648-199707000-00011>
- Horner, K., Rushton, V., Walker, A., Tsiklakis, K., Hirschmann, P. N., van der Stelt, P. F., Anne-Marie Glenny, Velders, X. L., & Pavitt, S. (2015). *European guidelines on radiation protection in dental radiology : the safe use of radiographs in dental practice.*

- Hubbell, J. H., Veigele, W. J., Briggs, E. A., Brown, R. T., Cromer, D. T., & Howerton, R. J. (1975). Atomic form factors, incoherent scattering functions, and photon scattering cross sections. *Journal of Physical and Chemical Reference Data*, 4(3), 471–538. <https://doi.org/10.1063/1.555523>
- Huda, W. (2015). *Categorical Course in Diagnostic Radiology Physics: From Invisible to Visible—The Science and Practice of X-Ray Imaging and Radiation Dose Optimization*. <https://archive.rsna.org/2006/4425855.html>
- Huda, W. (2016). *Review of Radiologic Physics. 3rd ed., Baltimore MD: Lippincott Williams & Wilkins. 255.*
- Hwang, S.-Y., Choi, E.-S., Kim, Y.-S., Gim, B.-E., Ha, M., & Kim, H.-Y. (2018). Health effects from exposure to dental diagnostic X-ray. *Environmental Health and Toxicology*, 33(4), e2018017. <https://doi.org/10.5620/eht.e2018017>
- IBA. (2013). *IBA Dosimetry GmbH, Schwarzenbruck*. <https://www.bloomberg.com/profile/company/7582580Z:US>
- ICRP. (1991). 1990 Recommendations of the International Commission on Radiological Protection. *Annals of the ICRP*, 21(1–3), 1–201.
- ICRP. (2002). *Basic anatomical and physiological data for use in radiological protection: reference values. ICRP Publication 89. Annals of the ICRP; 32 (3–4).*
- ICRP. (2007). The 2007 Recommendations of the International Commission on Radiological Protection. ICRP publication 103. *Annals of the ICRP*, 37(2–4), 1–332. <https://doi.org/10.1016/j.icrp.2007.10.003>

IPEM. (2005). *Institute of Physics and Engineering in Medicine. Recommended standard for the routine performance testing of diagnostic X-ray imaging systems. Report No.77. York.*

Izzetti, R., Nisi, M., Aringhieri, G., Crocetti, L., Graziani, F., & Nardi, C.

(2021). Basic Knowledge and New Advances in Panoramic Radiography Imaging Techniques: A Narrative Review on What Dentists and Radiologists Should Know. *Applied Sciences* 2021, Vol. 11, Page 7858, 11(17), 7858. <https://doi.org/10.3390/APP11177858>

Jackson, N., Menon, B. S., Zarina, W., Zawawi, N., & Naing, N. N. (1999). Why is acute leukemia more common in males? A possible sex-determined risk linked to the ABO blood group genes. *Annals of Hematology*, 78(5), 233–236. <https://doi.org/10.1007/s002770050507>

Jones, D., & Wall, B. (1985). *Organ doses from medical x-ray examinations calculated using Monte Carlo techniques, NRPB -R186. London: HMSO.*

Kapa, S. F., & Tyndall, D. A. (1989). A clinical comparison of image quality and patient exposure reduction in panoramic radiography with heavy metal filtration. *Oral Surgery, Oral Medicine, Oral Pathology*, 67(6), 750–759. [https://doi.org/10.1016/0030-4220\(89\)90020-0](https://doi.org/10.1016/0030-4220(89)90020-0)

Kapa, S. F., Tyndall, D. A., & Ouellette, T. E. (1990). Application of added beam filtration to intra-oral radiography. *Dento Maxillo Facial Radiology*, 19(2), 67–74. <https://doi.org/10.1259/dmfr.19.2.2079143>

Lecomber A. R., & Faulkner K. (1998). Dose and risk in Dental Radiography, Luxembourg 1997. Reference Doses and Quality in Medical Imaging: What the referring practitioner and directing medical staff should know. *Radiation*

Protection Dosimetry , 80, 23–25.

Lecomber, A. R., Downes, S. L., Mokhtari, M., & Faulkner, K. (2000).

Optimisation of patient doses in programmable dental panoramic radiography. *Dento Maxillo Facial Radiology*, 29(2), 107–112.

<https://doi.org/10.1038/sj/dmfr/4600513>

Lecomber, A. R., & Faulkner, K. (1993). Dose reduction in panoramic

radiography. *Dento Maxillo Facial Radiology*, 22(2), 69–73.

<https://doi.org/10.1259/dmfr.22.2.8375557>

Lecomber, A. R., Yoneyama, Y., Lovelock, D. J., Hosoi, T., & Adams, A. M.

(2001). Comparison of patient dose from imaging protocols for dental implant planning using conventional radiography and computed tomography. *Dento Maxillo Facial Radiology*, 30(5), 255–259.

<https://doi.org/10.1038/sj/dmfr/4600627>

Lee, C., Park, B., Lee, S. S., Kim, J. E., Han, S. S., Huh, K. H., Yi, W. J., Heo,

M. S., & Choi, S. C. (2019). Efficacy of the Monte Carlo method and dose reduction strategies in paediatric panoramic radiography. *Scientific Reports* 2019 9:1, 9(1), 1–10. <https://doi.org/10.1038/s41598-019-46157-0>

Lim, K. F., & Foong, K. W. (1997). Phosphor-stimulated computed

cephalometry: reliability of landmark identification. *British Journal of Orthodontics*, 24(4), 301–308. <https://doi.org/10.1093/ORTHO/24.4.301>

Longstreth, W. T., Phillips, L. E., Drangsholt, M., Koepsell, T. D., Custer, B. S.,

Gehrels, J.-A., & van Belle, G. (2004). Dental X-rays and the risk of intracranial meningioma. *Cancer*, 100(5), 1026–1034.

<https://doi.org/10.1002/cncr.20036>

Ludlow, J. B., Davies-Ludlow, L. E., & White, S. C. (2008). Patient risk related to common dental radiographic examinations: the impact of 2007 International Commission on Radiological Protection recommendations regarding dose calculation. *Journal of the American Dental Association* (1939), 139(9), 1237–1243.

<https://doi.org/10.14219/JADA.ARCHIVE.2008.0339>

Ludlow, J. B., Platin, E., & Mol, A. (2001). Characteristics of Kodak Insight, an F-speed intraoral film. *Oral Surgery, Oral Medicine, Oral Pathology, Oral Radiology, and Endodontics*, 91(1), 120–129.

<https://doi.org/10.1067/moe.2001.110575>

Ma, H., Hill, C. K., Bernstein, L., & Ursin, G. (2008). Low-dose medical radiation exposure and breast cancer risk in women under age 50 years overall and by estrogen and progesterone receptor status: results from a case-control and a case-case comparison. *Breast Cancer Research and Treatment*, 109(1), 77–90. <https://doi.org/10.1007/S10549-007-9625-5>

Macdonald-Jankowski, D. S., & Lawinski, C. P. (1992). The effect of thin K-edge filters on radiation dose in dental radiography. *The British Journal of Radiology*, 65, 990–995.

MacDonald-Jankowski, D. S., & Lawinski, C. P. (1991). The reduction in radiation dose for intra-oral radiographs by the use of thin K-edge filters. *The British Journal of Radiology*, 64(762), 524–528.

<https://doi.org/10.1259/0007-1285-64-762-524>

Maillie, H. D., & Gilda, J. E. (1993). Radiation-induced cancer risk in radiographic cephalometry. *Oral Surgery, Oral Medicine, Oral Pathology,*

75(5), 631–637. [https://doi.org/10.1016/0030-4220\(93\)90239-Z](https://doi.org/10.1016/0030-4220(93)90239-Z)

Manieri, E., Herrera-Melle, L., Mora, A., Tomás-Loba, A., Leiva-Vega, L., Fernández, D. I., Rodríguez, E., Morán, L., Hernández-Cosido, L., Torres, J. L., Seoane, L. M., Cubero, F. J., Marcos, M., & Sabio, G. (2019).

Adiponectin accounts for gender differences in hepatocellular carcinoma incidence. *The Journal of Experimental Medicine*, 216(5), 1108–1119.

<https://doi.org/10.1084/jem.20181288>

Mantebea, H. (2015). *Determination of doses and cancer risk to paediatric and young adult patients undergoing plain radiographic and fluoroscopic guided surgical procedures. A Master of Philosophy degree thesis, University of Ghana.*

Mauriello, S. M., Overman, V. P., & Mann, G. B. (1996). Clinical evaluation of a samarium compound filter and E-speed film. *Quintessence International (Berlin, Germany : 1985)*, 27(11), 769–773.

McCullough, C. H., Christner, J. A., & Kofler, J. M. (2010). How effective is effective dose as a predictor of radiation risk? *AJR. American Journal of Roentgenology*, 194(4), 890–896. <https://doi.org/10.2214/AJR.09.4179>

McDavid, W. D., Welander, U., Pillai, B. K., & Morris, C. R. (1982). The Intrex—a constant-potential x-ray unit for periapical dental radiography. *Oral Surgery, Oral Medicine, and Oral Pathology*, 53(4), 433–436. [https://doi.org/10.1016/0030-4220\(82\)90448-0](https://doi.org/10.1016/0030-4220(82)90448-0)

McMaster, W. H., Kerr Del Grande, N., Mallett, J. H., & Hubbell, J. H. (1970). Compilation of x-ray cross sections UCRL-50174, sections I, II revision 1, III, IV. *Atomic Data and Nuclear Data Tables*, 8(4–6), 443–444. [https://doi.org/10.1016/S0092-640X\(70\)80026-2](https://doi.org/10.1016/S0092-640X(70)80026-2)

Memon, A., Godward, S., Williams, D., Siddique, I., & Al-Saleh, K. (2010).

Dental x-rays and the risk of thyroid cancer: a case-control study. *Acta Oncologica (Stockholm, Sweden)*, 49(4), 447–453.

<https://doi.org/10.3109/02841861003705778>

Memon, A., Rogers, I., Paudyal, P., & Sundin, J. (2019). Dental X-Rays and the Risk of Thyroid Cancer and Meningioma: A Systematic Review and Meta-Analysis of Current Epidemiological Evidence. *Thyroid*, 29(11), 1572–1593. <https://doi.org/10.1089/thy.2019.0105>

Molander, B., Ahlqwist, M., & Gröndahl, H. G. (1995). Image quality in panoramic radiography. *Dentomaxillofacial Radiology*, 24(1), 17–22. <https://doi.org/10.1259/dmfr.24.1.8593902>

Moolgavkar, S. H., Day, N. E., & Stevens, R. G. (1980). Two-stage model for carcinogenesis: Epidemiology of breast cancer in females. *Journal of the National Cancer Institute*, 65(3), 559–569.

Neuberger JS, Brownson RC, Morantz RA, & Chin TD. (1991). Association of brain cancer with dental X-rays and occupation in Missouri - PubMed. 15(1). Retrieved August 21, 2021, from <https://pubmed.ncbi.nlm.nih.gov/1646072/>

Niroomand-Rad, A. (2003). Radiological protection of patients. *International Journal of Radiation Research*, 1(3), 125–131. Retrieved July 18, 2021 from <http://ijrr.com/article-1-18-en.html>

NRPB. (2001). *Guidance notes for dental practitioners on the safe use of X-ray equipment*. Department of Health, London.

NSW EPA. (2001). *Registration requirements and industry best practice for ionizing radiation apparatus used in diagnostic imaging. Radiation Standard 6: Part 3 - Dentistry*, 13-17.

Pasler, F. A. (2021). Vorwort. In *Zahnärztliche Radiologie*. Georg Thieme Verlag KG. <https://doi.org/10.1055/b-0041-181383>

Platin, E., Janhom, A., & Tyndall, D. (1998). A quantitative analysis of dental radiography quality assurance practices among North Carolina dentists. *Oral Surgery, Oral Medicine, Oral Pathology, Oral Radiology, and Endodontics*, 86(1), 115–120. [https://doi.org/10.1016/S1079-2104\(98\)90160-3](https://doi.org/10.1016/S1079-2104(98)90160-3)

Pradhan, A. S., Kim, J. L., & Lee, J. I. (2012). On the use of “effective dose” (E) in medical exposures. *Journal of Medical Physics*, 37(2), 63–65. <https://doi.org/10.4103/0971-6203.94739>

Preston-Martin, S., Henderson, B. E., & Bernstein, L. (1985). Medical and dental x rays as risk factors for recently diagnosed tumors of the head. *National Cancer Institute Monograph*, 69, 175–179.

Preston-Martin, S., Mack, W., & Henderson, B. E. (1989). Risk factors for gliomas and meningiomas in males in Los Angeles County. *Cancer Research*, 49(21), 6137–6143.

Preston-Martin, S., & White, S. C. (1990). Brain and salivary gland tumors related to prior dental radiography: implications for current practice. *Journal of the American Dental Association* (1939), 120(2), 151–158. <https://doi.org/10.14219/jada.archive.1990.0026>

Preston, D. L., Mattsson, A., Holmberg, E., Shore, R., Hildreth, N. G., & Boice, J. D. (2002). Radiation effects on breast cancer risk: a pooled analysis of

eight cohorts. *Radiation Research*, 158(2), 220–235.

[https://doi.org/10.1667/0033-7587\(2002\)158\[0220:reobcr\]2.0.co;2](https://doi.org/10.1667/0033-7587(2002)158[0220:reobcr]2.0.co;2)

Rosenstein, M. (1976). *Selected Organ Doses for Projections Common in Pediatric Radiology*.

Russo, J., & Russo, I. H. (1997). Toward a unified concept of mammary carcinogenesis. *Progress in Clinical and Biological Research*, 396, 1–16.

Scaf, G., Lurie, A. G., Mosier, K. M., Kantor, M. L., Ramsby, G. R., & Freedman, M. L. (1997). Dosimetry and cost of imaging osseointegrated implants with film-based and computed tomography. *Oral Surgery, Oral Medicine, Oral Pathology, Oral Radiology, and Endodontology*, 83(1), 41–48.
[https://doi.org/10.1016/S1079-2104\(97\)90089-5](https://doi.org/10.1016/S1079-2104(97)90089-5)

Sharma, S. (2021). Johns and cunningham's the physics of radiology. *Journal of Medical Physics*, 46(2), 128. https://doi.org/10.4103/jmp.JMP_102_21

Souza, E. M., Correa, C. A., Brito, A., Lima, M. A. F., Silva, A. X., & Kelecom, A. (2008). *Dose and Risk Evaluation to the Thyroid Gland in Intra-oral Dental Radiology*.

Stenström, B., Julin, P., & Karlsson, L. (1987). Comparison between panoramic radiographic techniques. Part IV. Absorbed doses and energy imparted from the Orthopantomograph, model OP10. *Dento Maxillo Facial Radiology*, 16(1), 11–15. <https://doi.org/10.1259/dmfr.1987.0001>

Storm, E., & Israel, H. (1970). *Photon cross sections from 1 keV to 100 MeV for elements Z=1 to Z=100. Nuclear Data Tables, Sect A; 7: 565–688*.

Svenson, B., & Petersson, A. (2009). Questionnaire survey on the use of dental X-ray film and equipment among general practitioners in the Swedish Public Dental Health Service. <Http://Dx.Doi.Org/10.3109/00016359509005978>,

53(4), 230–235. <https://doi.org/10.3109/00016359509005978>

Syriopoulos, K., Velders, X. L., Sanderink, G. C., & van Der Stelt, P. F. (2001).

Sensitometric and clinical evaluation of a new F-speed dental X-ray film.

Dento Maxillo Facial Radiology, 30(1), 40–44.

<https://doi.org/10.1038/sj/dmfr/4600575>

Syriopoulos K, Velders XL, van der Stelt PF, van Ginkel FC, & Tsiklakis K.

(1998). *Mail survey of dental radiographic techniques and radiation doses in Greece.*

https://www.researchgate.net/publication/12422862_Mail_survey_of_dental_radiographic_techniques_and_radiation_doses_in_Greece

Tapiovaara, M., Lakkisto, M., & Servomaa, A. (1997). *PCXMC. A PC-based Monte Carlo program for calculating patient doses in medical x-ray examinations. 2.*

http://inis.iaea.org/Search/search.aspx?orig_q=RN:28049612

Tapiovaara, M., & Siiskonen, T. (2008). *PCXMC : a Monte Carlo program for calculating patient doses in medical x-ray examinations.*

Tetradis, S., Scaf, G., Lurie, A. G., & Freedman, M. L. (1995). Niobium filtration of conventional and high-frequency x-ray generator beams for intraoral radiography. Effects on absorbed doses, image density and contrast, and photon spectra. *Oral Surgery, Oral Medicine, Oral Pathology, Oral Radiology, and Endodontics*, 80(2), 232–241.

[https://doi.org/10.1016/s1079-2104\(05\)80207-0](https://doi.org/10.1016/s1079-2104(05)80207-0)

Teunen, D. (1998). The European Directive on health protection of individuals against the dangers of ionising radiation in relation to medical exposures

(97/43/EURATOM). *Journal of Radiological Protection : Official Journal*

of the Society for Radiological Protection, 18(2), 133–137.

<https://doi.org/10.1088/0952-4746/18/2/009>

Thunthy, K. H., & Weinberg, R. (1995). Sensitometric comparison of Kodak EKTASPEED Plus, Ektaspeed, and Ultra-speed Dental Films. *Oral Surgery, Oral Medicine, Oral Pathology, Oral Radiology, and Endodontology*, 79(1), 114–116. [https://doi.org/10.1016/S1079-2104\(05\)80085-X](https://doi.org/10.1016/S1079-2104(05)80085-X)

Thunthy, K. H., & Weinberg, R. (1997). Film-screen systems: sensitometric comparison of Kodak Ektavision system to Kodak T-Mat/RA system. *Oral Surgery, Oral Medicine, Oral Pathology, Oral Radiology, and Endodontics*, 83(2), 288–292. [https://doi.org/10.1016/s1079-2104\(97\)90018-4](https://doi.org/10.1016/s1079-2104(97)90018-4)

UNSCEAR. (2001). *Hereditary effects of radiation : United Nations Scientific Committee on the Effects of Atomic Radiation, UNSCEAR 2001 report to the General Assembly, with scientific annex*. 160.
[//www.unscear.org/unscear/en/publications/2001.html](http://www.unscear.org/unscear/en/publications/2001.html)

UNSCEAR. (2010). 2008 Report to the General Assembly: Annex B Exposures of the Public and Workers from Various Sources of Radiation. *United Nations, I*, 66. [//www.unscear.org/unscear/en/publications/2008_1.html](http://www.unscear.org/unscear/en/publications/2008_1.html)

Velders, X. L., van Aken, J., & van der Stelt, P. F. (1991). Risk assessment from bitewing radiography. *Dento Maxillo Facial Radiology*, 20(4), 209–213.
<https://doi.org/10.1259/dmfr.20.4.1808009>

Visser, H., Rödiger, T., & Hermann, K. P. (2001). Dose reduction by direct-digital cephalometric radiography. *The Angle Orthodontist*, 71(3), 159–163.
[https://doi.org/10.1043/0003-3219\(2001\)071<0159:DRBDDC>2.0.CO;2](https://doi.org/10.1043/0003-3219(2001)071<0159:DRBDDC>2.0.CO;2)

Wakoh, M., Farman, A. G., Scarfe, W. C., Kelly, M. S., & Kuroyanagi, K. (1995). Perceptibility of defects in an aluminum test object: a comparison

of the RVG-S and first generation VIXA systems with and without added niobium filtration. *Dento Maxillo Facial Radiology*, 24(4), 211–214.

<https://doi.org/10.1259/dmfr.24.4.9161163>

Wakoh, M., Nishikawa, K., Kobayashi, N., Farman, A. G., & Kuroyanagi, K.

(2001). Sensitometric properties of Agfa Dentus OrthoLux, Agfa Dentus ST8G, and Kodak Ektavision panoramic radiographic film. *Oral Surgery, Oral Medicine, Oral Pathology, Oral Radiology, and Endodontics*, 91(2), 244–251. <https://doi.org/10.1067/moe.2001.112154>

Walker, C., & van der Putten, W. (2012). Patient dosimetry and a novel approach to establishing Diagnostic Reference Levels in dental radiology.

Physica Medica : PM : An International Journal Devoted to the Applications of Physics to Medicine and Biology : Official Journal of the Italian Association of Biomedical Physics (AIFB), 28(1), 7–12.

<https://doi.org/10.1016/J.EJMP.2010.12.003>

White, S. C. (2014). Assessment of radiation risk from dental radiography.

Dentomaxillofacial Radiology, 21(3), 118–126.

<https://doi.org/10.1259/dmfr.21.3.1397466>

White, S. C., & Gratt, B. M. (1991). Evaluation of Niobi-X filtration in intraoral radiology. *Oral Surgery, Oral Medicine, Oral Pathology*, 72(6), 746–755.

[https://doi.org/10.1016/0030-4220\(91\)90020-D](https://doi.org/10.1016/0030-4220(91)90020-D)

White, S. C., & Yoon, D. C. (2000). Comparison of sensitometric and diagnostic performance of two films. *Compendium of Continuing Education in Dentistry (Jamesburg, N.J. : 1995)*, 21(6), 530–532, 534, 536 passim.

Wingren, G., Hallquist, A., & Hardell, L. (1997). Diagnostic X-ray exposure and female papillary thyroid cancer: a pooled analysis of two Swedish studies.

European Journal of Cancer Prevention : The Official Journal of the European Cancer Prevention Organisation (ECP), 6(6), 550–556.

<https://doi.org/10.1097/00008469-199712000-00010>

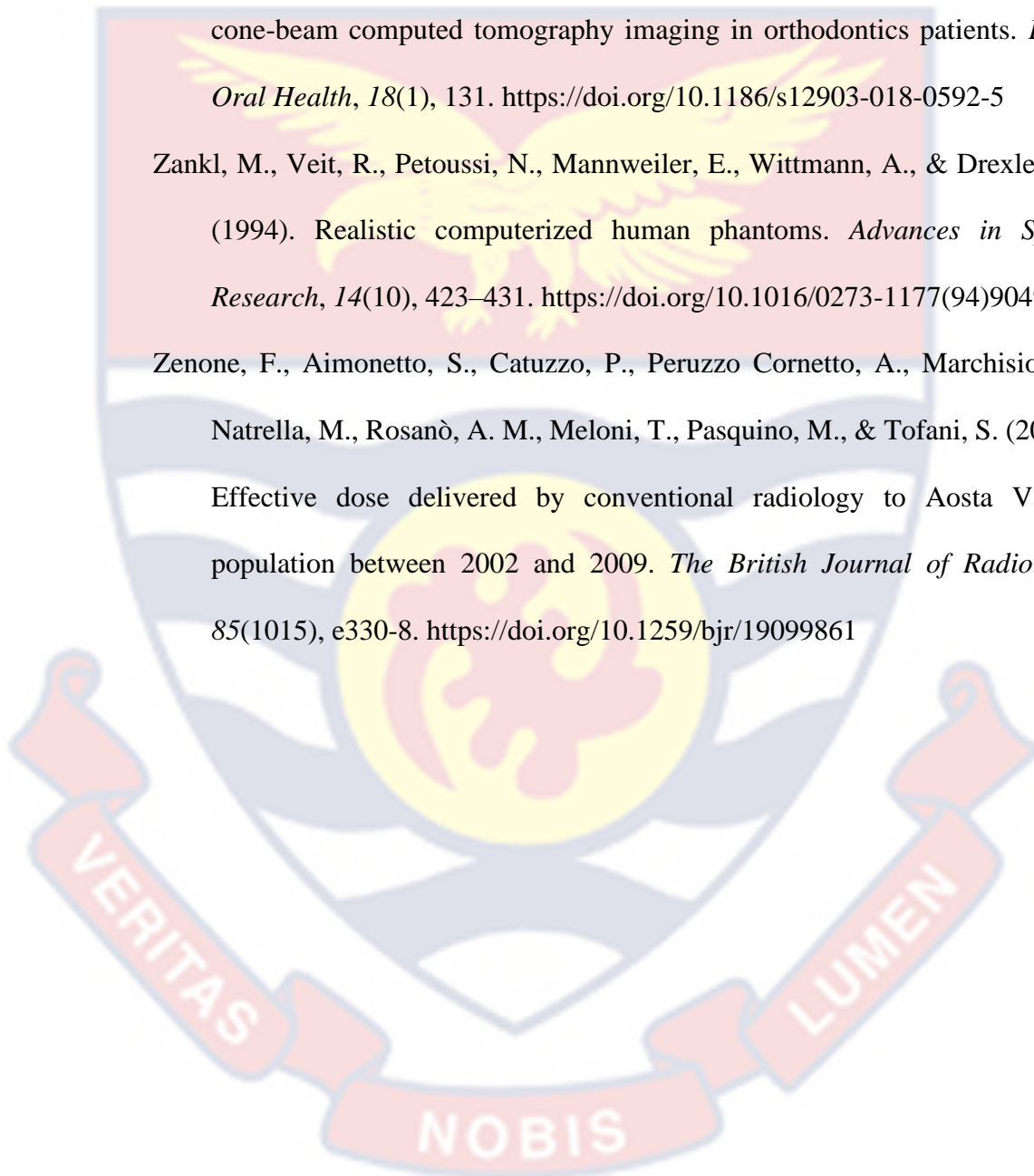
Yeh, J.-K., & Chen, C.-H. (2018). Estimated radiation risk of cancer from dental cone-beam computed tomography imaging in orthodontics patients. *BMC Oral Health*, 18(1), 131. <https://doi.org/10.1186/s12903-018-0592-5>

Zankl, M., Veit, R., Petoussi, N., Mannweiler, E., Wittmann, A., & Drexler, G.

(1994). Realistic computerized human phantoms. *Advances in Space Research*, 14(10), 423–431. [https://doi.org/10.1016/0273-1177\(94\)90496-0](https://doi.org/10.1016/0273-1177(94)90496-0)

Zenone, F., Aimonetto, S., Catuzzo, P., Peruzzo Cornetto, A., Marchisio, P., Natrella, M., Rosanò, A. M., Meloni, T., Pasquino, M., & Tofani, S. (2012).

Effective dose delivered by conventional radiology to Aosta Valley population between 2002 and 2009. *The British Journal of Radiology*, 85(1015), e330-8. <https://doi.org/10.1259/bjr/19099861>



APPENDICES

APPENDIX A

THE PCXMC 2.0 MODIFIED PRINCIPAL DIMENSIONS OF THE
MATHEMATICAL PHANTOMS.

	Weight (kg)	Total height (cm)	Trunk height (cm)	Trunk thickness (cm)	Trunk Width ¹⁾	Trunk Width ²⁾	Leg Length (cm)
Newborn	3.40	50.9	21.6	9.8	10.94	12.70	16.8
1-year-old	9.20	74.40	30.7	13.0	15.12	17.6	26.5
5-year-old	19.0	109.1	40.8	15.0	19.64	22.9	48.0
10-year-old	32.40	139.8	50.8	16.8	23.84	27.8	66.0
15-year-old	54.60	168.1	63.1	19.6	29.66	34.5	78.0
Adult	73.20	178.6	70.0	20.0	34.40	40.0	80.0

1) inclusive of arms

2) without arms

APPENDIX B

PCXMC 2.0 PERCENTAGE BY WEIGHT OF THE ELEMENTS IN THE
PHANTOM TISSUES

	Density (g/cm ³)	H (%)	C (%)	N (%)	O (%)	P (%)	Ca (%)
Skeleton (except newborn)	1.40	7.337	25.475	3.057	47.893	5.876	10.362
Newborn skeleton	1.22	7.995	9.708	2.712	66.811	4.623	8.151
Lung tissue	0.296	10.134	10.238	2.866	75.752	0.770	0.240
Other soft tissues (except newborn)	1.04	10.454	22.663	2.490	63.525	0.626	0.242
Other soft tissues (newborn)	1.04	10.625	14.964	1.681	71.830	0.592	0.308

